Theoretical and Experimental Study of The Effect Baffles Geometry and Nanofluid on Performance of Shell-U-Tube Heat Exchanger

A THESIS
SUBMITTED TO
THE COUNCIL OF BASRAH ENGINEERING TECHNICAL COLLEGE AT SOUTHERN TECHNICAL UNIVERSITY
IN PARTIAL FULFILLMENT OF THE REQUIREMENTS
FOR THE DEGREE OF MASTER OF SCIENCE
IN
THERMAL TECHNICAL ENGINEERING

BY

Murtadha Saeed Mohammed

(B.Sc. Air Conditioning and Refrigeration Eng.)

September - 2017

بسم الله الرحمن الرحيم

الله نور السموات والأرض مثل نوره

كمشكاة فيها مصباح المصباح في زجاجة

الزجاجة كأنها كوكب دري يوقد من شجرة

مباركة زيتونة لا شرقية ولا غربية يكاد زيتها يضيء ولو لم تمسسه نار نور

على نور يهدي الله لنوره من يشاء ويضرب الله الأمثال للناس

والله بكل شيء عليم

صدق الله العلي العظيم

سورة النور (٣٠)

Dedication

To

Allah Subhana WA taala,

My Country

And

My Family

Acknowledgements

*All praise and thanks are due to **Allah (subhana wa taala)** for bestowing me with health, knowledge and patience to complete this work.*

*Thereafter, I would like to express my sincere thanks to my first supervisor, **Prof. Dr. Sa'doon F. Dakhil** and **Assist. Prof. Dr. Ahmed K. Mohammed** for their valuable, professional guidance during the development of this work. Special thanks to **Assist. Prof. Dr. Adnan A. Ateeq,** the dean of the Basrah Engineering Technical College, **Dr. Dhia Kamel** the dean assistance for scientific affairs.*

*I am also extremely grateful to **Dr. Mohamed Abdel Wahab, Dr. Safaa Hameed**, **Mr. Tahseen Ali** and **Mr. Akeel Mohammed Ali**. Thanks are also extended to the staff of the higher education unit for being very helpful.*

*A part of this work was done in the fuel and energy laboratory, therefore my appreciation goes to **Dr. Amjad Ahmed**, the head of Department and all the staff of the laboratory.*

*I would like also to thank **Eng. Mahmood Shakir** who is in Alaq Annajah engineering industries for his help and support.*

I have no words to thank and express my indebtedness to my patient, kind and helpful family especially my parents for tolerating me during the period of the research.

Certification

We certify that this thesis titled "***Theoretical and Experimental Study of the Effect Baffle Geometry and Nanofluid on Performance of Shell-U-Tube Heat Exchanger***" Which is being submitted by **ENG. Murtadha Saeed Mohammed** was prepared under our supervision at the Basrah Engineering Technical College in partial fulfillment of requirements for the degree Master of Science in Thermal Technical Engineering.

Signature:

Name: **Prof. Dr. Sadoun F. Dakhil**

Date: / / 2017

Signature:

Name: **Assist. Prof. Dr. Ahmmad k. Mohammed**

Date: / / 2017

In view of the available recommendation, I forward this thesis for debate by Examining Committee.

Signature:

Name: **Assist. Prof. Dr. Adnan A. Ateeq**

Date: / / 2017

Examining Committee's Report

We certify that we have read this thesis titled **"*Theoretical and Experimental Study of the Effect Baffle Geometry and Nanofluid on Performance of Shell-U-Tube Heat Exchanger*"** which is being submitted by **Murtadha Saeed Mohammed** and as examining committee, examined the student in its contents. In our opinion, the thesis is adequate for the degree Master of Science in Thermal Technical Engineering.

Signature:

Name: **Prof. Dr. Abdul Muhsin A. Rageb**

(Chairman)

Signature:

Name: **Assist. Prof. Dr. Abdulwadood S. Shihab**

(Member)

Signature:

Name: **Dr. Mohammed A. Abdulwahid**

(Member)

Signature:

Name**: Prof. Dr. Sadoun F. Dakhil**

(Supervisor)

Signature:

Name: **Assist. Prof. Dr. Ahmed K. Mohammed**

(Supervisor)

Approval of the College of Engineering Technical

Signature:

Name: **Assist. Prof. Dr. Adnan A. Ateeq**

(Dean of Basrah Engineering Technical College)

Abstract

In this study, experimental and numerical investigations of the cylindrical three dimensional of laminar fluid flow and heat transfer in shell-and-tube heat exchanger, with baffles and Al_2O_3 nanofluid are used. The thermo-hydraulic performance of heat exchangers is predicted with finite volume method by CFD simulations using ANSYS 15.0.1 software. Shell-and-tube heat exchanger is consisting of one pass of warm water flow on the shell side and two passes single tube of cold water. The annular baffles are inserted in inner surface on the shell side, and on the facing distances from the outer surface of the tube. Baffles are inserted with staggered position to achieve good fluid circulation. The tube heat exchanger with baffles at different design style of angle inclination baffles (45º, 0º, -45º) and without baffles with Reynolds number ranging from 100 to 2000 were studied.

The main objective of this work is to identify the effect of several parameters such as: inclination angle of baffles, number of baffles, the height of baffles, hydraulic diameter of tube and volume concentrations of nanofluid on the heat exchanger performance. These parameters are investigated on the thermal performances as the average Nusselt number and effectiveness. The hydrodynamic parameters include analyzing the pressure drop and average friction factor are investigated.

The theoretical results show the high effect of baffles angles on the heat exchanger performance at high Reynolds number. Maximum heat transfer from the hot fluid occurs at baffle with Re_{sh}=2000 , α=0º, Nb=8, and

Bh=30mm with percentage increase in heat transfer rate 15.402% comparing with case without baffles. For nanofluid enhancement of the overall heat transfer coefficient 6.73% by using Al_2O_3-water nanofluid at 10 % volume concentration and Re_t=2000 comparing with base fluid which is due to the higher fluid thermal conductivity. Additionally, the increase in the number of baffles led to a high improvement in the effectiveness, which reached up to 7.94% in case of Nb=8 at Re_{sh}=2000 compared with case Nb=3.

The experimental part includes analyzing the thermal performance for laminar flow of U-tube heat exchanger unit. The effect of Re_{sh} and inclination angle of baffles are studied. The experimental results show that the increase in the inlet hot volume flow rate led to increasing the heat transfer rate. Also, the volume flow rate for shell side played a major role in effectiveness. Furthermore, it can be concluded that 0° baffle inclination angle gives the best performance compared to +45° and -45° inclination angles. All the experimental results were compared with theoretical results which analysis for the model and good agreement is obtained.

Contents

Subject	*Page*
Acknowledgments	I
Certification	II
Examining Committee's Report	III
Abstract	IV
Contents	VI
Nomenclatures	X
Chapter One : Introduction	
1.1 Background	2
1.2.1 Heat Exchanger Classification	2
1.2.2 Applications of Heat exchangers	4
1.3 Tubular heat exchanger	5
1.4 Fundamentals of Nanofluids	7
1.5.1 Numerical simulation	8
1.5.2 Modelling U-tube heat exchanger using CFD	9
1.5.3 Finite volume method	9
1.6 Experimental methods	10
1.7 Problem Statement	11
1.8 Objective of the research	11
1.9 Outlines of the thesis	12
Chapter Two : Literature Review	
2.1 General	15
2.1.1 Traditional fluid	15

2.1.2 Nanofluid	21
2.2 Summary	24
Chapter Three : Theoretical Analysis	
3.1 Introduction	27
3.2 Problem description	27
3.3 Governing equations	29
3.4 Boundary Conditions	30
3.5 Hydrodynamic parameters	32
3-6. Thermal parameters	33
3.7 Effectiveness	36
3.7 Thermophysical Properties of Nanofluid	38
3.8.1 Finite Volume Method	41
3.8.2 The Computational Grid	43
3. 8.3 Finite Volume Formulation of the Governing Equations	45
3.9 Solution procedures	55
3.9.1 Segregated solution algorithm	56
3.9.2 SIMPLE algorithm	56
3.9.3 Staggered grid	57
3.10 Solving by FLUENT software	57
3.10.1 Geometry creation	58
3.10.2 Mesh construction	58
3.10.3 Specifying zones types	60
3.10.3.1 Continuum specification	60
3.10.3.2 Boundary conditions	60
3.10.4 Physical properties model	61

3.10.5 Initial conditions	61
3.10.6 Under – Relaxation factors	61
3.10.7 Measure of Convergence	62
CHAPTER FOUR: Experimental Analysis	
4.1 Introduction	64
4.2 Experimental facilities	64
4.3 Main Components and Instrumentations	67
4.3.1 Test Rig Components	67
4.3.2 Measuring Instruments	71
4.4 Experimental procedures	73
4.5 Experimental Calculations	74
Chapter Five : Results and Discussion	
5.1 Introduction	76
5.2 Grid independence	77
5.3 Validation of numerical model	77
5.4 Numerical analysis	78
5.4.1. Hydrodynamic characteristics with pure fluid	78
5.4.2. Thermal characteristics with pure fluid	79
5.5 Performance analysis	80
5.5.1 Hydrodynamic Performance	80
5.5.2 Thermal Performance	82
5.5.2.1 Effect of inclination Angle of baffles	82
5.5.2.2 Effect of baffles height	85
5.5.2.3 Effect of baffles Number	88

5.5.2.4 Effect of tube diameter	91
5.5.2.5 Effect of nanofluid	93
5.6 Experimental analysis	96
5.7 Validation of the present model with experimental results	97
Chapter Six: Conclusions and Recommendations	
6.1 General	127
6.2 Conclusions	127
6.3 Recommendations	129
References	**132**
Appendices	
Appendix. A: Calibration of thermocouple	A1
Appendix. B: Calibration of rotameter	B1
Appendix. C: Submitted paper from the thesis 1	C1
Appendix. D: Submitted paper from the thesis 2	D1
Appendix. E: Submitted paper from the thesis 3	E1
Appendix. F: Submitted paper from the thesis 4	F1

Nomenclatures List

Symbols		
Symbol	***Description***	***SI Units***
A_c	cross section area	m²
Bh	height of baffle	m
b_f	Base fluid	-
Cp	constant pressure specific heat	kJ/kg. K
D_i	inner diameter of shell	m
d_o	outer diameter of tube	m
d_i	inner diameter of tube	m
D_h	hydraulic diameter of shell	m
d_h	hydraulic diameter of tube	m
h	heat transfer coefficient	W/K.m²
k	Thermal conductivity	W/m .K
LMTD	logarithm mean temperature difference	K
L_t	Tube length	m
Nu_{sh}	Nusselt number for shell	-
Nu_t	Nusselt number for tube	-
NTU	Number of transfer unit	-
P	Pressure	Pa
Per	Perimeter	m
m	Mass	kg
$\dot{m}$	Mass Flow rate	kg/s

n_f	Nanofluid	-
Nb	Number of baffle	-
$\dot{Q}$	Heat Transfer Rate	kW
Re_{sh}	Reynolds number for shell side	-
Re_t	Reynolds number for tube side	-
STHE	Shell-and-tube heat exchanger	-
S	Distance between center tube	m
T_{in}	Inlet temperature	K
T_{out}	Outlet temperature	K
U	Overall heat transfer coefficient	W/K.m²
$\dot{V}$	Volumetric flow rate	m^3/s

Greek Symbols

Symbol	***Description***	***SI Units***
Δ	Difference	-
ε	Effectiveness	-
ϕ	particle volume fraction %	-
ρ	Density	kg/m^3
μ	Dynamic viscosity	N·s/m²
α	angle of baffle	Degrees
δ_t	Tube thickness	m
$\delta_{b,sh}$	Baffle thickness of shell	m
$\delta_{b,t}$	Baffle thickness of tube	m

Subscripts

Symbol	***Description***
sh	Shell

t	Tube
c	Cold
h	Hot
i	Inlet
o	Outlet

Abbreviations

Symbol	***Definition***
CFD	Computational Fluid Dynamics
C.V	Control Volume
FEM	Finite element method
FVM	Finite volumes method
FDM	Finite difference method
HTSU	Heat transfer service unit
SIMPLE	Semi-implicit method for pressure–linked equations
SIMPLER	Semi-Implicit Method for Pressure-Linked Equations Revised
PDE	Partial differential equation
PVC	poly vinyl chloride

CHAPTER ONE

INTRODUCTION

Chapter one
Introduction

1.1 Background

Heat exchangers are one of the most used equipment in the process industries. Heat exchangers are used for transferring heat between two process streams [1]. One can realize their usage that any process which involves cooling, heating, condensation, boiling or evaporation will require a heat exchanger for these purposes. Process fluids, usually are heated or cooled before the process or undergo a phase change. Different heat exchangers are named according to their applications. For example, heat exchangers being used to condense are known as condensers, similarly, heat exchangers for boiling purposes are called boilers.

The Performance and efficiency of heat exchangers are measured through the amount of heat transfer using least area of heat transfer and pressure drop. A better presentation of its efficiency is done by calculating overall heat transfer coefficient. Pressure drop and area required for a certain amount of heat transfer, provides an insight about the capital cost and power requirements (Running cost) of a heat exchanger. Usually, there is lots of literature and theories to design a heat exchanger according to the requirements. A good design is referred to a heat exchanger with the least possible area and pressure drop to fulfill the heat transfer requirements [2].

1.2.1 Heat Exchanger Classification

At heat exchangers are available in many configurations. heat exchangers can be classified depending upon their application, process fluids, and mode of heat transfer and flow.

Heat exchangers can transfer heat through direct contact with the fluid or through indirect ways. They can also be classified on the basis of shell and tube passes, types of baffles, the arrangement of tubes (triangular, square etc.) and smooth or baffled surfaces. These are also classified through flow arrangements as fluids can be flowing in the same direction (parallel), opposite to each other (counter flow) and normal to each other (cross flow). The selection of a particular heat exchanger configuration depends on several factors. These factors may include, the area requirements, maintenance, flow rates, and fluid phase. Classification of heat exchangers are representing in flow chart below [3].

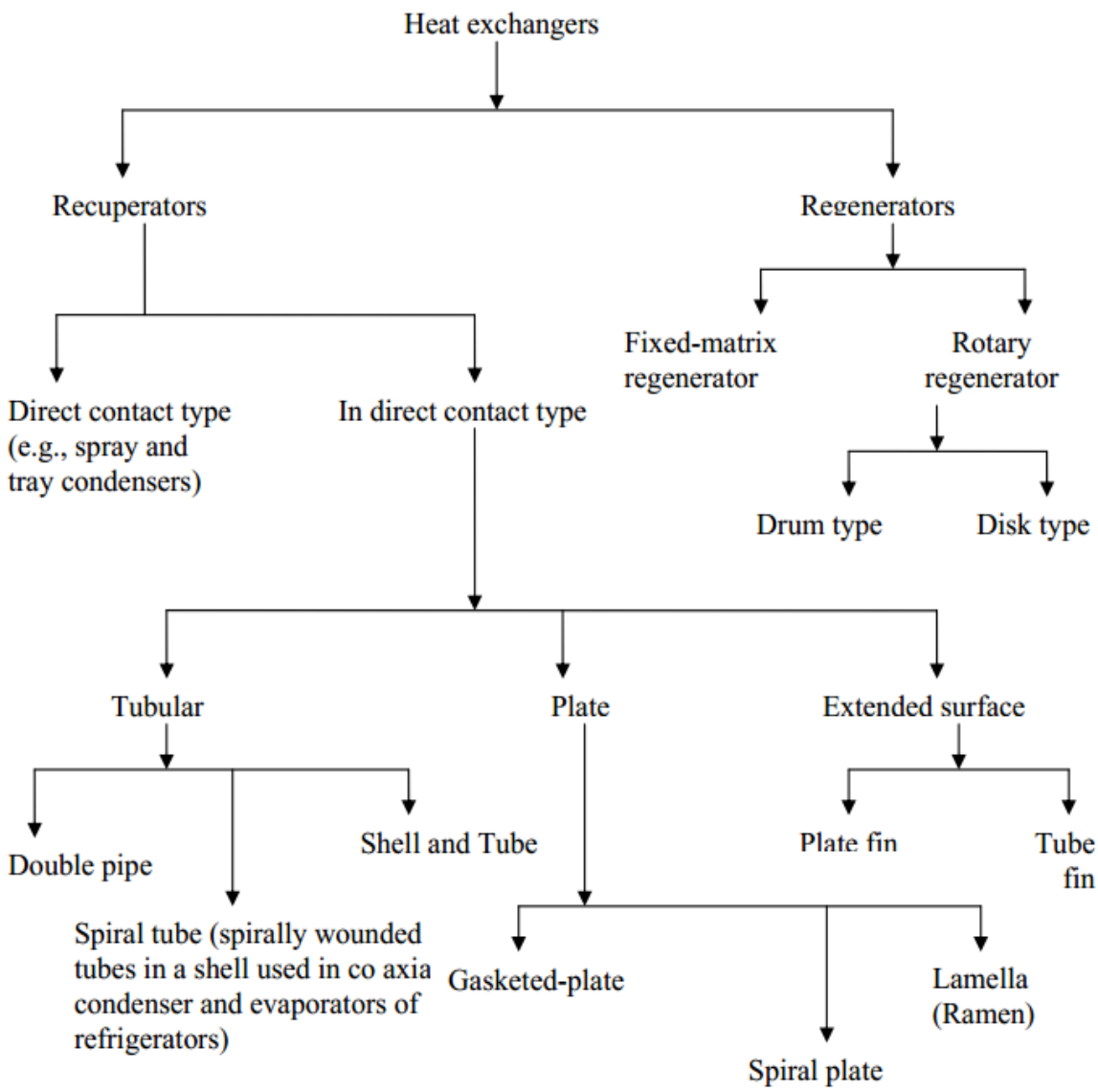

1.2.2 Applications of Heat exchangers

Applications of heat exchangers is a very vast topic and would require a separate thorough study to cover each aspect. Among the common applications are their use in the process industry, mechanical types of equipment industry and home appliances. Heat exchangers can be employed for heating district systems, largely being used now a day. Air conditioners and refrigerators also install the heat exchangers to condense or evaporate the fluid. Moreover, these are also being used in milk processing units for the sake of pasteurization. The more detailed in applications of the heat exchangers can be found in Table (1.1) different industries [4].

Table 1.1: Heat Exchanger Applications in Different Industries

Industries	Applications
Food and Beverages	Ovens, cookers, food processing and pre-heating, milk pasteurization, beer cooling and pasteurization, juices and syrup pasteurization, cooling or chilling the final product to desired temperatures.
Petroleum	Brine cooling, crude oil pre-heating, crude oil heat treatment, Fluid interchanger cooling, acid gas condenser.
Hydrocarbon processing	Preheating of methanol, liquid hydrocarbon product cooling, feed pre-heaters, recovery or removal of carbon dioxide, production of ammonia.
Polymer	Production of polypropylene, reactor jacket cooling for the production of polyvinyl chloride.

Pharmaceutical	Purification of water and steam, for point of use cooling on water for injection ring.
Automotive	Pickling, rinsing, priming, painting.
Power	Cooling circuit, radiators, oil coolers, air conditioners and heaters, energy recovery.
Marine	Marine cooling systems, Fresh water distiller, Diesel fuel pre-heating, central cooling, Cooling of lubrication oil.

1.3 Tubular heat exchanger

The heat exchange between flowing fluids is one of the important processes in engineering applications. It can be classified depending upon their application, process fluids, and mode of heat transfer and flow. One important type of tubular heat exchangers is called shell and tube which is widely used. Shell-and-tube heat exchangers (STHE) are extensively used in petroleum refining, chemical engineering, and power generation, among others [5].

The basic principle of operation is very simple as flows of two fluids with different temperature brought into close contact but prevented from mixing by a physical barrier. Then the temperature between two fluids tends to equalize by transfer of heat through the tube wall. The fluids can be either liquids or gases in either the shell or the tube side. In order to transfer heat efficiently, a large heat transfer area should be used, leading to the use of many tubes. In this way, waste heat can be put to use. This is an efficient way to conserve energy.

They have larger heat transfer surface area to volume ratios than the most of common types of heat exchangers, and they are manufactured easily for a large variety of sizes and flow configurations. They can operate at high pressures, and their construction facilitates disassembly for periodic maintenance and cleaning [6]. The shell and tube heat exchangers consist of a bundle of tubes enclosed within a cylindrical shell. One fluid flows through the tubes and a second fluid flows within the space between the tubes and the shell. Typical Shell-and-Tube heat exchanger is shown in Figure 1.1.

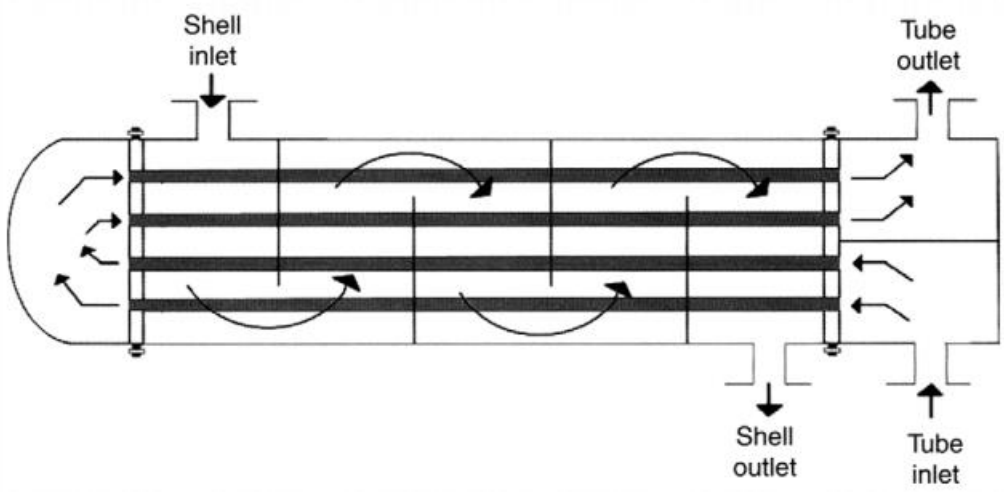

Fig 1.1 Shell and tube heat exchanger

There are several designs of shell and tube heat exchanger. Even though, the basic principle is still the same. The tubes may be straight or bent in the shape of a U, called U–tube heat exchanger. This U- tube type typically uses in nuclear power plants. The heat exchanger may be used to boil water recycled from a surface condenser into steam to drive a turbine to produce power. Most shell and tube heat exchangers are 1, 2, or 4 pass designs on the tube side. This refers to the number of times the fluid in the tubes passes through the fluid in the shell. In a single pass heat exchanger, the fluid goes in one end of each tube

and out the other [7]. Many factors have to be considered in heat exchanger selection. Generally, selection and sizing are related each other; changing in heat exchanger components, such as tube pattern and baffle, would affect the calculation.

1.4 Fundamentals of Nanofluids

With the recent enhancements in nanotechnology, the production of particles with sizes on the order of nanometers (nanoparticles) can be achieved with relative ease. As a consequence, the idea of suspending these nanoparticles in a base liquid for enhancing the thermal conductivity has been suggested recently. Such suspension of nanoparticles in a base fluid is well-known as Nanofluids. Due to their small size, nanoparticles liquefied easily inside the base fluid, and as a consequence, clogging of channels and erosion in channel walls are no longer a problem [8].

The Nanofluids presented great potential improving the heat transfer process. Suspended ultrafine particles remarkably increase the thermal conductivity of the Nanofluids. The volume fraction, shape, dimensions and properties of the nanoparticles affect the thermal conductivity of Nanofluids [9].

Increase in the thermal conductivity of the working fluid improves the efficiency of the associated heat transfer process. When forced convection in tubes is considered, it is expected that heat transfer coefficient enhancement obtained by using a Nanofluids is equal to the enhancement in thermal conductivity of the Nanofluids. However, research about the convective heat transfer of Nanofluids indicated that the enhancement of heat transfer coefficient exceeds the thermal conductivity enhancement of Nanofluids [10].

1.5.1 Numerical simulation

The numerical analysis approaches are very reliable and widely used in literature compared with other approaches. The importance of numerical simulation techniques is due to its reliability and ability to investigate and calculate the distribution and average values of any parameter in any location even in complex geometries. It is easily to repeat the solution and study the effect of any parameter for any range of values [11].

It is found from literature that, there is an increase in using of numerical techniques to study shell and tube in the present years especially using a CFD packages which include great abilities to study the flow and heat transfer problems and include a good means to show the results. One of the numerical methods which is widely used in the present years is the finite volume method. In which the governing equations are integrate about the control volume, yielding discrete equations.

From the above presentation for the different analysis approaches used to study the shell and tube, the analytical approaches are not widely used due to its less accuracy and low abilities to study the complex geometries and complex problems. Also the use of experimental approaches is very limited since it needs high technology apparatus. Compared with the two previous approaches the numerical methods are widely used to study the shell and tube and its applications devices and its using is increased in the present years especially using CFD software.

Computational Fluid Dynamics or CFD is the analysis of systems involving fluid flow, heat transfer and associated phenomena such as chemical reactions by means of computer based simulation. The technique is very powerful to perform the millions of calculations required to simulate the interaction of fluids and gases with complex surfaces used in engineering [12].

1.5.2 Modelling U-tube heat exchanger using CFD

The numerical methods are used to solve the physical model that can't be solved analytically. The main methods which are used in the numerical analysis are: finite difference (FDM), finite element (FEM) and finite volume (FVM). The finite volume method FVM augments the simplest of finite difference and accuracy of finite element. The Fluent software package uses the finite volume method [13].

The Fluent code is used to solve case of U-tube heat exchanger depending on the type of flow. It can be used to solve two and three dimensional geometries for both steady and transient flows, each of these models has its own continuity, momentum and energy equations and the need for using each of them depends on the type of flow.

In this study the laminar flow, three-dimensional steady state single phase flow in the horizontal U-tube heat exchanger is investigated. Several variables are studied for theoretical model such as: angle baffles of inclination, baffles height, number of baffles, hydraulic diameter of tube and using nanofluids for different concentrations all with different Reynolds numbers. The code involves several types of boundary conditions and a proper boundary conditions has been chosen for the shell and tube inlet and outlet (i.e. velocity inlet and pressure outlet respectively). The Fluent code uses finite volume method in solving the governing equations which are described in the next section.

1.5.3 Finite volume method

Finite volume methods are a class of discretization schemes that have proven highly successful in approximating the solution of a wide variety of conservation law systems. They are extensively used in fluid mechanics,

meteorology, electromagnetics, semi-conductor device simulation, models of biological processes and many other engineering areas governed by conservative systems that can be written in integral control volume form [14].

The finite volume method is a numerical method for solving partial differential equations that calculate the values of the conserved variables averaged across the volume. It was originally developed as a special finite difference formulation. The numerical algorithm consists of the three steps as: Grid generation, Discretisation and Solution of the algebraic equations [15].

1.6 Experimental method

The experimental techniques are used to measure and investigate the heat transfer in shell and tube. The experiments give more valid results compared with numerical approach but it includes many disadvantages and difficulties. Also in most of the experimental studies available in literature the distribution of temperature, pressure and other parameters did not measure along shell and tube since the values of these parameters are measured in the inlet and outlet of the shell and tube due to introducing the measuring devices inside shell and tube (with small diameter) lead to disturb the flow and cause many problems.

Experimental setup has been built with shell and tube one pass shell and two passes single tube heat exchanger with circle baffles. Design consideration are operating temperature, effective temperature difference, inclination angle of baffles and fluid velocity.

A new type of baffle, called the circle baffle, provides further improvement. They investigated the flow field patterns produced by such circle baffle geometry with different circler angles [16].

1.7 Problem Statement

Heat transfer is considered as transfer of thermal energy from physical body to another. Heat transfer is the most important parameter to be measured as the performance and efficiency of the shell and tube heat exchanger. By using CFD simulation software, it can be reducing the time and operation cost compared by experimental in order to measure the optimum parameter and the behavior of this type of heat exchanger.

1.8 Objective of the research

In this study an investigation of three dimensionless laminar flow along a U-tube heat exchanger developed with pure fluid and Nanofluids. Developing flow and conjugate heat transfer in a U-tube heat exchanger to investigate its overall performance (thermal and hydrodynamic) and studying the role of the affecting parameters to construct a procedure for design this U-tube heat exchanger. The specific objectives are following:

- To investigate the flow and heat transfer behavior in the U-tube heat exchanger at different number of baffles (Nb) (3, 5, and 8), different baffle height (Bh) (10, 20 and 30mm) and hydraulic diameter of tube (d_h) (16.91,19.9 and 26.04mm) on the heat transfer and the flow characteristics.
- Also the work of this thesis include the solve of the problem of the pressure drop associated with increasing the thermal performance by changing the inclination angle of baffles (α) (+45º, 0º, -45º and without baffles).
- To study the effects of nanofluids of Al_2O_3-H_2O nanoparticles volume fraction (Φ) (2, 5 and10%) at constant nanoparticles diameter 25 nm on the heat transfer and the flow characteristics.
- To analyze the heat transfer in U-tube heat exchanger experimentally and comparing the experimental results with simulation results.

1.9 Outlines of the thesis

The present thesis includes experimental and numerically modeling of the U-tube heat exchanger by using CFD software FLUENT 15.0.

The objectives, methodology and results of the research work are presented as follows:

Chapter 1 the introduction and objectives of the present thesis.

Chapter 2 describes the literature review for shell and tube heat exchangers.

Chapter 3 includes a detailed description of the mathematical model developed in the present thesis. And the numerical model used to solve the governing equations. Also include a description of grid generation and accuracy criteria used in addition to the boundary conditions used.

Chapter 4 includes a detailed description of the experimental work.

Chapter 5 results obtained in this thesis are presented and discussed.

Chapter 6 summarizes the conclusions done and recommendations for future works that can be done to further development of study the U-tube heat exchanger.

CHAPTER TWO

LITERATURE REVIEW

Chapter Two

Literature Review

2.1 Introduction

Due to the unique features of the flow and heat transfer in shell and tube, these heat exchangers have received much attention in the research works. Through the past decade the flow and heat transfer in shell and tube has been studied experimentally, numerically, and analytically and in now days the researches are focused on the applications of heat exchanger.

This chapter includes a review of the research publicized in this area. The reviewed literatures are divided into two main sections:

1- Researches include study of the fluid flow and heat transfer in shell and tube heat exchanger with traditional fluid.

2- Researches include study of the shell and tube heat exchangers with Nanofluids.

2.1.1 Pure fluid

In (2003), Vukic.M. et al. [17], carried out an experiment study on heat and flow for turbulent flow in STHE to show the effect of number of segmental baffles, baffle cut size on effectiveness of the shell and tube heat exchanger. They used heat exchanger with one pass shell and two passes 24tubes (U-tube) in shell. Three packages of segmental baffle cuts of 22, 27 and 32% were located in the shell. The results showed the heat exchange depends on the shell side geometry. The heat efficiency is decreasing with increasing of baffle cut from 22% to 32%. Also, the heat efficiency increase with one baffle with cut of 26% was 6.9% and for baffle cut of 32% was 5.6%, comparing with case without baffles in a shell.

In (2007), Cucumo.M. et al. [18], performed a numerical study to investigate the influence of the baffles type on the pressure drop and the heat transfer of shell and tube heat exchanger. They proposed a three dimensional model of shell and tube heat exchanger with different type of baffles, segmental and pseudo-helical. Exchangers with pseudo-helical baffles inclined by 7°, 20°, 30° and 40° are analyzed. In their model the mass, momentum and energy equations were solved numerically using software FLEUNT under laminar flow case. They studied the effects of baffles type and angles of inclination. Their results show that, the optimum baffles helix angle is 40°, although marked benefits are already obtained at an angle of 30°. Also, the use of a "helical baffles" heat exchanger with inclination angle less than 7° is not recommended either, since the pressure drops would be too high. They used correlations to compared with the results provided by the CFD analysis, present a deviation variable from 3.10 % to 3.70 % on the film heat transfer coefficient, and variable between 4.10% and 9.37 % on pressure drops.

In (2008), Yong-Gang et al. [19], studied a three dimensional numerical simulations for laminar, transitional and turbulent flow heat exchangers with different baffle inclination angles are performed to reveal the effects of baffle inclination angle on the heat transfer and pressure drop characteristic. They observed that the average Nusselt number increases with the increase of the baffle inclination angle α when $\alpha<30^{o}$. Whereas, the average Nusselt number decreases with the increase of the baffle inclination angle when $\alpha>30^{o}$. For $\alpha>40^{o}$, the effect of α on pressure drop is very small. Compared to the segmental heat exchangers, the heat exchangers with continual helical baffles have higher heat transfer coefficients to the same pressure drop Additionally, they found that with in the Reynolds number studied for the shell side, the

optimal baffle inclination angle is about 45º, with which the integrated heat transfer and pressure drop performance is the best.

In (2009), Ender.O and Ilker.T [20], investigated numerically three-dimensional steady state heat transfer and pressure drop for turbulent flow in shell-and-tube heat exchanger. The governing equations are solved for two types of k-ε turbulence model, standard and realizable. They solved Navier-Stokes equations and the energy equation with appropriate boundary conditions by using finite volume based CFD software FLUENT. Their study focused mainly on the effects of baffle spacing and baffle cut on heat transfer and pressure drop of the exchangers. Their results show that the differences between Bell–Delaware method and CFD predictions of the total heat transfer rate are below 2% for most of the cases. They also observed that the k–realizable turbulence model by comparing with Bell–Delaware results as the best simulation approach.

In (2012), Rajagapal.T and Srikanth.G [21], carried out the impacts of various baffle inclination angles on fluid flow and the heat transfer characteristics for turbulent flow of a STHE for three different baffle inclination angles namely 0°, 10°, and 20°. The simulation results for various tubular heat exchangers, one with segmental baffles perpendicular to fluid flow and two with segmental baffles inclined to the direction of fluid flow were compared for their performance. The results were concluded that the pressure drop is decreased by 4 %, for heat exchanger with 10° baffle inclination angle and by 16 % for heat exchanger with 20° baffle inclination compared to 0° baffle inclination heat exchanger. Also, the results were concluded that tubular heat exchanger with 20° baffle inclination angle better performance compared to 10° and 0° inclination angles.

In (2012), Usman Ur Rehman [22], studied the heat transfer and flow distribution in a shell and tube heat exchanger and compared them with the experimental results. The model showed an average error of around 20% in the heat transfer and the pressure difference. The study showed that the symmetry of the plane assumption worked well for the length of the heat exchanger but not in the outlet and inlet regions. The model could be improved by using Reynolds Stress models instead of k-ε models. The heat transfer was found to be on the lower side as there was not much interaction between the fluids. The design could be improved by improving the cross flow regions instead of the parallel flow. Thus the design can be modified to achieve the better heat transfer in two ways. Either, the shell diameter is reduced or tube spacing can be increased.

In (2012), Santosh K. Hulloli [23], studied fluid flow and heat transfer characteristics in shell and tube heat exchanger with different designs of baffles and semicircular turbulators. They proposed a three- dimensional model for turbulent flow of STHX with one shell pass and one tub pass. In their model the governing equation as mass, momentum and energy equations were solved numerically using software FLEUNT under five case of different baffles and turbulators. Their results showed that, the Enhanced heat transfer coefficient of 3.01% for baffles model, 7.1% for with baffles and turbulator model, and 6.5% for without sealer baffles and without turbulator model, 6.2% for without sealer with oval shaped holes on the baffles and without turbulator model compare to the plain model. Additionally, he found that The pressure drop increased more of about 25.07% for with baffles and turbulators compare with the plain model. Also, the fifth case is the best and safe design compare to all the cases.

In (2012), Rahim. A and Jameel [24], investigate the impacts of various baffle inclination angles on fluid flow and the heat transfer characteristics for turbulent flow of a shell-and-tube heat exchanger for three different baffle inclination angles namely 0°, 10° and 20°. The shell side of a small shell-and-tube heat exchanger is modeled with sufficient detail to resolve the flow and temperature fields.

- For the given geometry the mass flow rate must be below 2 kg/s, if it is increased beyond 2kg/s the pressure drop increases rapidly with little variation in outlet temperature.
- The pressure drop is decreased by 4 %, for heat exchanger with 10° baffle inclination angle and by 16 %, for heat exchanger with 20° baffle inclination angle.
- The maximum baffle inclination angle can be 20°, if the angle is beyond 20°, the center row of tubes is not supported. Hence the baffle cannot be used effectively.
- Hence it can be concluded tubular heat exchanger with 20° baffle inclination angle results in better performance compared to 10° and 0° inclination angles.

In (2013), Vyas. A and M.P. Sharma [25], investigated experimentally and numerically the heat transfer in Tubular Heat Exchangers, use of baffle has significant impact on tubular heat exchanger, numerical simulation of tubular heat exchanger is conducted to study the effect of baffle and its different orientations. They showed that the output results coming out from heat exchanger having baffles situated at outer pipe are more efficient from heat exchanger without baffles, the results of heat transfer coefficient coming out by use of 30º baffles are more efficient than 0ºbaffles. As the angle of inclination increases, the heat transfer rate of heat exchanger also increases. Use of helical baffles in heat exchanger reduces shell side pressure drop. For

the helical baffle heat exchangers, the ratios of heat transfer coefficient to pressure drop are higher than those of a conventional segmental heat exchanger. From the Numerical & experimental results it is confirmed that the performance of tubular heat exchanger can be improved by helical baffles instead of conventional segmental baffles, it can be concluded that proper baffle inclination angle will provide an optimal performance of heat exchangers.

In (2013), Shinde S.S. and Hadgekar H.p [26], presented a three-dimensional numerical simulation for shell and tube heat exchangers. They studied the effect of inclination angles on fluid flow and heat transfer analysis. Six different inclination angles were analyzed in single continuous helix style: 20º, 25º, 30º, 35º, 40º and 45º. The Reynolds number was simulated at the range (200-6000). The results showed that with constant flow rate and Reynolds number and varying helix angle, the heat transfer coefficient & pressure drop decreased slowly for helix angle less than 40 degrees. Also, they observed that the optimum helix inclination angle depended on the Reynolds number of the working fluid on the shell side of heat exchanger.

In (2014), Ajithkumar M.S et al [27], presented a three-dimensional numerical simulations analysis for turbulent flow of a single pass parallel flow Shell and Tube Heat Exchanger (STHX) with different baffle inclinations and type. They studied the effect of three different baffle inclinations namely 0°, 10°, and 20° on fluid flow and temperature field inside the shell side. The basic geometry of shell and tube heat exchanger has made by CATIA V5 and meshing has completed by using HYPER MESH (11.0). They used ANSYS-FLUENT (6.3) for studied the flow and temperature fields inside the shell. The governing equations used in their numerical simulations were momentum equations, energy equation in addition to the mass conservation equation. The numerical results showed that by comparing both segmental and helical baffle

STHE, the helical baffle with 0º inclination results were better performance than segmental baffle with 10º baffle inclination, i.e. minimum pressure drop with maximum heat transfer rate. Also, they observed that at 0° baffle inclination angle helical baffle STHE results are better performance compared to 10° and 0° inclination angles, i. e., with less pressure drop, maximum shell outlet temperature and. higher heat transfer rate.

In (2014), Arjun K.S. and Gopu K.B. [28], presented a numerical simulation to study pressure drop and heat transfer for turbulent flow in shell-and-tube heat exchanger with varying helix angle from 0º to 20º. They proposed a three-dimensional model of 7 tubes of outer diameter 20 mm and a 600 mm long shell of inner diameter 90 mm. The simulation show how the pressure vary in shell due to different helix angle and flow rate. They solved the governing equations numerically using software CFX for turbulent flows regimes. From their results, they found that the pressure decline inside the shell is decreased with the increase in baffle inclination angle. Also, they observed that unsupported behavior of center row of tubes makes the baffle use ineffective when the baffle angle is above 20º. Hence, the helix baffle inclination angle of 20º makes the best performance of shell and tube heat exchanger.

In (2015), Liu J.J et al [29], presented a numerical simulation to study the heat transfer and flow characteristics of shell-and-tube heat exchangers with rod-baffle. They focused improve the thermo-hydraulic performance in longitudinal flow heat exchangers and to obtain an understanding of the physical behavior of thermal and fluid flow in the RBHXsSCT. They proposed three-dimensional model for different heat exchangers Rod-baffle heat exchanger with plain tubes and with spirally corrugated tubes. The Reynolds number simulated between the ranges (6000 to 18,000). Their analysis carried out using the commercial software ICEM CFD14.0 on the

basis of the 3D geometry created in a commercial CAD program and a Gambit as preprocessor. His results showed the pressure drop in RBHX is 1.21, 1.16, 1.12, and 1.08 times than that in RBHXsSCT with one-start, two-start, three-start, and four-start spirally corrugated tubes, respectively. also, that the Nusselt number in RBHXSCT with one-start spirally corrugated tubes can be 1.2 times than that in RBHX when the Reynolds number is 18,000.

In (2016), Amirtharaj.P. et al [30], studied heat and flow for turbulent flow in shell and tube heat exchanger with different design style of baffle. They used CFD analysis for two models of shell and tube heat exchanger, the first with segmental baffles and second with inclined baffles. The Kern method was used to do the mathematical calculation. Results showed high effect of the heat transfer performance of shell and tube heat exchanger with inclined baffles. Also, They compared with both result, inclined baffles heat transfer coefficient is greater (72.5 w/m^2.k) then straight baffle heat transfer co efficient. They compared with both result, inclined baffles pressure drop is less (70 Pascal) than straight baffles pressure drop.

2.1.2 Nanofluid

In (2003), Shahmohammedi.P and Beikihe.H [31], studied the effect of γ-Al_2O_3 nanoparticles on heat transfer rate, baffle spacing and pressure drop for turbulent flow in the shell side of small shell and tube heat exchangers was investigated numerically under turbulent regime. They used γ-Al_2O_3-water nanofluids and pure water in the shell side and the tube side of heat exchangers, respectively. Their results showed that heat transfer and pressure drop were increased with mass flow rate as well as baffle numbers and suitable baffle spacing was 43.4% of the shell diameter. Also, the nanoparticles to the based fluid did not have a significant effect on pressure drop in the shell side. The best heat transfer performance of heat exchangers

was for γ-Al_2O_3-water 1 vol.% and higher nanoparticles concentration was not suitable.

In (2010), Etemad S.Gh and Farajollahi B [32], Studied experimentally the heat transfer performance of the water- Al_2O_3 nanofluid in a shell and tube heat exchanger. Heat transfer characteristics were measured under the turbulent flow condition and with range of nanoparticle concentrations. The results shown that the heat transfer characteristics of nanofluid enhance significantly with increasing Peclet number. They found that the use of a nanofluid with 0.5% nanoparticle volume concentration possesses about 20%, 56%, and 54% higher overall heat transfer coefficient, convective heat transfer coefficient and Nusselt number, respectively. Also there is an optimum for volume concentration in which the nanofluid shows the maximum heat enhancement.

In (2012), Dadui Guerrieri et al. [33], Investigated numerically the effects of the thermophysical properties of the fluids conventional water and ethylene glycol with nanofluids Al_2O_3 and CuO immersed in water and glycol etilenio. Their numerical simulations of shell and tube were presented by using software FLUENT to solve the momentum and energy equations in three-dimension momentum and energy equations. Their theoretical results showed that, the in this case water and ethylene glycol, provided a significant decrease in the dimensioning of the heat exchanger. The nanofluids of high particle concentration have shown higher thermal conductivity. The propylene glycol based nanofluids have low thermal conductivity compared to water based Nanofluids.

In (2012) P.C. Mukeshkumar et al. [34], carried out experimental study of a shell and helically coiled tube heat exchanger using γ-Al_2O_3/ water nanofluid. This study was done by changing the parallel flow configuration

into counter flow configuration under laminar flow regime. They γ-Al_2O_3 / water nanofluid at 0.4% and 0.8% particle volume concentration were prepared by using two step method. Their results show that, the overall heat transfer coefficient of counter flow was 4-8% higher than that of parallel flow at 0.4% nanofluid. The overall heat transfer coefficient was found to be 5-9% higher than that of parallel flow at 0.8% nanofluid.

In (2013) Jaafar Albadr et al. [35], studied experimentally on the forced convective heat transfer and flow characteristics of a nanofluid consisting of water and different volume concentrations of Al_2O_3 nanofluid (0.3–2) %. Their experiment was performed on shell and tube heat exchanger counter flow under turbulent flow conditions are investigated. The Al_2O_3 nanoparticles of about 30 nm diameter are used in the present study. The results show that the heat transfer coefficient of the nanofluid increases with an increase in the mass flow rate, also the heat transfer coefficient increases with the increase of the volume concentration of the Al_2O_3 nanofluid, however increasing the volume concentration cause increase in the viscosity of the nanofluid leading to increase in friction factor.

In (2014) Ramesh R and Dr. R. Vivekananthan. [36] performed a three-dimensional numerical and experimental investigations for thermal performance in shell and tube heat exchanger by using Al_2O_3 nanofluid and Ethylene glycol. Al_2O_3 has been mixed with water as a base fluid to increase the heat transfer rate. The experimental and numerical investigation has to be performed and the results have been compared to validate the performance of the heat Exchanger. Their experimental results show that the heat transfer coefficient increases by increasing the concentration of nanoparticles in nanofluid up to certain level. Also, at 2% volume fraction Nusselt number increases up to 30% for different Reynolds number. As a result, they obtained the increase in heat transfer coefficient due to presence of Al_2O_3 nanoparticles

is much higher than the conventional fluids and hence the shell and tube heat exchanger using nanofluid as a coolant has higher heat transfer rate than the conventional shell and tube heat exchanger.

In (2017), Akshay. K. S, et al [37], carried out the effect of number of tubes, unequal baffle spacing and tube diameter on heat transfer and pressure drop characteristics of a typical shell and tube type heat exchanger. Upon geometrical optimization, they studied the influence of Al_2O_3 nanofluid of 0.5%, 0.75%, 1%, 1.25% and 1.5% concentrations by admitting water along the tubes and Al_2O_3 nanofluid along the shell side. The heat transfers and fluid flow characteristics through the heat exchanger are obtained by solving the governing equations namely continuity, momentum and energy equations using ANSYS CFX 15 CFD code. Their results showed that using of nanofluid resulted increase of both the pressure drop and heat transfer coefficient. Also, they observed that the heat transfer coefficient at 1.25% volume concentration of nanofluid is found to be the optimum value.

2.2 Summary

The literature review has been found many investigations done on shell and tube heat exchanger with baffle both laminar and turbulent flow with pure fluid and Nanofluids. While, some studies were done to investigate the shell and tube with one pass shell and two passes tube both laminar and turbulent flow using pure fluid. Very few studies utilized Nanofluids in shell and U-tube using Nanofluids with baffles. I believe no study done laminar flow in U-tube with annular baffles with different inclination angle, number and height of baffles, under the thermal boundary condition of coupling boundary conditions at walls using Nanofluids.

From the literature we find that so much work had been done to find heat transfer characteristic of shell and tube heat exchanger with constant wall temperature and constant heat flux conditions. Also, by changing the working fluid heat transfer relation were found. But effect of outer boundary wall condition on inner fluid has not been yet predicted properly, as there is no investigation to study the effect of different inclination angle of baffle with coupling boundary conditions between hot water and cold water on performance of shell and U-tube heat exchanger.

CHAPTER THREE

THEORETICAL ANALYSIS

Chapter Three

Theoretical Analysis

3.1 Introduction:

In this chapter the hydrodynamic and thermal characteristics of one shell pass and two passes tube (U-tube heat exchanger) are investigated numerically and the parameters that affect its performance are examined. This investigation done by solving the cylindrical three dimensional developing laminar flow and conjugate heat transfer through the two fluids with and without baffles.

This chapter is divided into two main sections: The first is the mathematical formulation and the second is the numerical analysis as follow:

Part A: Mathematical formulation

This part includes explanation for the mathematical formulation of the present model flow as follow:

1- The geometry of the study is a three-dimensional into cylindrical coordinates of U-tube heat exchanger with baffle.
2- Description of the governing equations with their boundary conditions which govern the flow and heat transfer in U-tube heat exchanger.
3- Definition of the hydrodynamic and thermal parameters which are used to explain the fluids behavior.

3.2 Problem description

The physical model as shown in the schematic figure 3.1 represents the one shell pass and two passes tube with baffles on both inner shell and outer tube sides.

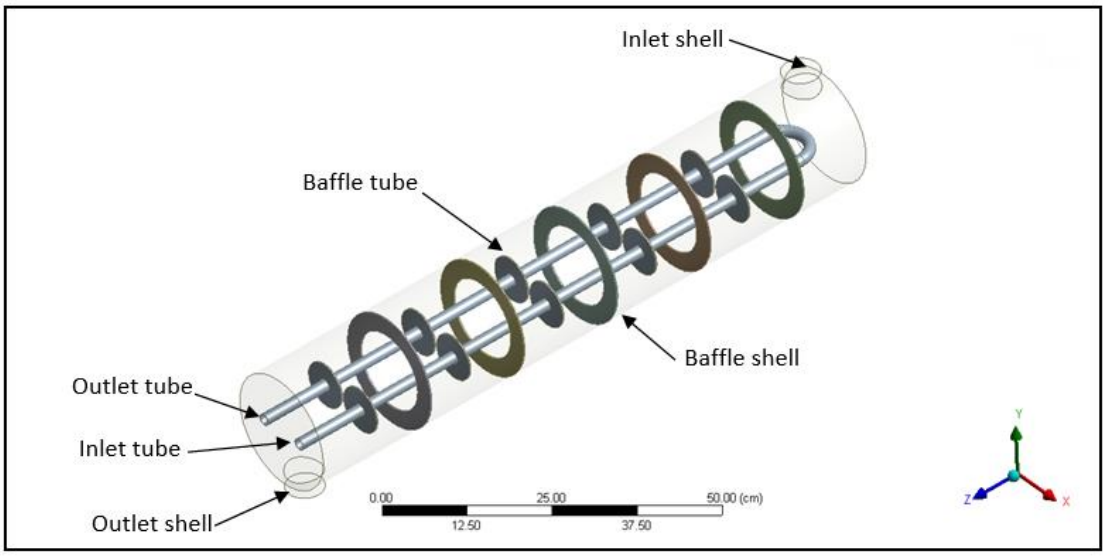

Fig.3.1: Isometric view of arrangement of baffles and tubes of shell and tube heat exchanger with baffle angle (α) 0°, NB 5, Bh= 20mm.

Also due to the geometrical the individual heat exchange unit will be considered as a physical model to represent the complete U-tube heat exchanger and study its flow and heat transfer characteristics. This individual heat exchange unit consists of cylinder and tube for hot and cold fluids and the tube wall separating them, as shown in the fig. 3.2 which represents the heat exchange units for different baffle angle studied in this work (0^0, $+45^0$, -45^0).

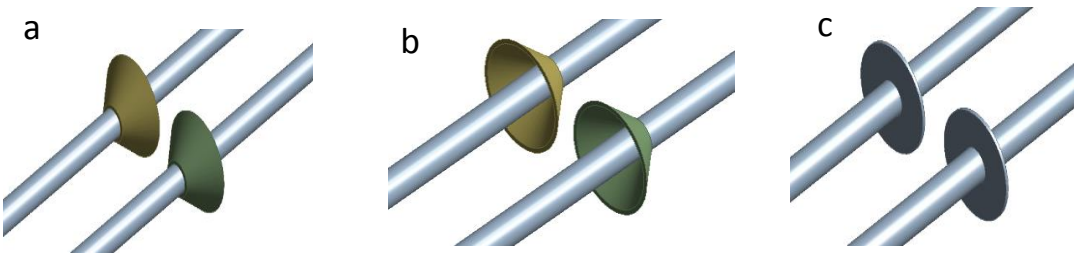

Fig.3.2: The model of the tube baffle angle in degree, Bh=20mm; (a) +45° ; (b) -45° ; (c) 0°.

In completing a CFD analysis of the entire domain of Shell and U-tube, it is necessary to set up the governing equations. For the specific case of heated flow through the tube, the governing equations could be solved with the aid of the following assumptions:

1. Steady state flow.
2. Incompressible fluids with single phase flow.
3. Laminar flow.
4. Negligible radiation and natural convection.
5. Constant properties (for fluids and solids).
6. Viscous dissipation is negligible.

3.3 Governing equations

The problem under consideration concerns the forced convection through the shell and tube heat exchanger. Heat transfer in the heat exchanger unit is a conjugate process combining heat conduction in the solid wall and convection in the working fluids. The system of equations governs the present model consists of continuity, momentum and energy equations which are written bellow [38], [39]:

The explanation of these equations and the boundary conditions used with the cylindrical coordinates are presented as the following:

(i) Continuity equation

$$\frac{\partial u_r}{\partial r} + \frac{u_r}{r} + \frac{1}{r}\frac{\partial u_\theta}{\partial \theta} + \frac{\partial u_z}{\partial z} = 0 \tag{3.1}$$

(ii) Momentum equation

θ-direction

$$\rho(u_r \frac{\partial u_\theta}{\partial r} + \frac{u_\theta}{r}\frac{\partial u_\theta}{\partial \theta} + \frac{u_r u_\theta}{r} + u_z \frac{\partial u_\theta}{\partial z}) = -\frac{1}{r}\frac{\partial P}{\partial \theta} + \mu(\frac{\partial^2 u_\theta}{\partial r^2} + \frac{1}{r}\frac{\partial u_\theta}{\partial r} - \frac{u_\theta}{r^2} + \\ + \frac{1}{r^2}\frac{\partial^2 u_\theta}{\partial \theta^2} + \frac{2}{r^2}\frac{\partial u_r}{\partial \theta} + \frac{\partial^2 u_\theta}{\partial z^2}) \tag{3.2}$$

r-direction

$$\rho(u_r \frac{\partial u_r}{\partial r} + \frac{u_\theta}{r}\frac{\partial u_r}{\partial \theta} - \frac{u^2{}_\theta}{r} + u_z \frac{\partial u_r}{\partial z}) = -\frac{\partial P}{\partial r} + \mu(\frac{\partial^2 u_r}{\partial r^2} + \frac{1}{r}\frac{\partial u_r}{\partial r} - \frac{u_r}{r^2} + \frac{1}{r^2}\frac{\partial^2 u_r}{\partial \theta^2} - \\ \frac{2}{r^2}\frac{\partial u_\theta}{\partial \theta} + \frac{\partial^2 u_r}{\partial z^2}) \tag{3.3}$$

z-direction

$$\rho(u_r \frac{\partial u_z}{\partial r} + \frac{u_\theta}{r}\frac{\partial u_z}{\partial \theta} + u_z \frac{\partial u_z}{\partial z}) = -\frac{\partial P}{\partial z} + \mu(\frac{\partial^2 u_z}{\partial r^2} + \frac{1}{r}\frac{\partial u_z}{\partial r} + \frac{1}{r^2}\frac{\partial^2 u_z}{\partial \theta^2} + \frac{\partial^2 u_z}{\partial z^2}) \tag{3.4}$$

(iii) Energy equation

- **For fluid region**

$$\rho Cp(u_r \frac{\partial T}{\partial r} + \frac{u_\theta}{r}\frac{\partial T}{\partial \theta} + u_z \frac{\partial T}{\partial z}) = k[\frac{1}{r} + \frac{\partial}{\partial r}(\frac{\partial T}{\partial r}) + \frac{1}{r^2}\frac{\partial^2 T}{\partial \theta^2} + \frac{\partial^2 T}{\partial z^2}] \tag{3.5}$$

- **For solid region**

$$\frac{\partial^2 Ts}{\partial r^2} + \frac{1}{r}\frac{\partial Ts}{\partial r} + \frac{1}{r^2}\frac{\partial^2 Ts}{\partial \theta^2} + \frac{\partial^2 Ts}{\partial z^2} = 0 \tag{3.6}$$

3.4 Boundary Conditions

Partial Differential Equations (PDEs) (eqs.3.1 to 3.6) are solved based upon on the boundary conditions as referring to Figure 3.1 which illustrates the boundary conditions in the shell and tube. Based on the previous assumptions the boundary conditions for the laminar flow can be summarized as follows:

1-The Inlet Boundary Conditions

a. inlet of cold fluid -tube

$$T_c = T_{ci}$$

$$W_c = W_{ci} \ , u_c = v_c = 0$$

b. inlet of hot fluid - shell

$$T_h = T_{hi}$$

$$u_h = u_{hi}, v_h = w_h = 0$$

2- Walls Boundary Condition

i- The Tube wall

a. The external walls of tube and baffles

No slip boundary condition, continuous boundary condition (fluid-solid interface).

$$u_h = v_h = w_h = 0$$

$$T_h = T_s$$

$$-k_s \frac{\partial T_s}{\partial n} = -k_h \frac{\partial T_h}{\partial n}$$

b. The Internal walls of tube

No slip boundary condition is applied to all of the Internal walls surfaces, continuous boundary condition (fluid-solid interface) i.e.

$$u_c = v_c = w_c = 0$$

$$T_c = T_s$$

$$-k_s \frac{\partial T_s}{\partial r} = -k_c \frac{\partial T_c}{\partial r}$$

ii-The shell wall

a. The external walls of shell

No-slip and adiabatic wall

$$u_h = v_h = w_h = 0$$

$$\frac{\partial T}{\partial r} = \frac{\partial T}{\partial \theta} = \frac{\partial T}{\partial z} = 0$$

b. The Internal walls of shell and baffles

No slip boundary condition, are insulated:

$$u_h = v_h = w_h = 0$$

$$\frac{\partial T}{\partial r} = \frac{\partial T}{\partial \theta} = \frac{\partial T}{\partial z} = 0$$

4- Outlet Boundary Conditions

a. For cold water (tube)

The outlet pressure is zero**,** $P_{out,c} = 0$

and out flow condition is fully developed **,** $\frac{\partial u_c}{\partial z} = \frac{\partial v_c}{\partial z} = \frac{\partial w_c}{\partial z} = \frac{\partial T_c}{\partial z} = 0$

b. For hot water (shell)

The outlet pressure is zero**,** $P_{out,h} = 0$

And out flow condition is fully developed **,** $\frac{\partial u_h}{\partial \theta} = \frac{\partial v_h}{\partial \theta} = \frac{\partial w_h}{\partial \theta} = \frac{\partial T_h}{\partial \theta} = 0$

3.5 Hydrodynamic parameters

The definitions of hydraulic parameters such as hydraulic diameter(D_h), Reynolds number(R_e), pressure drop(ΔP) and friction factor(f)are presented as the following:

1. Hydraulic Diameter

One of the important parameters which characterizing the flow in shell and tube is the hydraulic diameter [40].

$$D_h = \frac{4A_c}{Per} \tag{3.7}$$

Where: A_c: cross section area, Per: perimeter

For tube d_h = di

For shell $D_h = \frac{D_i^{\,2} - 2d_o^{\,2}}{D_i + 2d_o}$

2. Reynolds Number

This is used with fluid properties and inlet velocity to calculate Reynolds number.

$$\mathrm{Re} = \frac{Inertial\ \ forces}{Viscous\ \ forces} = \frac{\rho\, u_m\, D_h}{\mu} \tag{3.8}$$

3. Pressure Drop

The pressure drop across the shell and tube calculated as the difference between the inlet and outlet pressure.

$$\Delta P_s = P_i - P_o \tag{3.9}$$

4. Friction Factor

The friction factor for tube is described on the basis of wall friction forces per inertia forces and it is represented by equation [41]:

$$f = \frac{\Delta P_s}{(\rho u^2/2)(L/d_h)} \tag{3.10}$$

3.6 Thermal parameters

Due to small size of shell and tube and the relative thickness of the wall separating them the conduction in the walls cannot be ignored. The heat

transfer is a conjugate process therefore the energy equation must be solved in three adjacent zones (fluids inside shell and tube and the tube wall). Since the heat is transferred from the hot fluid to the wall by convection through the wall by conduction and then from the wall to the cold fluid by convection as shown in fig. 3.3.

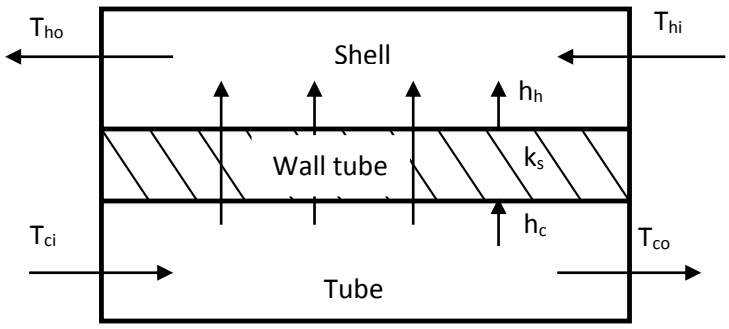

Fig.3.3: Two-dimensional schematic of the heat transfer process.

Convection heat transfer strongly depends on the fluid properties like dynamic viscosity, thermal conductivity, density, specific heat capacity and the fluid velocity. It is also depending upon the geometry of the shell and tube in addition to the type of fluid flow (such as being laminar or turbulent).

The region of the flow over which the thermal boundary layer develops and reaches the tube center is called the thermal entry region. The length of this region is called the thermal entry length. The region beyond the thermal entry region in which the dimensionless temperature remains unchanged is called the thermally fully developed region.

In convection studies are common practice to nondimensionalize the heat transfer coefficient, h, with local Nusselt number.

$$Nu = \frac{h\, D_h}{k_f} \tag{3.11}$$

The value of Nusselt number is a local value calculated based on the local values of heat transfer coefficient (h). Due to the conjugate heat transfer the boundary condition at the fluid - solid interface is coupled i.e. neither constant temperature nor constant heat flux also due to the existing of the radial conduction. The temperature distribution must be calculated from solving the energy equation and then the local heat transfer coefficient is calculated, and from its value the local Nusselt number is calculated.

$$h = \frac{q''}{T_w - T_b} \tag{3.12}$$

$$q'' = -k_s \frac{\partial T_s}{\partial r} \tag{3.13}$$

Where T_w is the wall temperature, T_b is the bulk temperature of fluid and q'' is the heat flux.

The average value of Nusselt number is obtained by integrating the local Nu along heat exchanger by using trapezoidal rule [42].

$$\overline{Nu} = \frac{1}{A}\int_0^A Nu\, dA \tag{3.14}$$

$$\overline{Nu} = \frac{\Delta z}{2L}[Nu_{z=0} + Nu_{z=L} + 2\sum_{i=2}^{N} Nu_{zi}] \tag{3.15}$$

Where

$Nu_{z=0}$, $Nu_{z=l}$, and Nu_{zi} are the values of the local average Nu at the first section (tube inlet), at the last section (tube outlet) and at the section (i) along heat exchanger respectively.

Δz is the increment in length.

N is the number of line along heat exchanger.

Due to combined the convection and conduction terms the Local value of overall heat transfer coefficient is:

$$U_x = \frac{1}{\frac{1}{h_h A} + \frac{\ln(r_2/r_1)}{k_s A} + \frac{1}{h_c A}} \tag{3.16}$$

Where h_h and h_c are the average local values of heat transfer coefficient for hot and cold fluids along heat exchanger respectively.

The average value $\overline{U}$ along entire heat exchanger can be calculated by integrating of the values of U_x along the heat exchanger using the trapezoidal rule.

Also the overall heat transfer coefficient can be calculated from:

$$U = \frac{q}{A\ LMTD} \tag{3.17}$$

Where LMTD is the logarithmic mean temperature difference

$$LMTD = \frac{(T_{h.o} - T_{c.i}) - (T_{h.i} - T_{c.o})}{Ln\frac{(T_{h.o} - T_{c.i})}{(T_{h.i} - T_{c.o})}} \tag{3.18}$$

3.7 Effectiveness

The heat exchanger effectiveness means the performance parameter and define as the ratio of the actual heat transfer to the maximum possible heat that can be transferred [43]:

$$\varepsilon = \frac{q_{act.}}{q_{\max.}} \tag{3.19}$$

Where the maximum heat transfer is the product of minimum heat capacity and the maximum temperature difference as:

$$q_{max} = c_{min}(T_{hi} - T_{ci}) \tag{3.20}$$

And the actual amount of heat lost by hot fluid or gained by the cold fluid is expressed as:

$$q_{act} = c_h(T_{hi} - T_{co}) = c_c(T_{co} - T_{ci}) \tag{3.21}$$

Where

$$C_h = \dot{m} Cp_h$$

$$C_c = \dot{m} Cp_c$$

$$\varepsilon = \frac{C_h(T_{hi} - T_{ho})}{C_{\min}(T_{hi} - T_{ci})} = \frac{C_c(T_{co} - T_{ci})}{C_{\min}(T_{hi} - T_{ci})} \tag{3.22}$$

For any heat exchanger the effectiveness is a function of NTU and the heat capacity ratio. ε=f (NTU, Cr)

Where NTU is the number of transfer units

$$NTU = \frac{UA}{C_{\min}} \tag{3.23}$$

And Cr is the heat capacity ratio $Cr = \frac{C_{\min}}{C_{\max}}$

For conventional counter flow heat exchanger where the overall heat transfer coefficient is constant the effectiveness as it explained in all references deals with heat exchangers given by the following relation [44].

$$\varepsilon = 2\{1 + Cr + (1 + Cr^2)^{½} * \frac{1 + e^{[-(NTU)(1+Cr^2)^{½}]}}{1 - e^{[-(NTU)(1+Cr^2)^{½}]}}\}^{-1} \tag{3.24}$$

From the above relation the conventional ε-NTU relation of conventional counter flow heat exchanger cannot be used directly to calculate the effectiveness of counter flow U-tube heat exchanger. Due to the existence of entrance regions and axial conduction which are the main parameters make the counter flow U-tube heat exchanger differ from the conventional counter flow heat exchanger.

3.8 Thermophysical Properties of Nanofluid

In order to perform the simulations for nanofluid, the effective thermophysical nanofluid properties must be calculated first. In this case, the nanoparticles being used are Al_2O_3. Basically, the required properties for simulations are effective thermal conductivity ($\boldsymbol{k_{eff}}$), effective dynamic viscosity ($\boldsymbol{\mu_{eff}}$), effective mass density ($\boldsymbol{\rho_{eff}}$) and effective specific heat ($\boldsymbol{cp_{eff}}$). The interest physical properties are specific heat, effective properties of density, viscosity and thermal conductivity which they are analyzed base on the mixing theory.

The density of nanofluid, $\boldsymbol{\rho_{nf}}$ can be obtained from the following equation as stated by Al-tayyeb. A. K [45].

$$\rho_{nf} = (1 - \emptyset)\rho_{bf} + \emptyset\rho_{np} \tag{3.25}$$

Where:

ρ_{bf} : mass densities of the based fluid.

ρ_{np} : mass densities of the solid nanoparticles.

The effective heat capacity of the nanofluid at constant pressure drop of nanofluid, $(\rho\ Cp)_{n_f}$ can be found from the following equation according to Al-tayyeb.A. K [45].

$$(\rho\ Cp)_{nf} = (1 - \emptyset)(\rho\ Cp)_{bf} + \emptyset(\rho\ Cp)_{np} \quad (3.26)$$

Where:

Cp_{bf} : heat capacities of the based fluid.

Cp_{np}: heat capacities of solid nanoparticles.

Thermal Conductivity: the thermal conductivity may be found according to Al-tayyeb.A. K [45].

$$K_{nf} = \frac{K_{np}+2K_{bf}+2(K_{np}-K_{bf})\emptyset}{K_{np}+2K_{bf}-2(K_{np}-K_{bf})\emptyset} K_{bf} \quad (3.27)$$

Dynamic Viscosity: The effective viscosity equation of the nanofluid can be calculated based on Al-tayyeb.A. K [45].

$$\mu_{nf} = \mu_{bf}(1 + 2.5\emptyset) \quad (3.28)$$

Table 3.1: Thermophysical Properties of Al_2O_3 types at T=300K [45]

Thermophysical Properties	Water	Al_2O_3
Density (kg/m³)	998.2	3970
Viscosity (N.s/m²)	0.000855	-
Heat Capacity (J/kg. K)	4179	765
Thermal Conductivity (W/m.K)	0.613	40

Table 3.2: Effective thermophysical properties of Al_2O_3-water at Ø 2%, 5% and 10% and dp of (25) nm at 300K [45].

Al_2O_3			
Properties	**Ø=2%**	**Ø=5%**	**Ø=10%**
ρ_{eff} (kg/m³)	1057.636	1146.79	1295.38
K_{eff} (W/m.K)	0.64882	0.70526	0.80726
μ_{eff} (N.s/m²)	0.00089775	0.000961875	0.00106875
Cp_{eff} (J/kg. K)	3922.7	3588.064	3132.699

Part B: Numerical analysis

This part includes a computational procedure for the governing differential equation. The description of the numerical analysis is explained by using finite volume method (FVM), through the solution of the continuity, momentum and energy equation to obtain the discretization equations for the velocity, pressure and temperature fields [46].

The mathematical model which is used to simulate the hydrodynamic and heat transfer for laminar through the U-tube heat exchanger is solved using the Computational Fluid Dynamic (CFD) software package FLUINT .15.0.

The discretization equations are solved in a formula of the Upwind scheme, with **SIMPLE** algorithm.

3.8.1 Finite Volume Method (Control Volume)

The finite- volume method (FVM) is a popular numerical technique for solving systems of differential equations that describe mass, momentum, and energy balances. It's have more use in Computational Fluid Dynamics (CFD) this is because, they combine the simplicity of the finite differences method with the local accuracy of the finite element method. Also, at the same dimension of the discretized problem, the accuracy is higher that with finite differences and nearly the same as with finite elements [47].

The key step of the finite volume method is the integration of the governing equations over a control volume to yield a discretised equation at its nodal point P and then convert the integral equations into a system of algebraic equations. The methods which depend on this technique such central differencing scheme, upwind differencing scheme, hybrid differencing scheme and others. However, the present work is adopted on the upwind differencing scheme.

The Upwind Scheme

Upwinding means that the face values are derived from quantities in the cell upstream relative to the direction of the normal velocity. The upwind differencing scheme takes into account the flow direction when determining the value at a cell face. The value of Φ at a cell face is taken to be equal to the value at the upstream node. In Fig. 3.5 if a strongly convective flow from west to east, the west cell face should receive much stronger influencing from node *W* than from node *P*. When the flow is in the positive direction as the flow in Fig. 3.6, the upwind differencing scheme sets become [48]:

$$\Phi_e = \Phi_P \;\; and \;\; \Phi_w = \Phi_W \tag{3.29}$$

where, Φ is any property such as velocity or pressure

When the flow is negative, that means reveres the flow direction in Fig. 3.5 as shown in Fig. 3.6. The upwind differencing scheme sets become:

$$\Phi_w = \Phi_P \;\; and \;\; \Phi_e = \Phi_E \tag{3.30}$$

Also, the point *e* lies at mid-way between *P* and *E*, and *w* between *P* and *W*. However, the current study depends on positive flow direction.

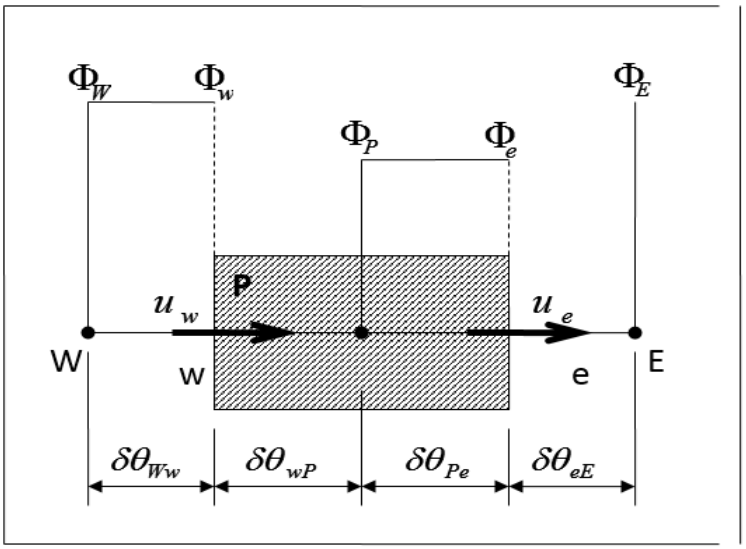

Fig.3.4 The positive flow direction.

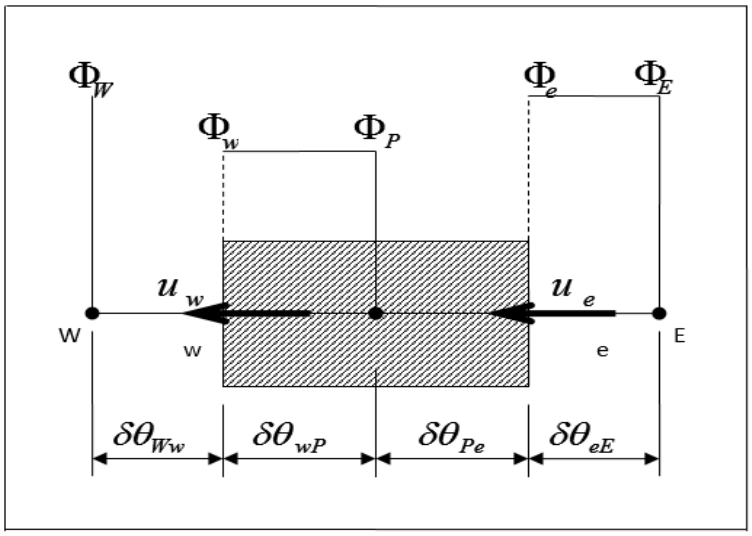

Fig.3.5 The negative flow direction.

3.8.2 The Computational Grid

The first step in the derivation of the finite volume equations is to divide the calculated domain completely into a set of control volumes. Both velocities components and the temperature at a set of chosen points are called the grid points. The algebraic equations for those values (called the discretization equations), are derived by converting the governing differential equations into finite volume form over a controlled volume surrounding each grid point.

For a given grid, the controlled volumes can be defined in many ways. The most obvious way of constructing the control volumes chosen in the present study is by placing their faces midway between the neighboring grid points, as shown in Fig. 3.7.

The calculated domain is divided into control volumes; the dashed lines denote by the control volume boundaries. Then, grid points which are denoted as dotes are placed at the intersection of the grid lines which are denoted as solid lines. To facilitate the understanding, the control volume (cell) the Fig. 3.8 bellow which is represent three-dimensional control volume. The node of interest is p and the neighboring nodes in three-dimension are W, E, S, N, T, B which are represent the west, east, south, north, top and bottom nodes respectively. The notations w, e, s, n, t, b is used to refer to the west, south, north, top, and bottom cell faces respectively.

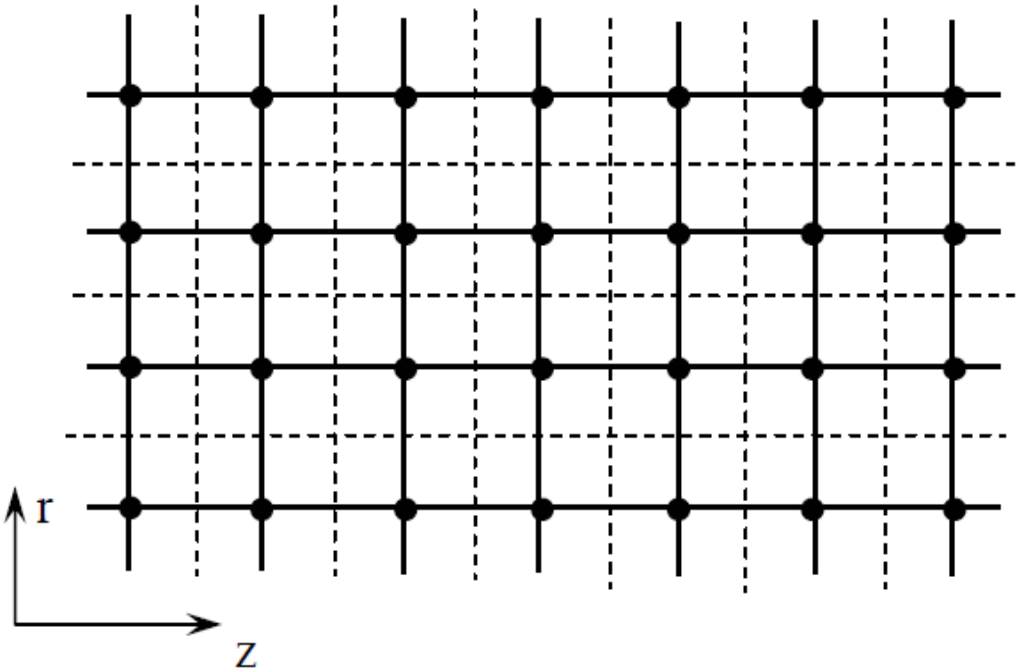

Fig.3.6 Grid of control volume in (r-z) plane.

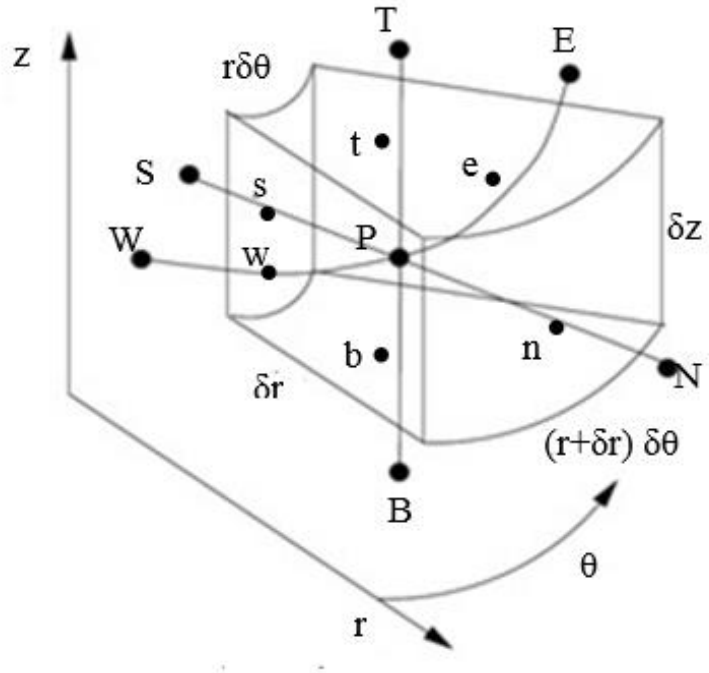

Fig.3.7 Three-dimensional control volume around node P.

3. 8.3 Finite Volume Formulation of Governing Equations

The first step in finite-volume method is the grid generation, and then discretization the governing equations by integration them over the spatial control volume for each one as a second step. To facilitate the understanding, the control volume (cell) for each velocity component and scalars like pressure and temperature, will be studied each one separately. The numerical transformation for all governing equations [49] as the following

The transform of the ***θ-momentum equation*** by using (FVM) to obtain the discretization equation in cylindrical coordinates is as follows:

Rewrite and arrangement Eq. (3.2)

$$\frac{\partial u_r u_\theta}{\partial r} + \frac{1}{r}\frac{\partial u_\theta u_\theta}{\partial \theta} + \frac{\partial u_z u_\theta}{\partial z} + \frac{u_r u_\theta}{r} = -\frac{1}{r}\frac{\partial p}{\partial \theta} + \frac{1}{Re}\left[\begin{array}{c}\frac{\partial^2 u_\theta}{\partial r^2} + \frac{1}{r}\frac{\partial u_\theta}{\partial r} - \frac{u_\theta}{r^2} + \\ \frac{1}{r^2}\frac{\partial^2 u_\theta}{\partial \theta^2} + \frac{2}{r^2}\frac{\partial u_r}{\partial \theta} + \frac{\partial^2 u_\theta}{\partial z^2}\end{array}\right] \tag{3.31}$$

The key step of the finite volume method is the integration of the governing equation over a control volume to yield a discretized equation at its nodal point (P). The integration over the CV gives:

$$\int_{cv}\left[\frac{\partial}{\partial r}(u_r u_\theta) + \frac{1}{r}\frac{\partial}{\partial \theta}(u_\theta u_\theta) + \frac{\partial}{\partial z}(u_z u_\theta) + \frac{u_r u_\theta}{r}\right] dv = \int_{cv}\left[-\frac{1}{r}\frac{\partial p}{\partial \theta} + \frac{1}{Re}\left(\begin{array}{c}\frac{\partial^2 u_\theta}{\partial r^2} + \frac{1}{r}\frac{\partial u_\theta}{\partial r} - \frac{u_\theta}{r^2} + \\ \frac{1}{r^2}\frac{\partial^2 u_\theta}{\partial \theta^2} + \frac{2}{r^2}\frac{\partial u_r}{\partial \theta} + \frac{\partial^2 u_\theta}{\partial z^2}\end{array}\right)\right] dv \tag{3.32}$$

By distributing the integral from on each term in equation (3.31).

The equation (3.30) can be written as

$$\int_s^n \frac{\partial}{\partial r}(u_r u_\theta)dv + \int_w^e \frac{1}{r}\frac{\partial}{\partial \theta}(u_\theta u_\theta)\,dv + \int_b^t \frac{\partial}{\partial z}(u_z u_\theta)\,dv + \int_p \frac{u_r u_\theta}{r}dv$$

$$= -\int_w^e \frac{1}{r}\frac{\partial p}{\partial \theta}dv$$

$$+ \frac{1}{Re}\left(\begin{array}{c} \int_s^n \frac{\partial^2 u_\theta}{\partial r^2}dv + \int_s^n \frac{1}{r}\frac{\partial u_\theta}{\partial r}dv - \int_s^n \frac{u_\theta}{r^2}dv + \\ \int_w^e \frac{1}{r^2}\frac{\partial^2 u_\theta}{\partial \theta^2}dv + \int_w^e \frac{2}{r^2}\frac{\partial u_r}{\partial \theta}dv + \int_b^t \frac{\partial^2 u_\theta}{\partial z^2}dv \end{array}\right) \tag{3.33}$$

The result of integration is

$$[(u_r A_r u_\theta)_n - (u_r A_r u_\theta)_s] + [(u_\theta A_\theta u_\theta)_e - (u_\theta A_\theta u_\theta)_w] + \left(\frac{u_r u_\theta dv}{r}\right)_p$$

$$+ [(u_z A_z u_\theta)_t - (u_z A_z u_\theta)_b] = -[(pA_\theta)_e - (pA_\theta)_w] +$$

$$\frac{1}{Re}\left[\left(A_r \frac{\partial u_\theta}{\partial r}\right)_n - \left(A_r \frac{\partial u_\theta}{\partial r}\right)_s\right.$$

$$+ \left(A_r \frac{u_\theta}{r}\right)_n - \left(A_r \frac{u_\theta}{r}\right)_s - \left(\frac{u_\theta dv}{r}\right)_p + \left(\frac{A_\theta}{r}\frac{\partial u_\theta}{\partial \theta}\right)_e - \left(\frac{A_\theta}{r}\frac{\partial u_\theta}{\partial \theta}\right)_w$$

$$+ \left(\frac{2A_\theta u_r}{r}\right)_e - \left(\frac{2A_\theta u_r}{r}\right)_w + \left(A_z \frac{\partial u_\theta}{\partial z}\right)_t$$

$$\left. - \left(A_z \frac{\partial u_\theta}{\partial z}\right)_b\right] \tag{3.34}$$

Where:

$$A_{\theta e} = A_{\theta w} = \delta r \delta z = A_\theta \tag{3.34a}$$

$$A_n = \left(r_p + \frac{\delta r}{2}\right)\delta\theta\delta z \tag{3.34b}$$

$$A_s = \left(r_p - \frac{\delta r}{2}\right)\delta\theta\delta z \tag{3.34c}$$

$$A_{zt} = A_{zb} = r_p\delta\theta\delta r = A_z \tag{3.34d}$$

The above areas represent the control volume (cell face) area in each direction. Now, based on the definitions in equations (3.34), and using forward differencing for first derivative in equation (3.33), this equation becomes

$$\begin{aligned}\left[\left(F_n u_{\theta,n}\right) - \left(F_s u_{\theta,s}\right) + \left(F_e u_{\theta,e}\right) - \left(F_w u_{\theta,w}\right) + \left(F_t u_{\theta,t}\right) - \left(F_b u_{\theta,b}\right)\right.\\ \left. + \left(F_p u_{\theta,P}\right)\right]\\ = -A_\theta(P_e - P_w)\\ + \left[D_n\left(u_{\theta,N} - u_{\theta,P}\right) - D_s\left(u_{\theta,P} - u_{\theta,S}\right) + D_e\left(u_{\theta,E} - u_{\theta,P}\right)\right.\\ \left. - D_w\left(u_{\theta,P} - u_{\theta,W}\right) + D_t\left(u_{\theta,T} - u_{\theta,P}\right) - D_b\left(u_{\theta,P} - u_{\theta,B}\right)\right]\\ + D_{ve}u_{r,e} - D_{vw}u_{r,w}\end{aligned} \tag{3.35}$$

From the upwind technique in equation (3.25) for positive flow direction, is

$$u_{\theta,e} = u_{\theta,P} \tag{3.35a}$$

$$u_{\theta,w} = u_{\theta,W} \tag{3.35b}$$

and the velocities at the faces ***s***, ***n***, ***b*** and ***t*** are

$$u_{\theta,s} = \frac{1}{2}\left(u_{\theta,P} + u_{\theta,S}\right) \tag{3.35c}$$

$$u_{\theta,n} = \frac{1}{2}\left(u_{\theta,P} + u_{\theta,N}\right) \tag{3.35d}$$

$$u_{\theta,b} = \frac{1}{2}\left(u_{\theta,P} + u_{\theta,B}\right) \tag{3.35e}$$

$$\mathrm{u}_{\theta,\mathrm{t}} = \frac{1}{2}\left(\mathrm{u}_{\theta,\mathrm{P}} + \mathrm{u}_{\theta,\mathrm{T}}\right) \qquad (3.35f)$$

Substituting the equations (3.33) in equation (3.32) with rearrangement, the equation (3.32) becomes

$$\begin{aligned}
&\begin{bmatrix} (D_w + F_w) + D_e + \left(D_s + \frac{F_s}{2}\right) + \left(D_n - \frac{F_n}{2}\right) + \left(D_b + \frac{F_b}{2}\right) \\ + \left(D_t - \frac{F_t}{2}\right) + \Delta F \end{bmatrix} \mathrm{u}_{\theta,\mathrm{P}} \\
&= -(p_e - p_w)A_\theta \\
&+ \begin{bmatrix} \left(D_n - \frac{F_n}{2}\right)\mathrm{u}_{\theta,\mathrm{N}} + \left(D_s + \frac{F_s}{2}\right)\mathrm{u}_{\theta,\mathrm{S}} + D_e \mathrm{u}_{\theta,\mathrm{E}} + \\ (D_w + F_w)\mathrm{u}_{\theta,\mathrm{W}} + \left(D_t - \frac{F_t}{2}\right)\mathrm{u}_{\theta,\mathrm{T}} + \left(D_b + \frac{F_b}{2}\right)\mathrm{u}_{\theta,\mathrm{B}} \\ + D_{ve}\mathrm{u}_{\mathrm{r,e}} - D_{vw}\mathrm{u}_{\mathrm{r,w}} \end{bmatrix}
\end{aligned} \qquad (3.36)$$

Where

$$\Delta F = (F_e - F_w) + (F_n - F_s) + (F_t - F_b) + F_P \qquad (3.35)$$

$$D_w = \frac{A_\theta}{Re r \delta\theta} \qquad (3.36a)$$

$$D_e = \frac{A_\theta}{Re r \delta\theta} \qquad (3.36b)$$

$$D_s = \frac{A_{rs}}{Re \delta r} \qquad (3.36c)$$

$$D_n = \frac{A_{rn}}{Re \delta r} \qquad (3.36d)$$

$$D_b = \frac{A_z}{Re \delta z} \qquad (3.36e)$$

$$D_{ve} = \frac{2A_\theta}{Re \mathrm{r_p}} \qquad (3.36f)$$

$$D_{vw} = \frac{2A_\theta}{Re \mathrm{r_p}} \qquad (3.36g)$$

The equation (3.34) reduced to

$$(a_W + a_E + a_S + a_N + a_B + a_T + \Delta F)\mathrm{u}_{\theta,\mathrm{P}} = -(p_e - p_{w)})A_\theta + a_N \mathrm{u}_{\theta,\mathrm{N}} + a_S \mathrm{u}_{\theta,\mathrm{S}} + a_E \mathrm{u}_{\theta,\mathrm{E}} + a_W \mathrm{u}_{\theta,\mathrm{W}} + a_T \mathrm{u}_{\theta,\mathrm{T}} + a_B \mathrm{u}_{\theta,\mathrm{B}} + D_{ve}\mathrm{u}_{\mathrm{r,e}} - D_{vw}\mathrm{u}_{\mathrm{r,w}} \quad (3.37)$$

where

$$a_W = D_w + F_w \quad (3.38a)$$

$$a_E = D_e \quad (3.38b)$$

$$a_S = D_s + \frac{F_s}{2} \quad (3.38c)$$

$$a_N = D - \frac{F_n}{2} \quad (3.38d)$$

$$a_B = D_b + \frac{F_b}{2} \quad (3.38e)$$

$$a_T = D_t - \frac{F_t}{2} \quad (3.38f)$$

equation (3.37) can be written as:

$$a_P \mathrm{u}_{\theta,\mathrm{P}} = -(p_e - p_w)A_\theta + a_W \mathrm{u}_{\theta,\mathrm{W}} + a_E \mathrm{u}_{\theta,\mathrm{E}} + a_S \mathrm{u}_{\theta,\mathrm{S}} + a_N \mathrm{u}_{\theta,\mathrm{N}} + a_B \mathrm{u}_{\theta,\mathrm{B}} + a_T \mathrm{u}_{\theta,\mathrm{T}} + D_{ve}\mathrm{u}_{\mathrm{r,e}} - D_{vw}\mathrm{u}_{\mathrm{r,w}} \quad (3.38)$$

where

$$a_P = a_W + a_E + a_S + a_N + a_B + a_T + \Delta F \quad (3.39)$$

The final shape of discretized equation (3.38) is

$$a_{(i,J,K)}u_{\theta(i,J,K)}$$
$$= \left(p_{(I-1,J,K)} - p_{(I,J,K)}\right)A_\theta + a_W\, u_{\theta(i-1,J,K)} + a_E\, u_{\theta(i+1,J,K)} + a_S u_{\theta(i,J-1,K)}$$
$$+ a_N u_{\theta(i,J+1,K)} + a_B u_{\theta(i,J,K-1)} + a_T u_{\theta(i,J,K+1)} + D_{ve}\left(\frac{u_{r(I,j+1,K)} + u_{r(I,j,K)}}{2}\right)$$
$$- D_{vw}\left(\frac{u_{r(I-1,j+1,K)} + u_{r(I-1,j,K)}}{2}\right) \qquad (3.40)$$

Where: $a_{(i,J,K)} = a_P$

For R-momentum equation, the control volume of R-momentum equation solution as the same procedures for θ-momentum equation is adopted here in equations from (3.27) to (3.33), therefore the discretization equation for *v*-component becomes.

$$\left(F_e u_{r,e} - F_w u_{r,w}\right) + \left(F_n u_{r,n} - F_s u_{r,s}\right) + \left(F_t u_{r,t} - F_b u_{r,b}\right) + F_P u_{r,P}$$
$$= -\left(A_{rn} p_n - A_{rs} p_{s)}\right) + \begin{bmatrix} D_n\left(u_{r,N} - u_{r,P}\right) \\ -D_s\left(u_{r,P} - u_{r,S}\right) \end{bmatrix}$$
$$+ \begin{bmatrix} D_e\left(u_{r,E} - u_{r,P}\right) \\ -D_w\left(u_{r,P} - u_{r,W}\right) \end{bmatrix} + \begin{bmatrix} D_t\left(u_{r,T} - v_P\right) \\ -D_b\left(v_P - u_{r,B}\right) \end{bmatrix} - D_{ue} u_{\theta,e}$$
$$+ D_{uw} u_{\theta,w} + F_{up} u_{\theta,p} \qquad (3.41)$$

The upwind technique sets

$$u_{r,n} = u_{r,P} \qquad (3.42a)$$

$$u_{r,s} = u_{r,S} \qquad (3.42b)$$

Substituting the equation (3.42) in equation (3.41) with rearrangement, the equation (3.41) becomes

$$\left[\begin{array}{c}\left(D_w+\frac{F_w}{2}\right)+\left(D_e-\frac{F_e}{2}\right)+(D_s+F_s)+D_n+\left(D_b+\frac{F_b}{2}\right)\\ +\left(D_t-\frac{F_t}{2}\right)+\Delta F\end{array}\right]u_{r,P}=$$

$$=-\left(A_{rn}p_n-A_{rs}p_{s)}\right)$$

$$+\left[\begin{array}{c}D_n u_{r,N}+(D_s+F_s)u_{r,S}+\left(D_e-\frac{F_e}{2}\right)u_{r,E}+\left(D_w+\frac{F_w}{2}\right)u_{r,W}\\ +\left(D_t-\frac{F_t}{2}\right)u_{r,T}+\left(D_b+\frac{F_b}{2}\right)u_{r,B}\\ -D_{ue}u_{\theta,e}+\ D_{uw}u_{\theta,w}+F_{up}u_{\theta,p}\end{array}\right] \tag{3.43}$$

where

$$\Delta F=(F_e-F_w)+(F_n-F_s)+(F_t-F_b)+F_P \tag{3.44}$$

the diffusion conductance at cell faces D is same as in equations from (3.36a) to (3.36g). The equation (3.43) reduced to

$$\begin{aligned}a_P u_{r,P}=&-\left(A_{rn}p_n-A_{rs}p_{s)}\right)+a_N u_{r,N}\\ &+a_S u_{r,S}+a_E u_{r,E}+\ a_W u_{r,W}+a_T u_{r,T}+a_B u_{r,B}+a_{up}u_P\\ &-a_{ue}u_{\theta,e}+a_{uw}u_{\theta,w}\end{aligned} \tag{3.45 }$$

The final shape of discretized equation (3.45) becomes

$$\begin{aligned}a_{(I,j,K)}u_{r(I,j,K)}&\\ &=-\left(A_{rn}p_{(I,J,K)}-A_{rs}p_{(I,J-1,K)}\right)+a_W u_{r(I-1,j,K)}\\ &+a_E u_{r(I+1,j,K)}+a_S u_{r(I,j-1,K)}+a_N u_{r(I,j+1,K)}\\ &+a_B u_{r(I,j,K-1)}+a_T u_{r(I,j,K+1)}\\ &+a_{up}\left(\frac{u_{\theta(i+1,J,K)}+u_{\theta(i+1,J-1,K)}+u_{\theta(i,J,K)}+u_{\theta(i,J-1,K)}}{4}\right)\\ &-a_{ue}\left(\frac{u_{\theta(i+1,J,K)}+u_{\theta(i+1,J-1,K)}}{2}\right)\\ &+a_{uw}\left(\frac{u_{\theta(i,J,K)}+u_{\theta(i,J-1,K)}}{2}\right)\end{aligned} \tag{3.46}$$

Where: $a_{(I,j,K)} = a_P$

For z-momentum equation, the control volume of z-momentum equation solution as the same procedures for θ-momentum equation is adopted in equations from (3.27) to (3.33). therefore, the discretization equation for *w*-component is

$$\left(F_n u_{z,n} - F_s u_{z,s}\right) + \left(F_e u_{z,e} - F_w u_{z,w}\right) + \left(F_t u_{z,t} - F_b u_{z,b}\right)$$
$$= -(p_t - p_b)A_z + \begin{bmatrix} D_n\left(u_{z,N} - u_{z,P}\right) \\ -D_s\left(u_{z,P} - u_{z,S}\right) \end{bmatrix} + \begin{bmatrix} D_e\left(u_{z,E} - u_{z,P}\right) \\ -D_w\left(u_{z,P} - u_{z,W}\right) \end{bmatrix}$$
$$+ \begin{bmatrix} D_t\left(u_{z,T} - u_{z,P}\right) \\ -D_b\left(u_{z,P} - u_{z,B}\right) \end{bmatrix} \qquad (3.47)$$

For positive flow direction in equation (3.25), the upwind technique sets

$$u_{z,t} = u_{z,P} \qquad (3.48a)$$

$$u_{z,b} = u_{z,B} \qquad (3.48b)$$

Substituting the equation (3.48) in equation (3.47) with rearrangement, the equation (3.47) becomes

$$\begin{bmatrix} \left(D_w + \frac{F_w}{2}\right) + \left(D_e - \frac{F_e}{2}\right) + \left(D_s + \frac{F_s}{2}\right) + \left(D_n^* - \frac{F_n^*}{2}\right) + (D_b + F_b) \\ +D_t + \Delta F \end{bmatrix} u_{z,P}$$
$$= -(p_t - p_b)A_z + \begin{bmatrix} \left(D_n - \frac{F_n}{2}\right) u_{z,N} + \left(D_s + \frac{F_s}{2}\right) u_{z,S} \\ + \left(D_e - \frac{F_e}{2}\right) u_{z,E} + \left(D_w + \frac{F_w}{2}\right) u_{z,W} \\ +D_t u_{z,T} + (D_b + F_b) u_{z,B} \end{bmatrix} \qquad (3.49)$$

The diffusion conductance at cell faces *D* is the same as that in equations from (3.36a) to (3.36g).The equation (3.49) is reduced to

$$a_P u_{z,P} = a_W u_{z,W} + a_E u_{z,E} + a_S u_{z,S} + a_N u_{z,N} + a_B u_{z,B} \tag{3.50}$$

The final shape of discretized equation (3.50) is

$$a_{(I,J,k)} u_{z(I,J,k)} = -\left(p_{(I,J,K)} - p_{(I,J,K-1)}\right) A_z + a_W\, u_{z(I-1,J,k)} + a_E u_{z(I+1,J,k)}$$

$$+ a_S u_{z(I,J-1,k)} + a_N u_{z(I,J+1,k)}$$

$$+ a_B u_{z(I,J,k-1)} + a_T u_{z(I,J,k+1)} \tag{3.51}$$

Where: $a_{(I,J,k)} = a_P$

For energy equation of fluid, the first discretization step is rearrangement the equation (3.5) and then integral

$$\int_{cv} \left[\frac{\partial}{\partial z}(u_z T) + \frac{\partial}{\partial r}(u_r T) + \frac{1}{r}\frac{\partial}{\partial \theta}\,(u_\theta T)\right] dv$$

$$= \int_{cv} \left[\frac{1}{Pe}\left(\frac{\partial^2 T}{\partial z^2} + \frac{1}{\mathrm{r}}\frac{\partial}{\partial \mathrm{r}}\left(\mathrm{r}\frac{\partial \mathrm{T}}{\partial \mathrm{r}}\right) + \frac{1}{r^2}\frac{\partial^2 T}{\partial \theta^2}\right)\right] dv \tag{3.52}$$

$$\int_b^t \frac{\partial}{\partial z}(u_z T) dv + \int_s^n \frac{\partial}{\partial r}(u_r T) dv + \int_w^e \frac{1}{r}\frac{\partial}{\partial \theta}(u_\theta T) dv$$

$$= \frac{1}{Pe}\left(\int_b^t \frac{\partial^2 T}{\partial z^2} dv + \int_s^n \frac{1}{\mathrm{r}}\frac{\partial \mathrm{T}}{\partial \mathrm{r}} dv + \int_s^n \frac{\partial^2 \mathrm{T}}{\partial \mathrm{r}^*} dv\right.$$

$$\left. + \int_w^e \frac{1}{r}\frac{\partial^2 T}{\partial \theta^2} dv\right) \tag{3.53}$$

result of integration is

$$\left\{\begin{bmatrix}(u_{z,t}A_{zt})T_t\\-(u_{z,b}A_{zb})T_b\end{bmatrix}+\begin{bmatrix}(u_{r,n}A_{rn})T_n\\-(u_{r,s}A_{rs})T_s\end{bmatrix}+\begin{bmatrix}(u_{\theta,e}A_{\theta e})T_e\\-(u_{\theta,w}A_{\theta w})T_w\end{bmatrix}\right\}$$
$$=\frac{1}{Pe}\left\{\begin{bmatrix}A_{zt}\left(\frac{\partial T}{\partial z}\right)_t\\-A_{zb}\left(\frac{\partial T}{\partial z}\right)_b\end{bmatrix}+\begin{bmatrix}A_{rn}\left(\frac{\partial T}{\partial r}\right)_n\\-A_{rs}\left(\frac{\partial T}{\partial r}\right)_s\end{bmatrix}+\left(\frac{A_{rn}}{r_n}T_n\right)-\left(\frac{A_{rs}}{r_s}T_s\right)\right.$$
$$\left.+\begin{bmatrix}\frac{A_{\theta e}}{r_e}\left(\frac{\partial T}{\partial \theta}\right)_e\\-\frac{A_{\theta w}}{r_w}\left(\frac{\partial T}{\partial \theta}\right)_w\end{bmatrix}\right\} \tag{3.54}$$

and the area of opposite directions is to be equal, therefore

$$A_{\theta e}=A_{\theta w}=\delta r\delta z=A_\theta \tag{3.55a}$$

$$A_n=\left(r_p+\frac{\delta r}{2}\right)\delta\theta\delta z \tag{3.55b}$$

$$A_s=\left(r_p-\frac{\delta r}{2}\right)\delta\theta\delta z \tag{3.55c}$$

$$A_{zt}=A_{zb}=r\delta\theta\delta r=A_z \tag{3.55d}$$

based on the definitions in equation (3.55), the forward differencing is applied for first derivative in equation (3.54), this equation becomes:

$$(F_tT_t-F_bT_b)+(F_nT_n-F_sT_s)+(F_eT_e-F_wT_w)$$
$$=\begin{bmatrix}D_t(T_T-T_P)\\-D_b(T_P-T_B)\end{bmatrix}+\begin{bmatrix}D_n(T_N-T_P)\\-D_s(T_P-T_S)\end{bmatrix}$$
$$+\begin{bmatrix}D_e(T_E-T_P)\\-D_w(T_P-T_W)\end{bmatrix} \tag{3.56}$$

For positive flow direction in equation (3.25), the upwind technique sets

$$T_e=T_P \tag{3.57a}$$

$$T_w=T_W \tag{3.57b}$$

$$T_n=T_P \tag{3.57c}$$

$$T_s = T_S \tag{3.57d}$$

$$T_t = T_P \tag{3.57e}$$

$$T_b = T_B \tag{3.57f}$$

Substituting the equation (3.57) in equation (3.56) with rearrangement, therefore equation (3.56) becomes

$$\lfloor (D_w + F_w) + D_e + (D_s + F_s) + D_n + (D_b + F_b) + D_t + \Delta F \rfloor T_P = \begin{pmatrix} (D_w + F_w)T_W + D_e\, T_E + (D_s + F_s)T_S \\ +D_n T_N + (D_b + F_b)T_B + D_t T_T \end{pmatrix} \tag{3.58}$$

the final shape of discretized equation (3.54) is

$$a_{(I,J,K)}T_{(I,J,K)} = a_W\, T_{(I-1,J,K)} + a_E T_{(I+1,J,K)} + a_S T_{(I,J-1,K)} + a_N T_{(I,J+1,K)} + a_B T_{(I,J,K-1)} + a_T T_{(I,J,K+1)} \tag{3.59}$$

Where: $a_{(I,J,K)} = a_P$

All discretisation equations are solved by using the SIMPLE algorithm method.

3.9 Solution procedures:

In the present model it's required to calculate the temperature and velocity distribution in addition to the pressure drop for the various cases under consideration. The pressure gradient is unknown in the present work, and the continuity equation may be used as a transport equation for pressure.

The problem associated with the pressure –velocity coupling can be solved by adopting an iterative solution strategy such as SIMPLE algorithm.

3.9.1 Segregated solution algorithm:

The segregated solver was used to solve the governing integral equations for the conservation of the mass, momentum and energy.

In this approach the non – linear governing equations are solved sequentially (i.e. segregated from each another) using the iterative technique. The steps of iteration are as follows [50]:

1- Fluid properties are updated (for temperature dependent properties), based on the current solution (or the initial conditions) if just starting.
2- The u, v, and w momentum equations are each solved in turn using current values of pressure and face mass flux, in order to update the velocity field.
3- The velocity may not satisfy the continuity equation locally; therefore, a pressure correction equation is derived from the continuity equation and momentum equations. This equation is then solved to obtain the necessary correction of the pressure and velocity field and the face mass fluxes so that the continuity is satisfied.
4- Using the previously solved variables, energy and if exists, turbulence and radiation equations are solved.
5- Following these steps a convergence check is done.

These steps are continued until the convergence criteria are met.

3.9.2 SIMPLE algorithm:

To solve the pressure-velocity coupling problem when the pressure gradient is not known the SIMPLE algorithm is used.

The SIMPLE algorithm uses the relationship between velocity and pressure correction to enforce mass conservation and to obtain the pressure field. The momentum equation then solved using a guessed pressure field to obtain the face flux. If the resulting face flux does not satisfy the continuity

equation a correction face flux is added to obtain the corrected face flux which is satisfying the continuity equation.

Further explanation and formulation of the SIMPLE algorithm will be presented after discretising the governing equations of the present model to complete the numerical formulation of the governing equations.

3.9.3 Staggered grid:

The finite volume method starts, as always, with the discretisation of the flow domain and of the relevant transport equations. First need to decide where to store the velocities. It seems logical to define these at the same locations as the scalar variables such as pressure, temperature. etc. However, if the velocities and pressure are both defined at the nodes of an ordinary control volume a highly non – uniform pressure field can act like a uniform field in the discretised momentum equations.

If the velocities are defined at the scalar grid nodes, the influence of pressure is not properly represented in the discretised momentum equations. A remedy of this problem is to use a staggered grid for the velocity components.

The idea of staggered grid is to evaluate scalar variables, such as pressure, density, temperature... etc. at ordinary nodal points. While to calculate the velocity components on staggered grids centered around the cell faces.

3.10 Solving by FLUENT software:

The previous discretised governing equations are ready to solve by writing a code or the problem can be solved by using one of the available CFD packages. In this thesis a CFD software FLUENT 15.1 is used to solve the present model. Since FLUENT is widely used in this field and its considered one of the more powerful among other available codes.

FLUENT is a state –of –art computer program for modeling fluid flow and heat transfer problems especially for complex geometries and provides complete mesh flexibility.

The steps of simulation by FLUENT are the same for any other CFD code [51]:

1- Define the modeling goals.

2- Create the model geometry and grid.

3- Set up the solver and physical models.

4- Compute and monitor the solution.

5- Examine and save the results.

3.10.1 Geometry creation:

The first step in numerical simulation using ANSYS FLUENT is a creating or drawing the geometry under consideration. This step is done using separate software called design modeler.

Design modeler is software used to create the geometry, generating the mesh required and specify the zones of the geometry with its types and boundary conditions.

To draw a 3D geometry in design modeler it's necessary to begin with the vertices, then these vertices are linked together to form the edges of geometry. From the edges the faces are generated, then these faces are linked together to form the 3D volumes of the geometry.

3.10.2 Mesh construction:

The second part of the pre – processing is the mesh generation. Mesh is the key components of a high quantity solution. The software design modeler was used to meshing the geometries studied. Design modeler offers many types of

meshes such as hexahedral and tetrahedral and the mesh may be structured or non – structured.

The geometrical modeling and grid generation procedure are carried out with commercial CFD preprocessor ANSYS 15.1, grid generation is performed using meshing [ANSYS WORK BENCH]. In the most flow region, the models are discretized the tetrahedral meshes for shell and the hexahedral meshes for the U-tube and baffle region. The grid distribution of the physical model is presented in Fig.3.9. One of the most important tests of numerical analysis of a problem which should be done is grid independence test. The grid independence test was completed for this model in numerical problem. These results depend on the number of grids generated which shown in Fig.5.1. The number of grids without change in results were selected as best grid size and the results become independent of grids (the number of nodes=453467 and number of elements=1942789). In Fig. 5.1, the temperature of hot fluid at the outlet is considered for check the grid independence.

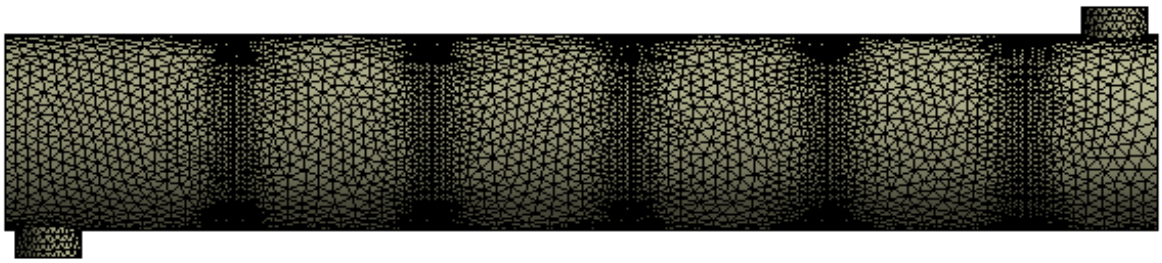

(a) overall meshes of heat exchanger

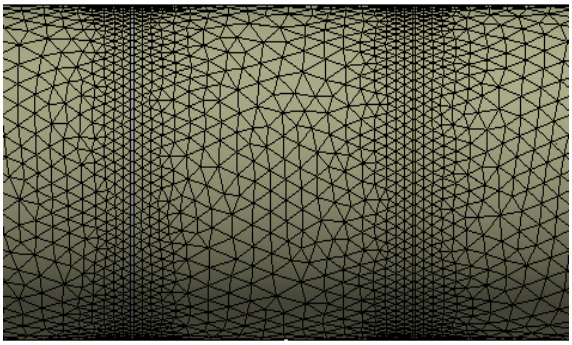

(c) partial meshes of shell

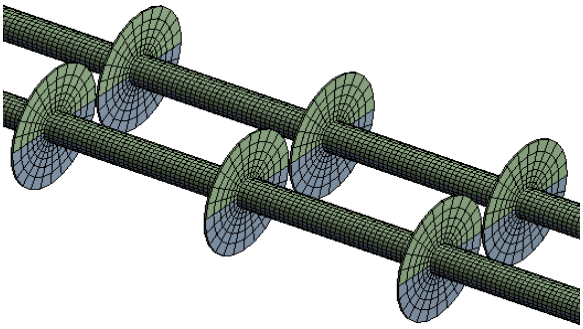

(b) partial meshes of tube baffle(0°)

Fig.3.9 Meshes of computational model.

3.10.3 Specifying zones types:

Zone type specifications define the physical and operational characteristics of the model at its boundaries within specific regions of its domain. There are two classes of zone-type specifications in FLUENT.

- Continuum types.

- Boundary types.

3.10.3.1 Continuum specification:

Continuum type specifications such as fluid or solid define the characteristics of the model within specified regions of its domain to specify the governing equations to be solve.

3.10.3.2 Boundary conditions

The boundary conditions specify the flow and thermal variables on the boundaries of the physical model. They are therefore, critical components of

the simulations and it is important that they are specified appropriately. There are many types of boundary conditions available in FLUENT and it is selected according to the case studied.

3.10.4 Physical properties model

An important step in the setup of the numerical model is the definition of the physical properties. The physical properties may be dependent or independent of temperature depending upon the type of approach chosen. In the calculations of this study the fluid properties are assumed constant.

3.10.5 Initial conditions

Initial velocities and temperatures are defined. Initial pressure is taken to be the ambient pressure. The initialization of the model is important for convergence. If the initial conditions are poor, then it takes longer time to converge or it may even result in divergence.

3.10.6 Under – Relaxation factors

These values have direct impact on the convergence. Generally, default values are used, but if convergence problems occur, then these values are modified. Decreasing these factors gradually helps convergence, on the other hand, for less computational times they may be increased Its values ranged from 0 to 1.

The expression for under – relaxation factors is given as:

$$E_{new} = E_{old} + \lambda\ (E_{Calculated} - E_{old})$$

Where

E_{new} : new value of the computed parameter.

$E_{calculated}$: newly computed value of the parameter.

λ : under relaxation factor.

3.10.7 Measure of Convergence

It is tried to have a good convergence throughout the simulations. The solution time increases if the convergence criteria are made strict. Good thing about this model is that it doesn't take too much time to converge. Thus strict criteria are possible to get good accurate results, as shown in table 3.2.

Table 3.2: Residuals

Variable	**Residual**
x-velocity	10^{-6}
y-velocity	10^{-6}
z-velocity	10^{-6}
Continuity	10^{-6}
Energy	10^{-8}

CHAPTER FOUR

EXPERIMENTAL WORK

CHAPTER FOUR
EXPERIMENTAL WORK

4.1 Introduction

The experimental rig for shell and tube heat exchanger system is built at collage to assistant in the practical analysis. This rig is designed to obtain and study the actual behavior of heat transfer in U-tube heat exchanger and appropriate with theoretical part for different angle of inclined baffle and water mass flow rates. The experimental work includes an investigation of the effect of some parameters of the U-tube heat exchanger in the steady-state conditions.

4.2 Experimental Facilities

The experimental apparatus consists of one pass of warm water flow through the shell side and two passes single tube of cold water. The annular baffles in shell side and on the facing distances from the outer surface of the length of the tube are inserted to impede the flow. The water is heated in a storage tank to provide the shell with hot water by a suitable Pump. The inlet and outlet temperature are measured by using thermocouples (K- Type). The mass flow rate of shell and tube was measured by a flow meter type (rotameter). The schematic diagram is shown in Fig. 4.1 and the experimental installation is shown in Fig. 4.2. This rig was building in the lab of the thermal engineering department faculty in engineering technical college in Basra.

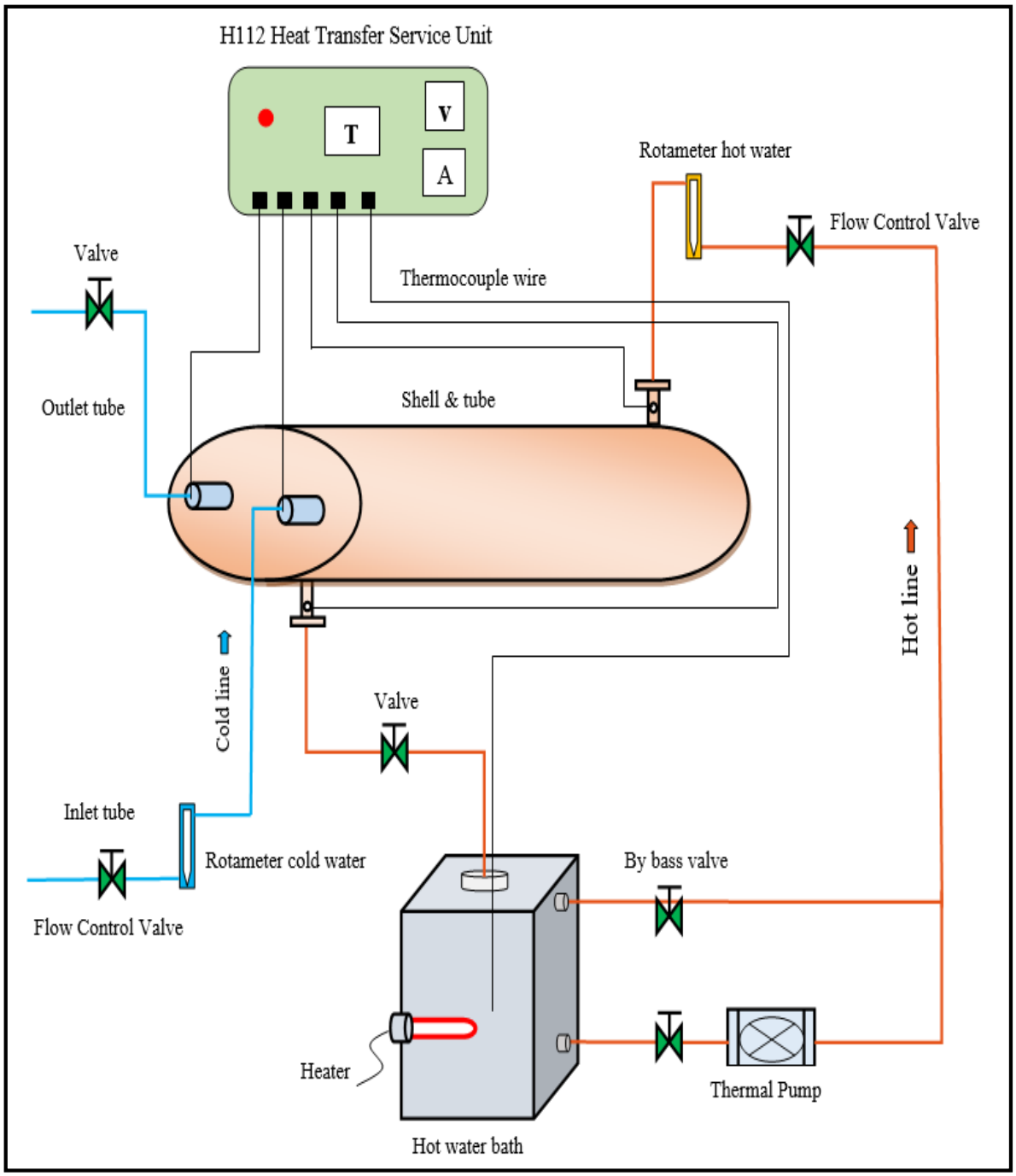

Fig.4.1 Schematic Diagram of the experimental test apparatus

Fig.4.2 Photograph of the experimental rig

1-thermal pump	2-bybass valve	3-inlet shell	4-outlet shell
5-shell	6-flow meter of shell	7- Flow control valve of shell	
8-flow meter of tube	9- Flow control valve of tube	10-discharge valve	
11-inlet tube	12-outlet tube	13-hot water bath	14- HTSU

4.3 Main Components and Instruments of the Experimental Rig.

The test rig consists of the following components and instruments.

4.3.1 Test Rig Components

The main components used in the test rig are U-tube heat exchanger, shell, hot water bath, thermal pump, flow control valve and extension pipe. The details of each component are explained as following:

1. The U-tube and baffles

It is the main part of the heat exchanger, which is supported by the tube plate. The cold water run through tube, which flows from the cold tank at the top of the building through the PVC pipe line of cold water. The U-tube is made of copper metal. The baffles inserted around the tube as annulus from the outer surface of the length of the tube with different angle (+45°, 0°, -45º), the number of baffles tube the used are ten. The baffles tube is made of aluminum metal. The specifications of the U-tube and baffles are given in tables 4.1 and 4.2 respectively. Fig. 4.3 shows the U-tube with baffles.

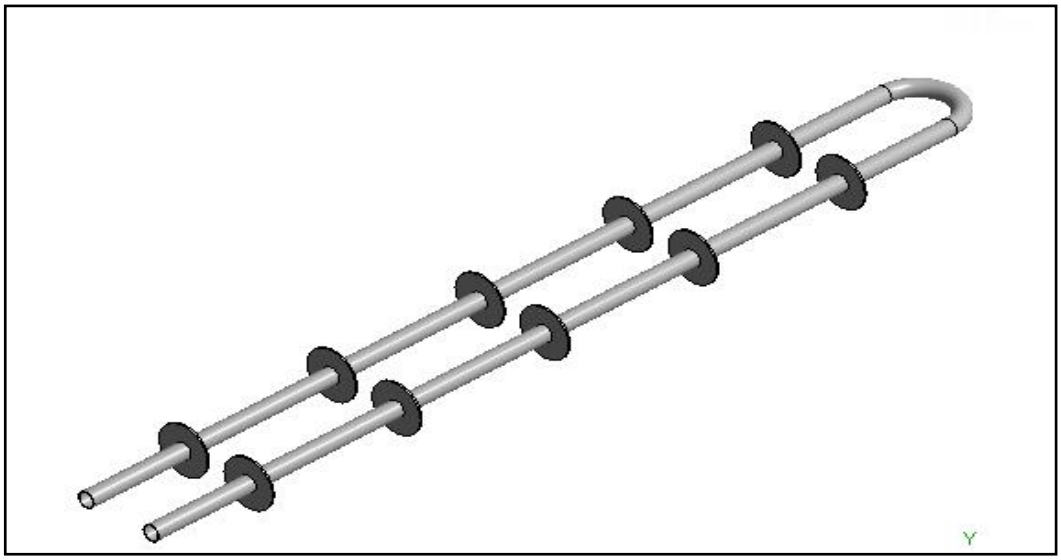

Fig.4.3 U-tube heat exchanger

Table 4.1: Specifications of the U-tube

No.	Geometric Parameters	Value
1.	Tube outer diameter (d_o)	19.05mm
2.	Tube thickness (δ_t)	1.07 mm
3.	Tube length (L_t)	2100 mm
4.	Distance between tube center (S)	50 mm

Table 4.2: Specifications of the tube baffles

No.	Geometric Parameters	Value
1.	Baffle inner diameter ($B_{d,t}$)	19.05mm
2.	Baffle thickness ($\delta_{b,t}$)	1.5 mm
3.	Baffle height ($B_{h,t}$)	20 mm
4.	Baffle spacing ($B_{s,t}$)	170 mm

2. The Shell

It is made of poly vinyl chloride (PVC), schedule 100 with internal diameter 188.9mm and length 2100mm. Inside shell contains U-tube, the system is called one-shell pass and two-tube passes heat exchangers. Baffles are commonly placed inside the shell to force the shell side fluid to flow across the tube to enhance heat transfer. The baffles are made of Alubond material, it's placed in the shell as annular to the inner diameter with constant angle and stagger position of the tube baffles, the baffles number used are five. The shell inlet is at the end of the cylinder from the top and outlet in the foreground at the bottom. The hot water enters the shell at inlet by the pump from hot water bath. The discharge valve is used to release the air from shell side at the start of the experiment. The specifications of the baffle shell are given in table 4.3.

Table 4.3: Specifications of the shell baffle

No.	Geometric Parameters	Value
1.	Baffle inner diameter ($B_{d,sh}$)	148.9mm
2.	Baffle thickness ($\delta_{b,sh}$)	1.5 mm
3.	Baffle height ($B_{h,sh}$)	20 mm
4.	Baffle spacing ($B_{s,sh}$)	170 mm

3. Hot Water Bath

The hot water tank which is made of a galvanize iron, is heated by an electric element of (3000W) that, it's placed at the bottom of this tank and fabricated as a boiler and has capacity of 180 L. The hot water bath contains two entrances and one outlet, the first inlet to the tank from the reservoir to fill the tank before the operating. The second inlet to the tank it regulating valve (by bass) to control the amount of the water going to the shell. The outlet from hot water bath is provided by thermal pump to the hot line PVC pipe.

4. Thermal pump

One thermal pump model VA 35/180 X is used to circulate the hot water in the shell side. The discharge of the 8 L/min, it is working at high temperature from -10 ^{O}C to + 110 ^{O}C. Also, it contains three selector of velocity range from 0.04 to 0.14 kg/s and with head up to (9m). For regulate the hot water amount velocity selector is used, and the discharge valve to control on the amount of the circulated water in shell side. Table 4.4 shows the properties of thermal pump. Fig. 4.4 shows simple picture of the Circulating Pump.

Table 4.4: Properties of thermal pump

Speed	N (r.p.m.)	P1 MAX (W)	I (A)	Measured mass flow rate (Kg/s)
1.	**1440**	**44**	**0.24**	**0.04**
2.	**1910**	**60**	**0.31**	**0.09**
3.	**2370**	**71**	**0.36**	**0.14**

Fig.4.4 Thermal Circulating Pump

5. Flow Control Valve and Extension Pipe

To control the mass flow for shell and tube a flow control valve is used. More valves are used in the rig, the first for control hot water flow through shell side, the second to control the cold water flow in the tube side, the third used for by bass of the hot water and other valves for closed or open drains every component. The poly vinyl chloride (PVC) pipe schedule 60 used in rig for extension between main components.

4.3.2 Measuring Instruments:

1. H112 Heat Transfer Service Unit

The unit has three digital displays on the front panel including a push button digital temperature indicator allowing all relevant parameters to be displayed. Parameters displayed on the Heat Transfer Service Unit H112 are temperature, voltage of range 0-240V ac and current of range 0-2A ac.

Miniature type K thermocouple sockets allow the connection of up 12 temperature sensors from the range of optional experimental units available with resolution is 0.1°C. Fig 4.5 shows heat transfer service unit.

Fig.4.5: H112 Heat transfer service unit (HTSU)

2. Thermocouple Wires

The temperatures in the shell and tube are measured by K- type thermocouples wires that are made of Ni-Cr and Ni-Cd with range -50 to 700°C, as shown in fig 4.6. Heat transfer service unit is used to connect all thermocouples, as shown in Fig 4.2. Also, five thermocouples are used to measure the temperature at inlet-outlet shell, inlet-outlet tube and hot bath

water. These wires are carefully inserted into the main flow stream and supported by spot welded. A selector switch in the heat transfer service unit is used to change among these four locations.

The Calibration is done against mercury thermometer and the outputs from the thermocouples are measured by **H112** HTSU which is made by (Paul Hilton Ltd) which is shown in the Fig 4.6. It is containing a regulated and variable AC power supply and single conditioning with three digital displays and selector switch tor up 5 type "K" thermocouple, AC current and voltage. The resolution is 0.1°C. Appendix (A) shows the results of the calibration.

3. Flow Meter

The volume flow rate of the water was measured by floating type rotameter. The rig is used two rotameters, the first for hot water shell side with range of 1 L/m to 16 L/m and second for cold water with range of 0.75 L/m to 5 L/m, as shown in the Fig. 4.6. The rotameter is calibrated after mounted in the experimental rig and before tests are performed using a measuring cylinder and stop watch, the details of calibration are mentioned in Appendix (B).

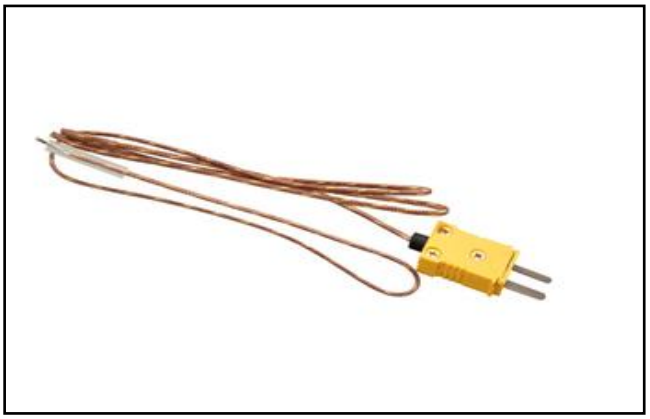

Fig. 4.6 thermocouple wire

Fig. 4.7 Rotameter

4.4 Experimental procedures

1. At first the hot water bath is filled with water.
2. The valves that must be open or closed.
3. Connect the rig to the electric source and thermocouples to heat transfer service unit.
4. Powered on the immersion heater at the hot water bath.
5. Operate the heat transfer service unit to reader of thermocouples to measure the temperature for hot water bath
6. Operate the thermal pump, after until the water in the hot water bath reach to 60C^{o}.
7. Adjust the mass flow rate for cold and hot fluids.
8. The air vent valve is opened to release the air when start the experiment, and closed the air vent valve after extract the air from the system.
9. No records were done during the unsteady operation. When the recorded temperature from the previous period is less than that of the later period not more than (±0.15 ^{O}C), the experiment is assumed to reach a steady state condition.
10. Changing mass flow rate five times for hot fluid (2, 3, 4, 5 and 6 L/min) and three time for cold fluid (0.75,1 and 1.25 L/min).
11. The H112 heat transfer service unit is used to select the temperature reading for each thermocouple.
12. The same procedure is repeated for three angle of baffle (+45°,0°, -45°)
13. Switch off the electrical power supply to the rig, after the end of the experiment, and leave the rig to return to its original temperature before starting a new run.

4.5 Experimental Calculations

The data reduction of the measured results is summarized in the following procedures:

The rate heat transfer from hot water can be calculated from

$$Q_h = \dot{m}_h Cp(T_{hi} - T_{ho}) \tag{4.1}$$

Rate heat transfer to the cold water can be calculated from

$$Q_c = \dot{m}_c Cp(T_{co} - T_{ci}) \tag{4.2}$$

The logarithmic mean temperature difference (LMTD) is determined from the following equation.

$$LMTD = \frac{(T_{h.i} - T_{c.o}) - (T_{h.o} - T_{c.i})}{Ln\dfrac{(T_{h.i} - T_{c.o})}{(T_{h.o} - T_{c.i})}} \tag{4.3}$$

Heat exchanger effectiveness (ε) is the ratio of the actual heat transfer to the maximum possible heat that can be transferred:

$$\varepsilon = \frac{q_{act.}}{q_{\max.}} = \frac{C_h(T_{hi} - T_{ho})}{C_{\min}(T_{hi} - T_{ci})} = \frac{C_c(T_{co} - T_{ci})}{C_{\min}(T_{hi} - T_{ci})} \tag{4.4}$$

the number of transfer unit as it explained in all references deals with heat exchangers given by the following relation [44].

$$NTU = -\frac{1}{\sqrt{1+c^2}}\ln\left(\frac{2/\varepsilon - 1 - c - \sqrt{1+c^2}}{2/\varepsilon - 1 - c + \sqrt{1+c^2}}\right) \tag{4.5}$$

CHAPTER FIVE

RESULTS AND DISCUSSION

Chapter Five
Results and Discussion

5.1 Introduction

The results of both theoretical and experimental investigation of the heat exchanger will be discussed in this chapter. The discussion includes the flow and heat transfer characteristics of fluid flow in the three dimensional single U-tube heat exchanger. It's tried to cover all aspects that may affect thermal and hydraulic performance of U-tube heat exchanger; since the computations of this thesis include study the effect of the angle baffles of inclination, Baffles height, Number of baffles, Hydraulic diameter of tube and using nanofluid for different volume concentrations with different Reynolds numbers.

First verification is made to be sure that the present numerical model is working properly by comparing specific results with numerical results from same literature.

Table 5.1 below indicates the ranges of values of parameters studied in this work.

Table 5.1 Ranges of parameters values which were studied

Parameter	Value
inclination angle of baffles (α)	(45º - 0º - º45 and without baffles)
Baffles height (Bh)	(10 - 20 - 30) mm
Number of baffles (Nb)	3 - 5 - 8
Hydraulic diameter of tube (d_h)	(16.91 - 19.9 - 26.04) mm
volume concentrations of nanofluids (Φ)	(2 - 5 - 10) %
Re_{sh}	150 - 500 - 1000 - 1500 - 2000
Re_t	400 - 800 - 1200 - 1600 - 2000

5.2 Grid Independence

Grid independence test is one of the most important test which should be done in numerical analysis of the problem. Grid independence test was done to check that the final results that should be independent of the number of grids. In numerical problem the results are always dependent on the number of grids generated. So if we change the number of grids the results well be changed. While with changing the number of grids a stage may come when the results are independent of the number of grids. These minimum number of grids after which there is no change in results are observed known as optimum grid size and the results are independent of grids. The properties considered for checking the grid independence are at temperature of cold and hot fluid at the outlet.

In Fig. 5.1 show two graphs for outlet fluid temperatures were taken in Y axis and number of grids in X axis. The grids divisions are increased corresponding to the temperature of the hot fluid in Fig. (5.1.a) and outlet of the cold fluid temperature in Fig. (5.1.b) are shown. After 1942789 numbers of divisions the results not independence on grids hence the more than result is grid independent.

5.3 Validation of Numerical Model

To check the validity of the present numerical model, verification is made by comparing the results of the Gang Lei [19] reported in the literature with numerical results for the same model.

The verification is made by solving the work of Gang Lei [19] numerically by fluent and comparison the results with present results for the same model. The model of Gang Lei [19] a shell and tube heat exchanger consists of one pass tube with helical baffles. Oil as the working fluid. The Shell inside

diameter (110mm), tube outside diameter (19mm), tube pitch (25mm) and number of tube (9). The helical inclination angles various (15º, 20º, 30º, 40º, 45º, 50º), the numerical investigation has been performed for several shell-side Reynolds numbers ranging from 500 to 3500. The thermal boundary condition used constant temperature of 300 K applied at the inlet of the tubes. Constant mass flow rate is assumed in the flow direction rather than constant pressure drop.

The numerical results are obtained using the present model and that obtained by Gang Lei [19] shown in Fig. 5.2 which appear the variation of average Nussult number with shell Reynolds number for inclination angles baffle (15º). From this figure the agreement is excellent and the mean error is 1.2 % with maximum Nussult number difference.

From the previous verification, it can be concluded that, the present numerical model is reliable and can be used precisely to simulate and design the U-tube heat exchanger and study the role of various affecting parameters on thermal and hydraulic performance.

5.4 Numerical Analysis

This section includes details of computational results for the hydrodynamics and heat transfer characteristics of laminar flow through the shell and tube heat exchanger with different inclination angle of baffles, baffles height, number of baffles, Hydraulic diameter of tube and used nanofluid as mentioned in the next sections:

5.4.1 Hydrodynamic Characteristics with pure Fluid

In this section the results of hydrodynamic parameters (velocity and pressure) in counter flow U-tube heat exchanger will be presented. These parameters play an important role in the performance of U-THE. The heat

exchanger studied consists of shell and tube with dimensions and parameters values are listed in table 5.1.

Fig. 5.3 shows contour of the distribution of central plain velocity along the heat exchanger. From this figure can be seen that, the flow is developing and the central velocity in tube side increased in flow direction until reach its maximum value in the fully developed region. Also one can see the length of entrance region has considerable value compared with the length of U-tube due to short length of the shell.

Fig.5.4 presents contour of the fluid behavior as streamline velocity at Re_{sh}=2000, Nb=3 and Bh=30mm. Results show the effect of baffles on the hot fluid flow pattern. There is guidance for fluid flow by baffle which helps in a grueling movement around the tube and thus increase heat transfer between fluids. So the high velocity reach to 0.04 m/s outside the tube compared to surface far away from the tube.

Fig.5.5 illustrates the distribution of pressure drop along shell and tube heat exchanger unit at Re_{sh}=2000, α (0º), Nb=8 and Bh=30mm, for different values of Re with respect to pressure at inlet as a reference value. From this figure the pressure drop increased with length of shell due to the increasing resistance to the flow of fluid.

5.4.2 Thermal characteristics with pure fluid

In this section the thermal characteristic represented by temperature distribution is discussed, also the inlet temperatures of hot and cold fluids used are T_{hi} = 360 K and T_{ci} = 300 K respectively.

Fig. 5.6 shows the temperature distribution of hot fluids along U-tube heat exchanger with baffles angels α (+45º) at Re_{sh}= 150, Nb=5 and Bh=20mm. From this figure it can be seen that, the temperature of hot fluid decreased along the shell due to the transfer of heat from hot to the cold fluid through the separating wall. Also it can be seen that the trend of temperature change is similar for hot and cold fluids since both fluids have the same heat capacity. This distribution of temperatures is similar as for conventional counter flow heat exchangers.

The contour of a temperature distribution in entire heat exchange unit (U-tube heat exchanger) with baffles angels α (0º) at Re_{sh}= 150, Nb=8 and Bh=30mm is shown in Fig. 5.7. The shell contains a hot fluid while the cold fluid flow in the tube. As expected the temperature of hot fluid decreased with length along heat exchanger while the temperature of cold fluid increased in the opposite direction because the flow is counter-current. The temperature of the wall separating of tube is increased along the heat exchanger in flow direction of the hot fluid.

5.5 Performance Analysis

5.5.1 Hydrodynamic Performance

In this section the study of the hydrodynamic performance such as: average friction factor and pressure drop will be focused on the effect of baffles inclination angle, baffles height, baffles number, tube hydraulic diameter and volume concentrations of nanofluids.

Fig.5.8 shows the variation of shell side fluid pressure drop with shell Reynolds number for different baffle inclination angles (+45º, 0º, -45º) at Bh=20mm and Nb=5. It is clear that the fluid pressure drop increases with the increase of shell-side Reynolds number and its increase more evident in large

Re_{sh} range. It is very interesting to note that the effect of baffle inclination angle on the pressure drop is relatively large for inclination angle of baffle. The pressure drop increases with the increase of baffle inclination angle at positive direction and decrease at negative direction. For the shell-side Reynolds number of 2000, the pressure drop increases (12.18%,16.17% and 7.03%) when baffle inclination angle varying (+45, 0, -45) respectively, comparing with case without baffles. It is understood that the increasing of inclination angle is more effective for decreasing pressure drop in higher shell-side Reynolds number region.

It can also be seen from Fig.5.9 and Fig.5.10 the variation of shell side fluid pressure drop with shell Reynolds number for different height and number of baffles at α=0˚. It is seen from this figure that, the shell-side pressure drop increases when the number and height baffle increases. It means that, the increases due to the increasing resistance to the flow of fluid. Also the pressure drop increase with increase Reynolds number due to increase the velocity of flow, and the increases in the number and height of baffle to decrease the hydraulic diameter of shell side. This is related to the fact that forcing the liquid to flow through a small hydraulic diameter shell produces a higher pressure drop compared to large hydraulic diameter.

Fig.5.11 shows the variation of fluid average friction factor of tube side with tube Reynolds number for different values of tube hydraulic diameter at α=0˚, Nb=5 and Bh=25mm. As seen in this figure, the friction factor decreases with increasing tube Reynolds number for all range of selected hydraulic diameter, due to increase of the velocity. Also, the results show that the friction factor increases when the hydraulic diameter increased due to the obstruction of the flow by the larger diameter, which produce a smaller pressure drop, thereby increasing the flow frictional resistance.

Fig.5.12 illustrates the variation of tube side fluid pressure drop with tube Reynolds number for different values of tube hydraulic diameter at α=0˚and

Nb=5 and Bh=25mm. From this figure it can be seen that, the water pressure drop increases when the diameter of tube decreased leads to decrease the hydraulic diameter of fluid flow. This related to the fact that forcing the liquid to flow through a small hydraulic diameter tube produces a higher pressure drop compared to large hydraulic diameter. Therefore, for all the value of tube hydraulic diameter the pressure drop increased with increase tube Reynolds number, due to increase the velocity of flow, according to equation (3.10).

Fig.5.13 represents the variation of fluid pressure drop across tube side with tube Reynolds number for different volume concentrations at α=0˚, Bh=25mm and Nb=5. From this figure the fluid pressure drop increased with increased volume concentrations of nanofluid which is due to increase its viscosity. Also, there is a small difference between pressure drop in pure water and Al_2O_3-water nanofluid in 2% volume concentration which is due to the difference in density and viscosity between them.

The percentage pressure drop increase associated with using three volume concentrations nanofluid compared with pure water is 15.1% for volume concentrations 10% ,10.1% for 5% and 3.9% for 2 % at Re_t=2000.

5.5.2 Thermal Performance

5.5.2.1 Effect of inclination angle of baffles

One of the important parameters which have a considerable effect on both of hydrodynamic and thermal performance of U-tube heat exchanger is the inclination angle of baffles. Therefore, this study aimed to investigate the effect of inclination angle of baffles on the performance of this heat exchanger.

The comparison between the effects of inclination Angle is performed for the same values of Bh, Nb and Re_{sh}. The values of parameters and dimensions are indicated in table 5.2 below.

Table 5.2 values of parameters used

Parameter	Value
α	+45º , 0º , -45º, without
Bh	20mm
Nb	5
d_h	16.91mm
Re_{sh}	150 - 2000
T_{hi}	360 K
T_{ci}	300 K

Fig. 5.14 indicates the variation of average Nussult number of shell side with shell Reynolds number for different inclination angles baffle (+45˚, 0˚, -45˚) and without baffles at Bh=20mm and Nb=5. From this figure it is clear that, the Nussult number increases when shell Reynolds number increase too for all range of varying baffle angles. The Nusselt number for inserted baffles is higher than that of the smooth tube without baffles. Because the presence of inserted circular baffles causes the dispersion and random movement of the flow field leads to higher heat transfer rate. In addition, it limits the growth of fluid boundary layer close to the heat transfer surface caused by periodic disruption of the layer due to repeated changes in the flow direction. The Nusselt number for α > 0˚ i.e. at negative direction to the flow is lower than those of other tubes for α < 0° i.e. at positive direction to the flow. Whereas the Nusselt number of the shell side when α=0° is the highest due to increase the circulation which leads to larger heat transfer coefficient according to equation 3.11.

Fig. 5.15 illustrates the effect of baffles inclination on the average overall heat transfer coefficient at various shell side Reynolds numbers at Bh=20mm and Nb=5. From this figure can see that, the average overall heat transfer coefficient increases significantly for all case with increase shell Reynolds

number as a result of enhance heat transferred due to the higher convection at high Reynolds number.

The maximum percentage in enhancement of the average overall heat transfer coefficient results from using three inclination angle baffles (+45˚, 0˚, -45˚) and without baffles compared with that case without baffles is 7.09% at α=0˚, 5.66% for α=+45˚and 3.5% for α=-45˚ at Re_{sh}=2000.

Fig. 5.16 shows the variation of heat exchanger effectiveness with shell side Reynolds number for different baffle inclination angle (+45˚, 0˚, -45˚) and without baffles at Bh=20mm and Nb=5. From this figure it can be seen that, the effectiveness for all cases increase with increase the Reynolds number of shell side. It indicates that the effectiveness at α=0˚ is optimum angle baffle. This may be attributed to resistance that obtained from the right angle (0˚) which gives more time for heat exchange between solid and hot fluid. The modification in the effectiveness at α=0˚for different values of Re compared with and without baffles indicated in table 5.3 below.

Table 5.3 Enhancement in (ε) with Re_{sh} at α=0°

Re_{sh}	$[\frac{\varepsilon_{\alpha=0^0} - \varepsilon_{without}}{\varepsilon_{without}}]x\ 100\%$
100	4.733%
500	6.15%
1000	7.361%
1500	8.55%
2000	9.38%

Fig. 5.17 illustrates the variation of number of transfer unit (NTU)with shell side Reynolds numbers for three cases of baffle inclination angle (+45˚,

0˚, -45˚) and without baffles at Bh=20mm and Nb=5. It's clear that the number of transfer unit increases with increase Reynolds number for all cases. Also the number of transfer unit increases with the increased of angle inclination at positive direction to the flow, which is due to increase overall heat transfer according to equations (3.23).

Fig 5.18 illustrated the variation of total heat transfer rate at various shell side Reynolds number for three inclination angle baffles (+45˚, 0˚, -45˚) and without baffles at Bh=20mm and Nb=5. From this figure the heat exchanged between hot and cold fluids increased with increase shell Reynolds number due to the increase of flow rate which leads to increase the heat transfer rate. The increase in heat transfer rate is higher at α=0˚while it's smaller at without baffles i.e. the heat transfer rate increase with inclination angle baffles at positive direction to the flow and decreases in negative direction for flow. Due to increase the circulation which leads to higher heat transfer rate between the two fluids.

The percentage increase in heat transfer rate results from using of the three inclination angle baffles compared with that case without baffles is 9.38% for α=0˚, 8.14% for α= +45˚ and 4.95% for α= -45˚ at Reynolds number 2000.

5.5.2.2 Effect of baffles height

In this section the evaluation of the effect of baffles height on the performance is carried out. In this investigation of the heat exchanger with the same angle and number of baffles. The values of parameters are indicated in table 5.4 below.

Table 5.4 values of parameters used

Parameter	Value
α	0º
Bh	(10, 20, 30) mm
Nb	5
d_h	16.91mm
Re_{sh}	150 - 2000
T_{hi}	360 K
T_{ci}	300 K

Fig. 5.19 indicates the variation of average Nusselt number of shell side with shell Reynolds number for different baffles height at α=0˚and NB=5. From this figure it is clear that, the Nusselt number increases when shell Reynolds number increased for all range of baffles height. Also the Nusselt number of the shell side when Bh=30mm is the highest due to increasing the disability which leads to larger heat transfer coefficient according to equation (3.11). However, the increase baffle height it causes higher degree of turbulence is created and hence the heat transfer coefficient increases as the baffle height increased.

Fig. 5.20 illustrates the effect of baffles height on the average overall heat transfer coefficient at various shell side Reynolds number at α=0˚and NB=5. From this figure one can see that, the average overall heat transfer coefficient increases significantly for all case with the increase of shell side Reynolds number as a result of enhance heat transferred due to higher convection at higher Reynolds number.

The maximum percentage in enhancement of average overall heat transfer coefficient results from using three cases of baffles height compared with the case of Bh=10mm is 5.53% at Bh=30mm and 3.46% for Bh=20mm at Re_{sh}=2000.

Fig. 5.21 shows the variation of heat exchanger effectiveness with Reynolds number for different baffles height at α=0˚and NB=5. From this figure it can be seen that, the effectiveness for all cases increase with increase Reynolds number of shell side. The increase of effectiveness with increasing baffles height is due to increase the disability which leads to larger heat transfer rate between the two fluids. Also the increasing in effectiveness in case of Bh=30mm is larger than the remaining cases. The modification in the effectiveness at Bh=30mm for different values of Re compared with case Bh=10mm indicated in table 5.5 below.

Table 5.5 modification of (ε) with Re_{sh}

Re_{sh}	$[\frac{\varepsilon_{Bh=30} - \varepsilon_{Bh=10}}{\varepsilon_{Bh=10}}]x\ 100\%$
100	4.06%
500	5.39%
1000	6.01%
1500	6.03%
2000	6.74%

Fig. 5.22 illustrates the variation of the number of transfer unit with shell side Reynolds number for three cases of baffles height at α=0˚and NB=5. It's clear that the number of transfer unit increases with increase Reynolds number for all cases. The number of transfer unit increases with increased baffles height which is due to increase overall heat transfer according to equation (3.23). The increasing in NTU in the case of Bh=30mm is larger than in all case which is due to the higher disability of than the remaining cases.

Variation of heat transfer rate at various shell side Reynolds number for different baffles height at α=0˚and NB=5 is illustrated in Fig. 5.23. From this figure, it can be seen that the increase in heat transfer rate is high at Bh=30mm while it's small at Bh=10mm, i.e. the heat transfer rate increase with baffles height. Due to increase the disability which leads to larger heat transfer rate between the two fluids. Also, the heat exchange between the hot and cold fluids increases with increase Reynolds number due to increase the flow rate which leads to increase the heat transfer rate.

The percentage increase in heat transfer rate results from using of the three cases of baffles height (10mm, 20mm, 30mm) compared with that case for Bh=10mm is 0.0671 for Bh=30mm and 0.0421 for Bh=20mm at Re_{sh}=2000.

5.5.2.3 Effect of Baffles Number

In this section, the study is made to investigate the effect of the number of baffles on the performance of U-tube heat exchanger. The U-tube heat exchanger used in this section with dimensions and values of parameters is the same as listed in table 5.1 in addition to the values listed in table 5.6 below.

Table 5.6 values of parameters used

Parameter	Value
α	0º
Bh	30mm
Nb	3-5-8
d_h	16.91mm
Re_{sh}	150 – 2000
T_{hi}	360 K
T_{ci}	300 K

Fig. 5.24 indicates the variation of the average Nusselt number of shell side with shell Reynolds number for different baffles number at α=0˚and Bh=30mm. From this figure, it is clear that the Nusselt number increases when shell Reynolds number increases for all range of baffles number. Whereas the Nusselt number of the shell side when Nb=8 is the highest due to increasing the disability which leads to larger heat transfer coefficient. However, the baffle number increases a higher degree of turbulence is created and hence the heat transfer coefficient increases as the baffle number and baffle height increases.

Fig. 5.25 illustrates the effect of baffles number on the average overall heat transfer coefficient at various shell side Reynolds number at α=0˚and Bh=30mm. From this figure, one can see that, the average overall heat transfer coefficient increases significantly for all case with increase shell side Reynolds number as a result of enhancing heat transferred due to higher convection at higher Reynolds number.

The maximum percentage of an enhancement of the average the overall heat transfer coefficient results from using three cases of baffles number compared with case Nb=3 is 13.8% at Nb=8 and 5.87% for Nb=5 at Re_{sh}=2000.

Fig. 5.26 shows the variation of heat exchanger effectiveness with Reynolds number for different baffles number at α=0˚and Bh=30mm. From this figure, it can be seen that the effectiveness for all cases increases with increase Reynolds number of shell side. The increase of effectiveness with increased number of baffles is due to the increase of the circulation which leads to larger heat transfer rate between the two fluids. Also, the increasing in effectiveness in case of Nb=8 is larger than the remaining cases. The modification in the effectiveness at Nb=8 for different values of Re compared with case Nb=3 indicated in table 5.7 below.

Table 5.7 modification in (ε) with Re_{sh}

Re_{sh}	$[\frac{\varepsilon_{Nb=8} - \varepsilon_{Nb=3}}{\varepsilon_{Nb=3}}]x\ 100\%$
100	3.98%
500	5.72%
1000	6.65%
1500	7.47%
2000	7.94%

Fig. 5.27 illustrates the variation of number of transfer unit(NTU) with shell side Reynolds number for three cases of baffles number at α=0˚and Bh=30mm. It's clear that the number of transfer unit increases with increase Reynolds number for all cases. Also the increasing in NTU in case of Nb=8 is larger than the remaining cases which are due to the increase of overall heat transfer coefficient.

Variation of heat transfer rate at various shell side Reynolds number for different baffles number at α=0˚and Bh=30mm is illustrated in Fig. 5.28. From this figure, the heat exchanged between hot and cold fluids increased with increased Reynolds number due to increasing the flow rate which leads to increase the heat transfer rate. The increase in heat transfer rate is higher at Nb=8 while it's smaller at Nb=3, i.e. the heat transfer rate increase with baffles number due to increasing the disability which leads to larger heat transfer rate between the two fluids.

The percentage increase in heat transfer rate results from using of the three cases of baffles number (3, 5, 8) compared with that case for Nb=3 is 7.9% for Nb=8 and 4.8% for Nb=5 at Re_{sh}=2000.

5.5.2.4 Effect of tube diameter

The aim of this section is to study the effect of tube diameter on thermal performance of U-tube heat exchanger. The heat exchange unit studied in this section consists of U-tube with values of dimensions and parameters indicated in table 5.8 below.

Table 5.8 Values of parameters used.

Parameter	Value
α	0º
Bh	25 mm
Nb	5
d_h	(16.91 - 19.9 - 26.04) mm
Re_t	400 – 2000
T_{hi}	360 K
T_{ci}	300 K

Fig. 5.29 shows the variation of average Nusselt number of tube side with tube Reynolds number for different diameter of tube at α=0˚and Nb=5, Bh=25mm. From this figure, it can be seen that the Nusselt number increases with increasing of tube Reynolds number for all range of selected hydraulic diameter. This is due that the increment in the tube Reynolds number yields an improvement in the convection coefficient of the heat exchanger. It is also found that, the Nusselt number increases when hydraulic diameter increased. This is due to increasing the tube diameter leads to increase the area of the thermal contact surface between the two fluids. Also, the increment in the tube diameter permits a greater water flow across the heat exchanger which reinforces the cooling capacity of the walls. Therefore, this behavior is attributed to the enhancing the heat transfer rate.

Variation of average overall heat transfer coefficient of tube side with tube Reynolds number for different diameter of tube at α=0˚and Nb=5, Bh=25mm is illustrated in Fig.5.30. From this figure, one can see that the average overall heat transfer coefficient increases significantly for all case with increase tube Reynolds number as a result of enhance heat transferred due to higher convection at higher Reynolds number. As clearly shown in fig. (5.30), the maximum enhancement of the overall heat transfer coefficient of three cases of the different hydraulic diameter of tube occurs at dh=16.9mm which is due to the higher heat transfer coefficient than the remaining cases.

Fig. 5.31 shows the variation of heat exchanger effectiveness with Reynolds number for different diameter of the tube at α=0˚and Nb=5, Bh=25mm. From this figure, one can find that the effectiveness decreased with increase Reynolds number of tube side due to increasing the velocity of flow and then decreases the residence time taken by the certain amount of fluids inside heat exchanger and therefore reduce the temperature change of both fluids. The increase of effectiveness with decrease hydraulic diameter is due produces a higher velocity, which leads to increase convection coefficient.

The maximum percentage in enhancement of heat exchanger effectiveness results from using different hydraulic diameter compared with case d_h=26.04 is 25.9% for hydraulic diameter d_h=16.9mm and 18.9% ford_h=19.9mm at Re_t=2000.

Fig. 5.32 illustrates the variation of the number of transfer unit with tube Reynolds number for different diameter of the tube at α=0˚and Nb=5, Bh=25mm. It's clear that the number of transfer unit decreased with increase Reynolds number for all cases due to increase overall heat transfer. Also the number of transfer increases with decrease hydraulic diameter of the tube which is due to produces a higher velocity, which leads to increase heat

transfer coefficient. The maximum enhancement of the number of transfer unit for different hydraulic diameter is d_h=16.9mm.

Fig. 5.33 illustrates the effect of hydraulic diameter of tube on the heat transfer rate with various Reynolds number at α=0˚and Nb=5, Bh=25mm. As shown in fig. 5.33, it's clear that the heat exchanged between two fluids increased with increase Reynolds number of tube side due to increase flow rate the heat transfer is directly proportional to the flow rate. Also, the heat transfer rate with case d_h=26.04mm is larger than the remaining cases is due to the increase the area of the thermal contact surface between the two fluids.

The enhancement of the heat transfer rate for three cases of hydraulic diameter compared with case d_h=16.9mm is 0.22 for d_h=26.04mm and 0.116 for d_h=19.9mm at Re_t=2000.

5.5.2.5 Effect of nanofluid

The aim of this study is to modify the thermal performance by using nanofluid as the cooling medium and to investigate the effect of thermal conductivity of additives in nanofluid on its cooling abilities.

In this thesis one of the nanofluid are used in the calculations Al_2o_3-water to modify the thermal performance of a U-tube heat exchanger under consideration. The advantages of nanofluid is to enhance the heat transfer with a little penalty of increase the pressure drop due to the small volume fractions of ultra-fine particle used.

The heat exchange unit under consideration consists of α=0º, Nb=5 and Bh=25mm. The simulation is made first using pure water and then repeated with nanofluid for different volume fractions for Al_2o_3-water nanofluids studied. Other required values of parameters and dimensions of channels are listed in table 5.9 below.

Table 5.9 values of parameters

Parameter	Value
α	0°
d_h	19.9mm
Bh	25mm
Nb	5
Re_t	400-2000
Φ	(0, 2, 5, 10) %
T_{hi}	360 K
T_{ci}	300 K

The comparisons are made between different cases of volume concentrations with case pure water. The properties of pure water and nanofluid are shows in table 3.2.

Fig. 5.34 indicate the variation of average heat transfer coefficient of tube side with tube Reynolds number for different volume concentrations at α=0˚and Nb=5, Bh=25mm. From this figure, it can be seen that the heat transfer coefficient increased with increasing the Reynolds number. The increase of heat transfer coefficient with increased volume concentrations is due to increase the thermal conductivity of nanofluid according to table 3.3. Also, the increasing in heat transfer coefficient in case of volume concentrations 10% is larger than in all case which is due to the higher thermal conductivity of than the remaining cases.

The percentage increase in heat transfer coefficient results from using of the three volume concentrations nanofluid compared with that for pure water is 17.57% for 10%, 11.22% for 5% and 6.01% for 2% at Re_t=2000.

Variation of average overall heat transfer coefficient of tube side with tube Reynolds number for different volume concentrations at α=0˚and Nb=5, Bh=25mm is illustrated in Fig. 5.35. From this figure, one can see that the average overall heat transfer coefficient increases significantly for all case with increase tube Reynolds number as a result of enhancing heat transferred due to higher convection at higher Reynolds number. The overall heat transfer coefficient at a constant Reynolds number increases with nanoparticle concentration compared to the pure fluid. As clearly shown in fig. (5.35), the maximum enhancement of the overall heat transfer coefficient of Al_2o_3-water nanofluid occurs at 10 % volume concentration.

Fig. 5.36 shows the variation of heat exchanger effectiveness with Reynolds number for different volume concentrations at α=0˚and Nb=5, Bh=25mm. From this figure, one can find that the effectiveness decreased with increase Reynolds number due to increasing the velocity of flow and then decreases the residence time taken by the certain amount of fluids inside heat exchanger and therefore reduce the temperature change of both fluids. The increase of effectiveness with increased volume concentrations is due to increase the thermal conductivity of nanofluid. Also, the increase in effectiveness in case of 10% volume concentrations Al_2o_3-water is larger than in pure water which is due to the higher thermal conductivity of Al_2o_3-water than pure water.

The maximum percentage in the enhancement of heat exchanger effectiveness results from using nanofluid compared with pure water is 13.8% at volume concentrations 10 %, 5.87% for 5% and 2.38% for 2% at Re_t=2000.

Fig. 5.37 illustrates the variation of the number of transfer unit with tube Reynolds number for different volume concentrations at α=0˚and Nb=5, Bh=25mm. It's clear that the number of transfer unit increases with increased Reynolds number for all cases. Also, the number of transfer increases with

increased volume concentrations of particles which is due to increase thermal conductivity. The maximum enhancement of the number of transfer unit for nanofluid is particularly significant at their optimum with nanoparticle concentrations 10%.

Fig. 5.38 illustrates the effect of nanoparticles concentrations on the heat transfer rate of the nanofluid at various Reynolds number. As shown in figs. 5.38, it's clear that the heat exchanged between two fluids increased with the increase of volume concentrations of particles. Also, the heat transfer rate with using Al_2o_3-water is larger than that for using pure water is due to the higher thermal conductivity of Al_2o_3-water than pure water. The enhancement of the heat transfer rate for nanofluid is particularly significant at their optimum nanoparticle concentrations 10% and its value 6.5% at Re_t=2000.

5.6 Experimental Analysis

In this part, the experimental results are presented which include the parameters that affect the heating process in the U-tube heat exchanger. These parameters are volume flow rate and the inclination angle of baffles.

Fig. 5.39 shows the variation of heat exchanger effectiveness with the volume flow rate of hot water for the different inclination angle of baffles at Nb=5 and Bh=20mm. From this figure, one can see that the effectiveness increased with the increase of volume flow rate of hot water. This refers to the large hot Reynolds number which attributed to the higher velocity leading too to enhance the heat transfer rate between two fluids. Also, the α=0º beast inclination baffles angle due to increasing the circulation which leads to larger heat transfer rate between the two fluids.

Fig. 5.40 illustrates the variation of the number of transfer unit for experimental results with the volume flow rate of hot water for three cases of the inclination angle of baffles at Bh=20mm and NB=5. It's clear that the number of transfer unit increases with increasing volume flow rate for all cases is due to increase overall heat transfer according to equation (4.5). Also, the increasing in NTU in case of α=0º is larger than in all case which is due to the higher disability of than the remaining cases.

Fig. 5.41 indicates the variation of the total heat transfer rate with different values of the volume flow rate of hot water for the different inclination angle of baffles at Nb=5 and Bh=20mm. It can be noticed that the heat transfer rate increases as the volume flow rate increases. This is due to increase in temperature difference of hot water between the inlet and the outlet, then leads to higher heat transfer rate.

5.7 Validation of the present model with experimental results

A comparison is made between the results obtained from the current numerical model by using Fluent and experimental results involving for U-tube heat exchanger and shown in Fig. 5.42 to 5.50 respectively in order to check the validation of the present model for U-tube heat exchanger.

Fig. 5.42 illustrates the variation of the effectiveness with different values of the volume flow rate of hot water for α=0º Bh=20mm and Nb=5. A comparing the experimental results with the results obtained from the numerical analysis. As shown in this figure that the effectiveness increases as volume flow rate increases. This refers to the large volume flow rate which attributed to the higher velocity leading too to enhance the heat transfer rate between two fluids. This figure indicates that the numerical results are in close agreement with experimental results and the maximum relative error is 7.9%.

Fig. 5.43 indicates the variation of effectiveness of heat exchanger with different values of volume flow rate of hot water for α=+45º Bh=20mm and Nb=5. A comparison between the experimental results with the results obtained from numerical is analyzed. As seen in the figure, that the effectiveness increases with increases of the volume flow rate of hot water. This behavior is due to increase the velocity of flow and then enhance the heat transfer rate between two fluids. It can be decided that the numerical results correlate well with experimental results and the maximum relative error is 8.7%.

Fig. 5.44 indicates the variation of the effectiveness with different values of volume flow rate of hot water for α= -45º Bh=20mm and Nb=5. A comparing the experimental results with the results obtained from the numerical analysis. As shown in this figure that the effectiveness increases as volume flow rate increases. This refers to the large volume flow rate which attributed to the higher velocity leading too to enhance the heat transfer rate between two fluids. This figure indicates that the numerical results are in close agreement with experimental results and the maximum relative error is 9.4 %.

Fig. 5.45 to 5.47 illustrates the variation of number of transfer unit (NTU) with shell side volume flow rate for three cases of baffle inclination angle (+45˚, 0˚, -45˚) at Bh=20mm and Nb=5. It's clear that the number of transfer unit increases with increasing volume flow rate for all cases. Also the number of transfer increases with increased angle inclination at the positive direction to the flow, which is due to increase overall heat transfer according to equations 4.5.

When the baffle inclination angle is α=+45º and volume flow rate is (3 L/m) the number of transfer unit results obtained experimentally were found approximate to theoretical results by about (9.7%), by about (8.9%) when the

baffle inclination angle is α= 0º and by about (11.1%) when the baffle inclination angle is α=-45º.

Fig. 5.48 to 5.50 illustrated the variation of total heat transfer rate at the various shell side volume flow rate for three inclination angle baffles (+45˚, 0˚, -45˚) at Bh=20mm and Nb=5. From this figure the heat exchanged between hot and cold fluids increased with increase shell volume flow rate due to increase the flow rate which leads to increase the heat transfer rate. The increase in heat transfer rate is higher at α=0˚while it's smaller at α=-45ºi.e. the heat transfer rate increase with inclination angle baffles at the positive direction to the flow and decrease in the negative direction for flow due to increasing the circulation which leads to larger heat transfer rate between the two fluids.

When the baffle inclination angle is α=+45º and volume flow rate is (3 L/m) the heat transfer rate results obtained experimentally were found approximate to theoretical results by about (11.2%), by about (10.3%) when the baffle inclination angle is α= 0º and by about (12.5%) when the baffle inclination angle is α=-45º.

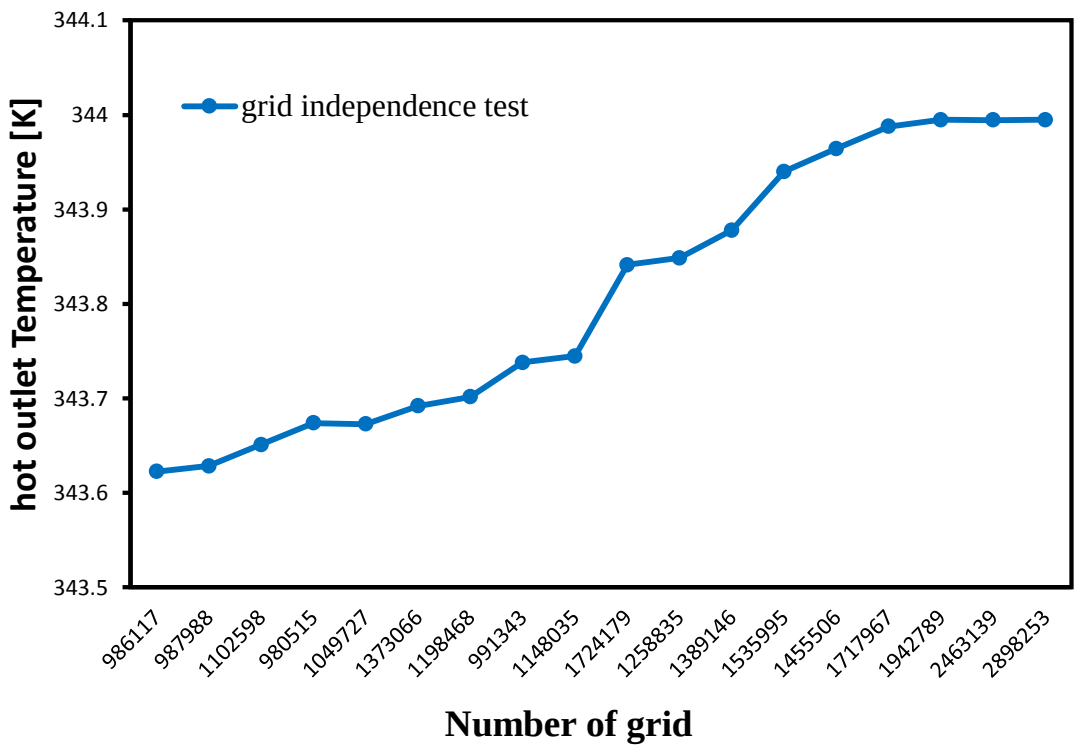

Fig. (5.1.a) grid independence test based on the outlet of hot fluid temperature

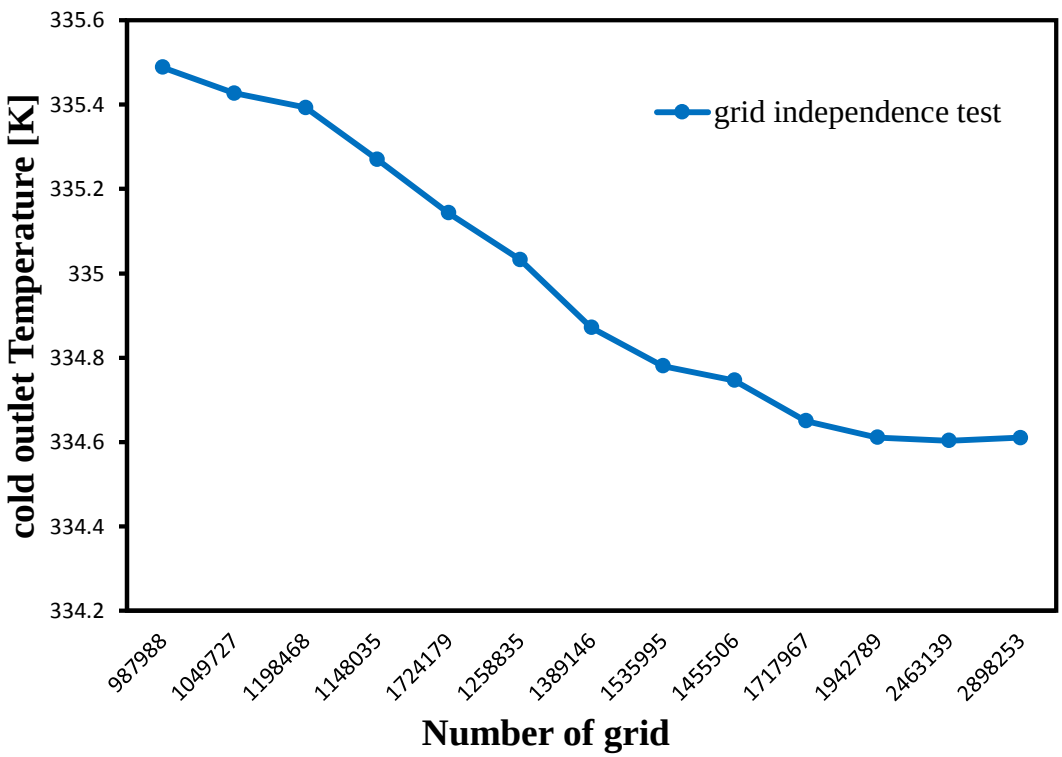

Fig. (5.1.b) grid independence test based on the outlet of cold fluid temperature

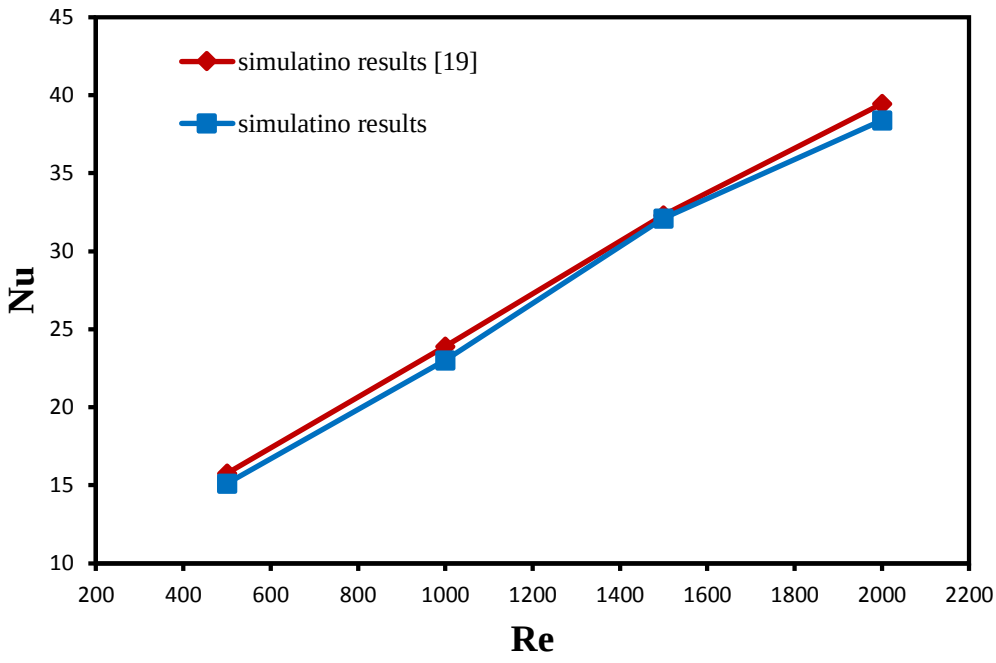

Fig. 5.2 Comparison of the present results with the results of Gang Lei [19] Variation of average Nusselt number with Reynolds number of shell.

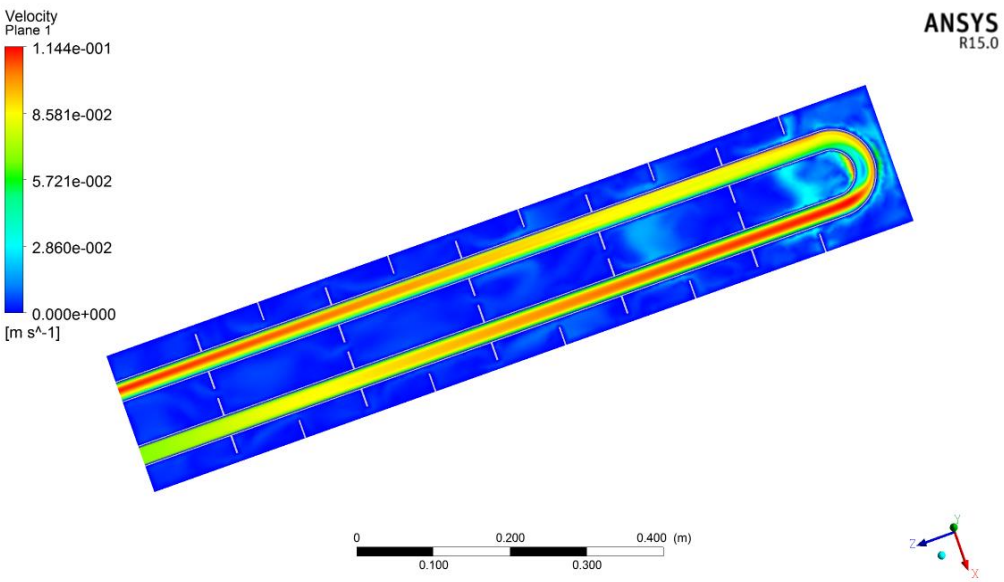

Fig. 5.3 Velocity contour for along the heat exchanger at Re_{sh}=2000, α=0º, Nb=5 and Bh=30mm.

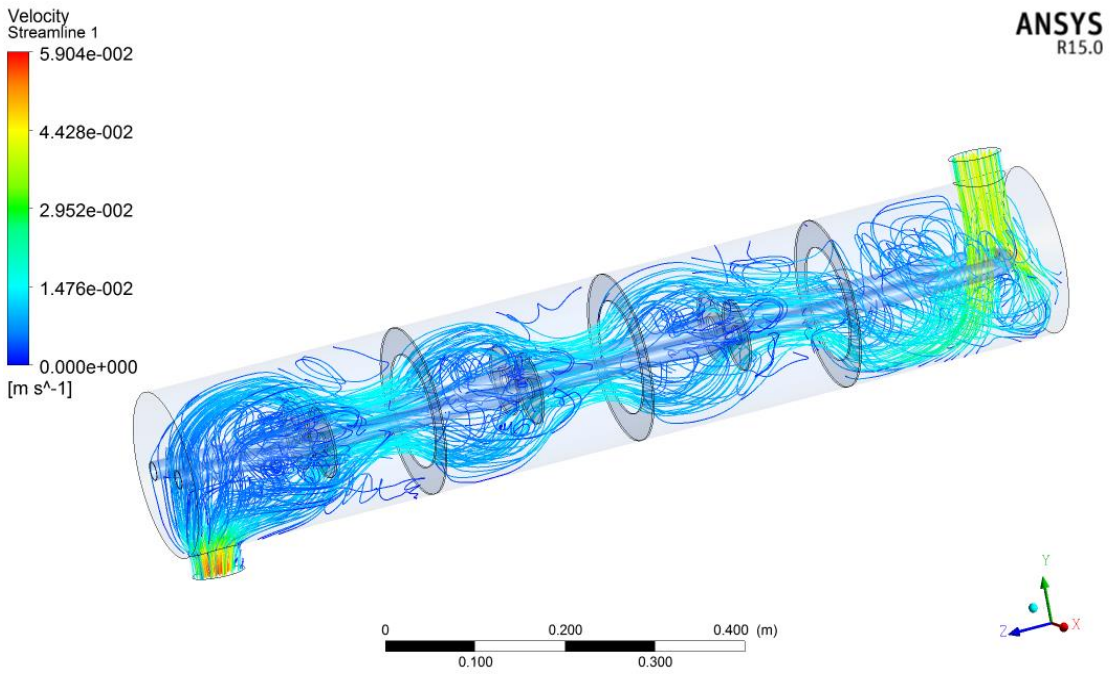

Fig. 5.4 Hot fluid velocity streamline distribution with vertical baffles at Re_{sh}=2000, α=0º, Nb=3 and Bh=30mm.

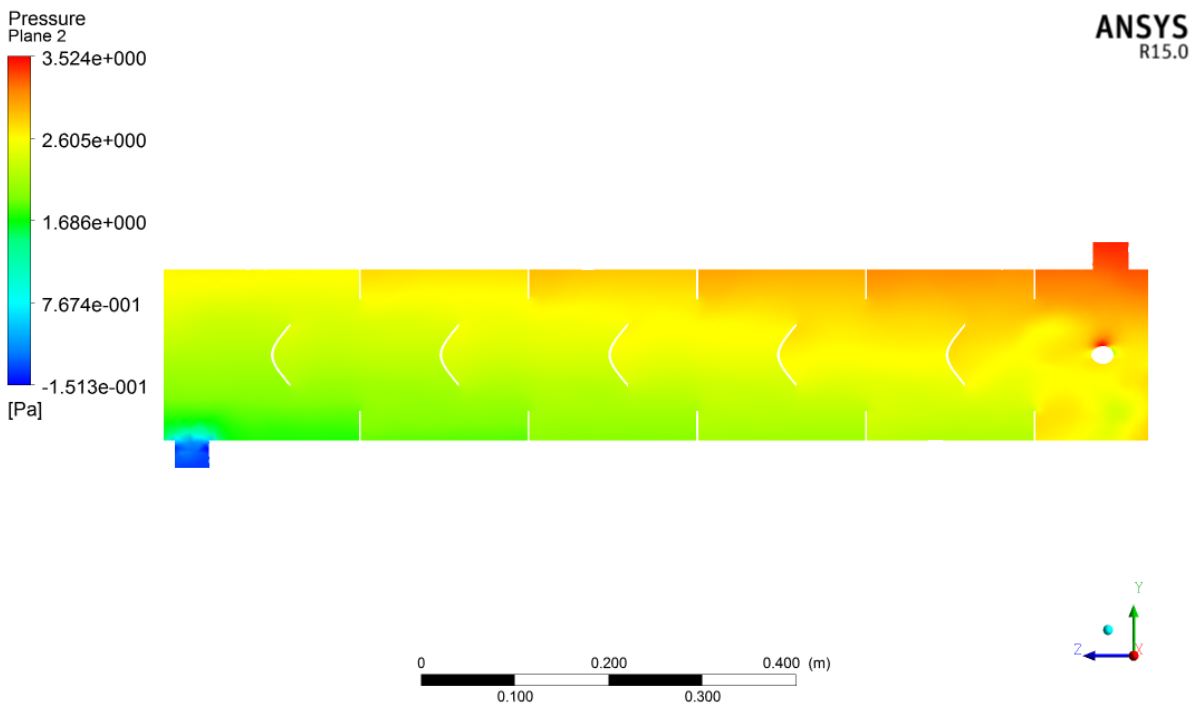

Fig. 5.5 Static pressure distribution contour for along the heat exchanger at Re_{sh}=2000, α=+45º, Nb=5 and Bh=20mm.

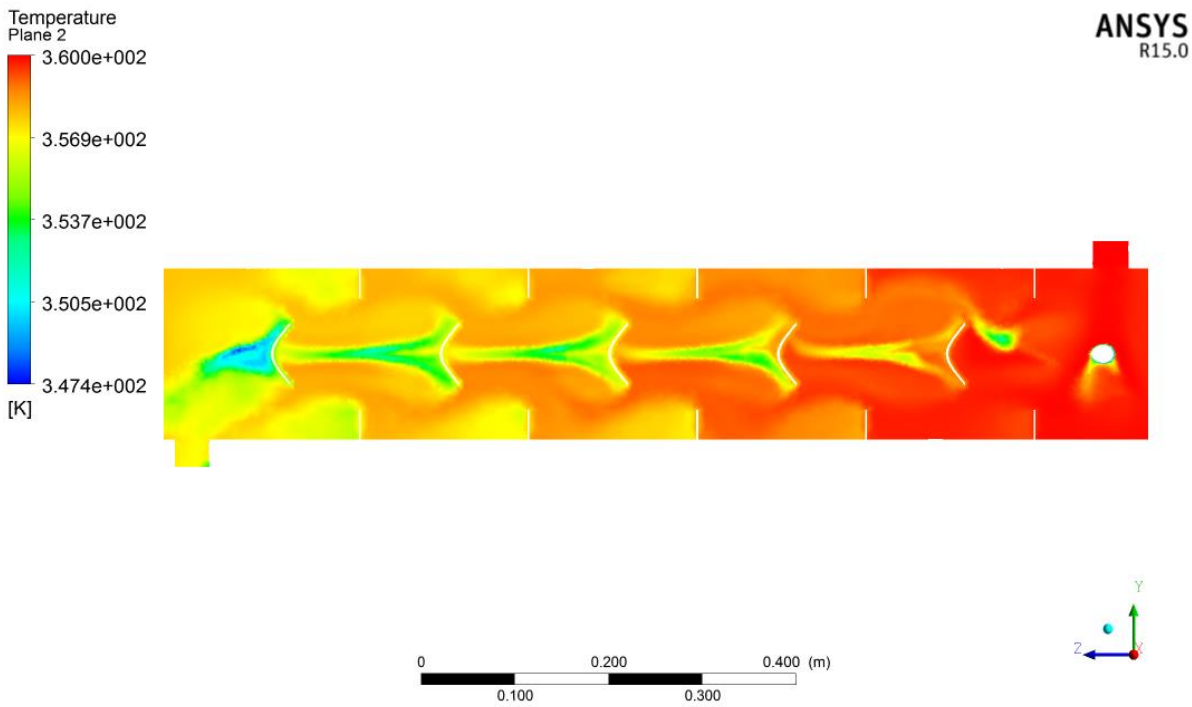

Fig. 5.6 Temperature distribution contours at center plane of hot water at α=+45º, Nb=5 and Bh=20mm

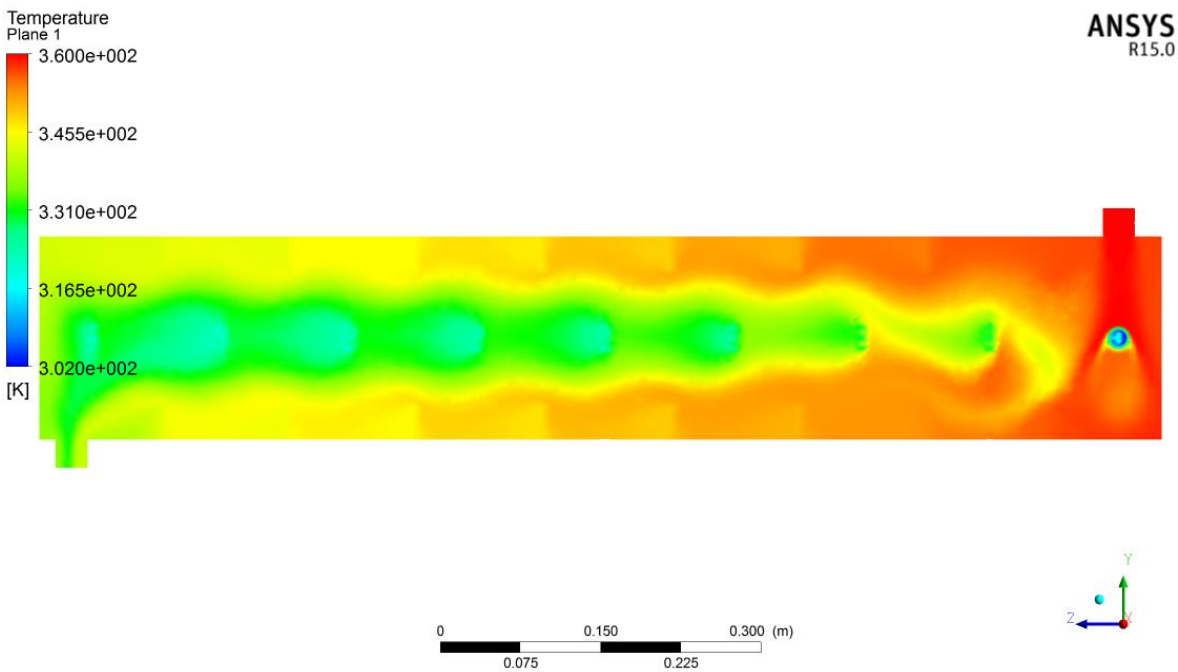

Fig. 5.7 Temperature distribution contours at center plane of hot water at α=0º, Nb=8 and Bh=30mm

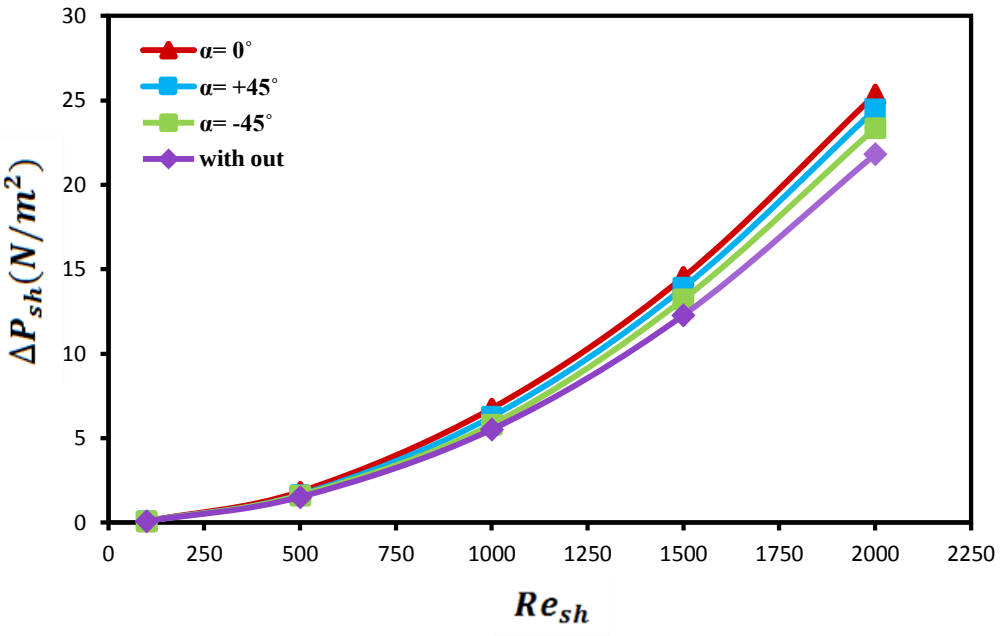

Fig. 5.8 Variation of shell side pressure drop with shell Reynolds number for different inclination of angle baffle(α) at Bh=20mm, Nb=5 T_{ci}=300K and T_{hi}=360K.

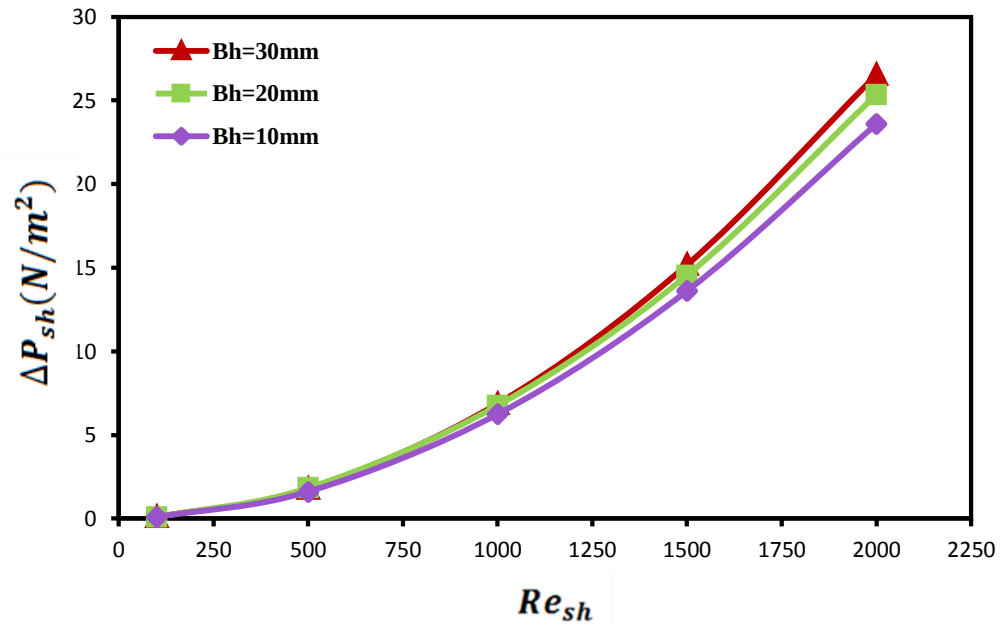

Fig. 5.9 Variation of shell side pressure drop with shell Reynolds number for different baffle height at α (0˚), dh=16.9mm, T_{ci}=300K and T_{hi}=360K.

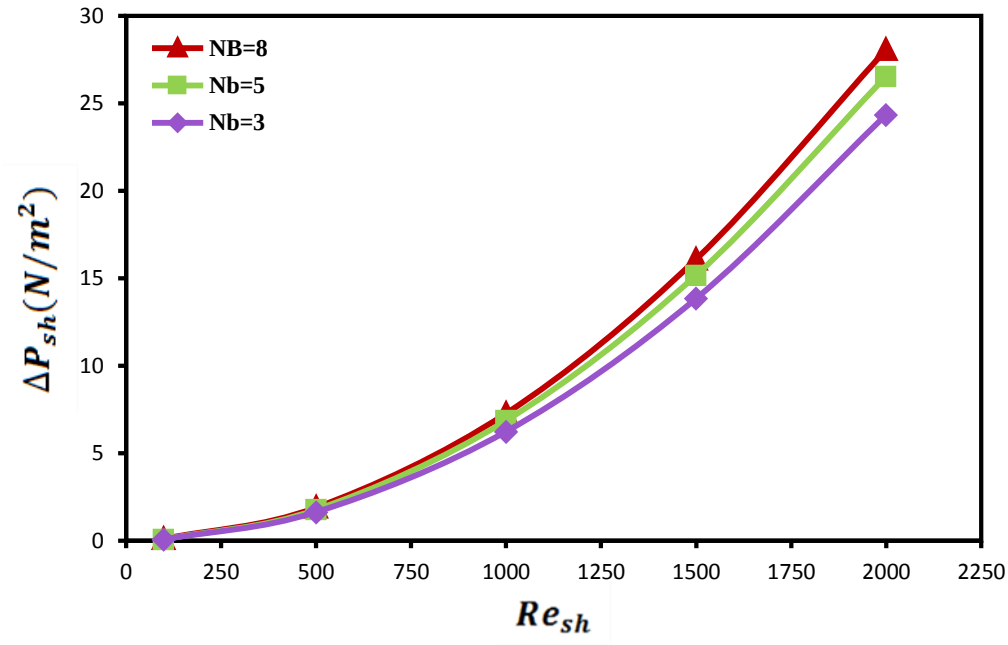

Fig. 5.10 Variation of shell side pressure drop with shell Reynolds number for different baffle number at α (0˚), Bh=30mm, dh=16.9mm, T_{ci}=300K and T_{hi}=360K.

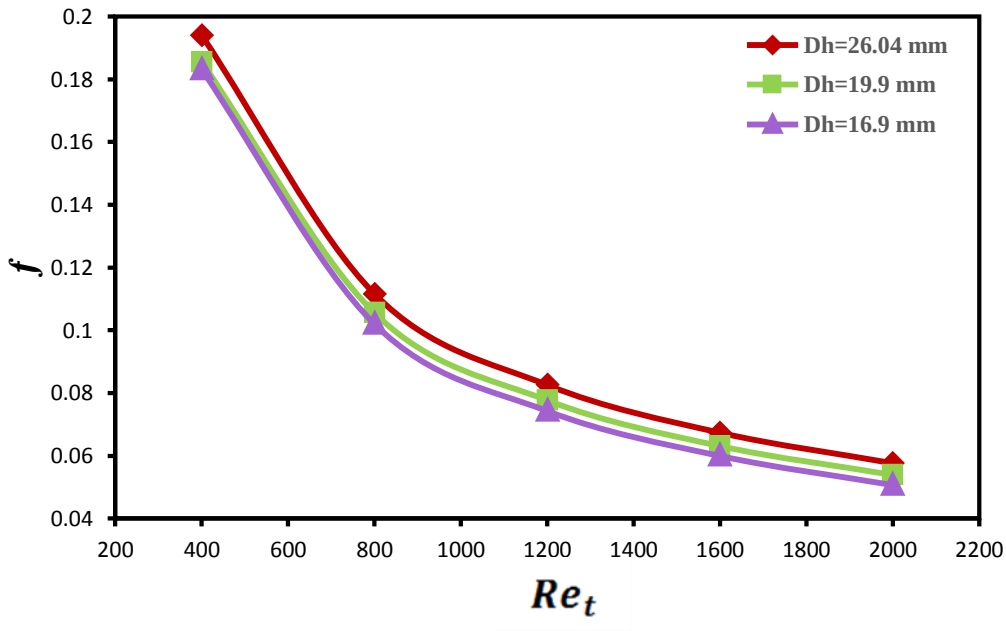

Fig. 5.11 Variation of average friction factor of tube side with tube Reynolds number for different tube hydraulic dimeter at T_{ci}=300K and T_{hi}=360K.

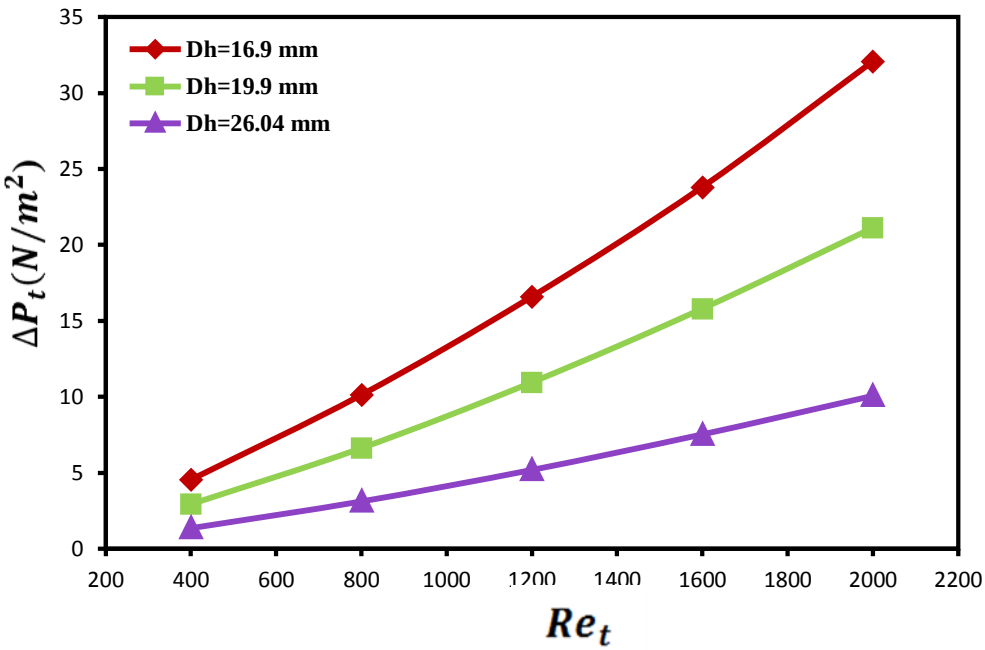

Fig. 5.12 Variation of pressure drop of tube side with tube Reynolds number for different tube hydraulic dimeter at α(0˚), Re_{sh}=1000, T_{ci}=300K and T_{hi}=360K.

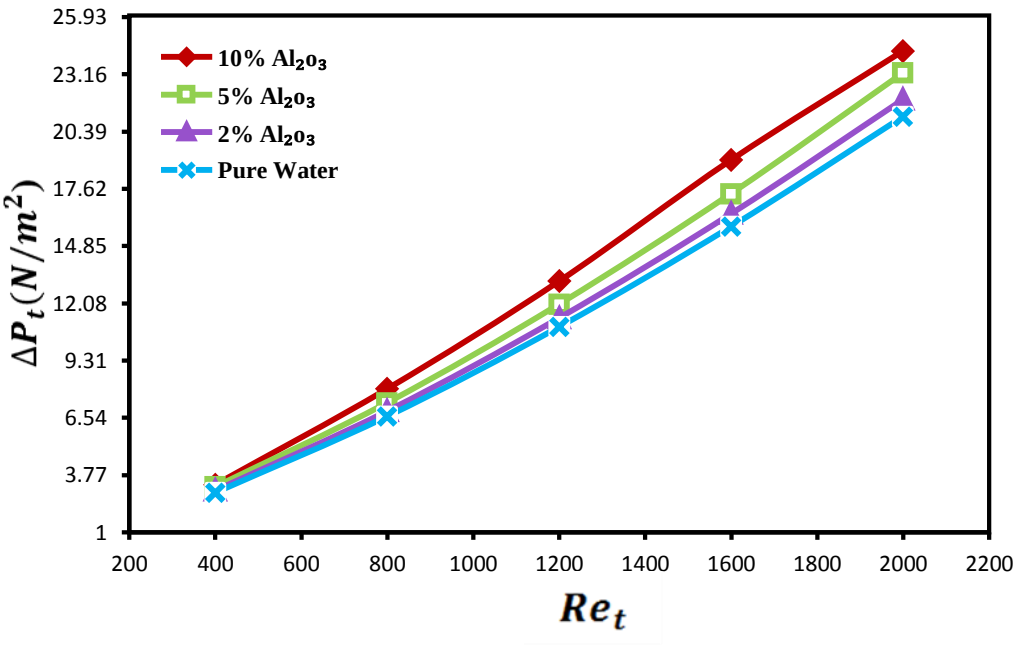

Fig. 5.13 Variation of pressure drop of tube side with tube Reynolds number for different volume concentrations at α(0˚), Re_{sh}=1000, dh=19.9mm, T_{ci}=300K and T_{hi}=360K.

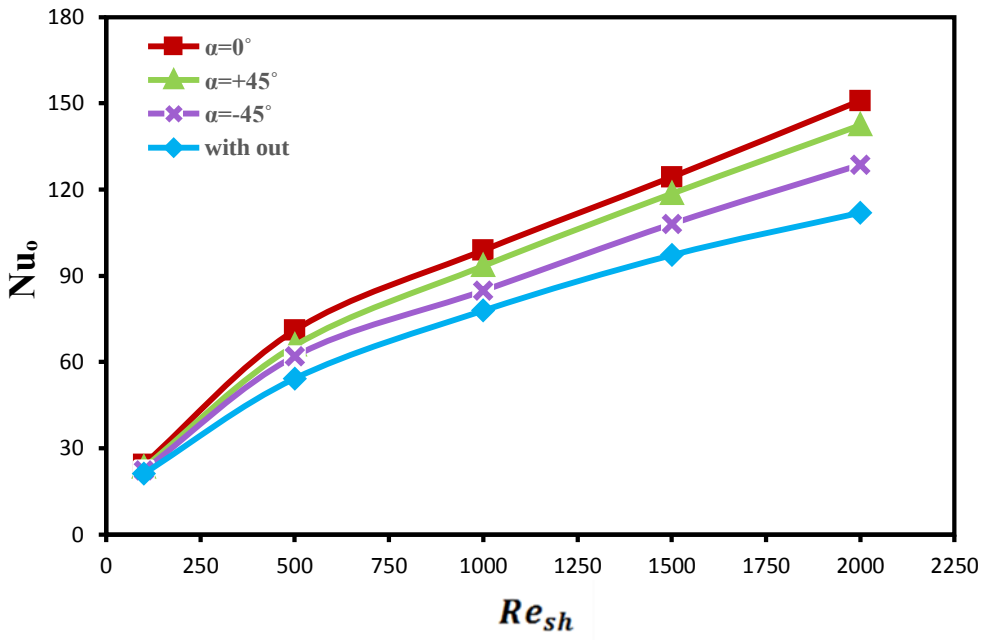

Fig. 5.14 Variation of average Nussult number with shell side Reynolds number for different inclination angle of baffles(α) at Re_t=600, dh=16.9mm, T_{ci}=300K and T_{hi}=360K.

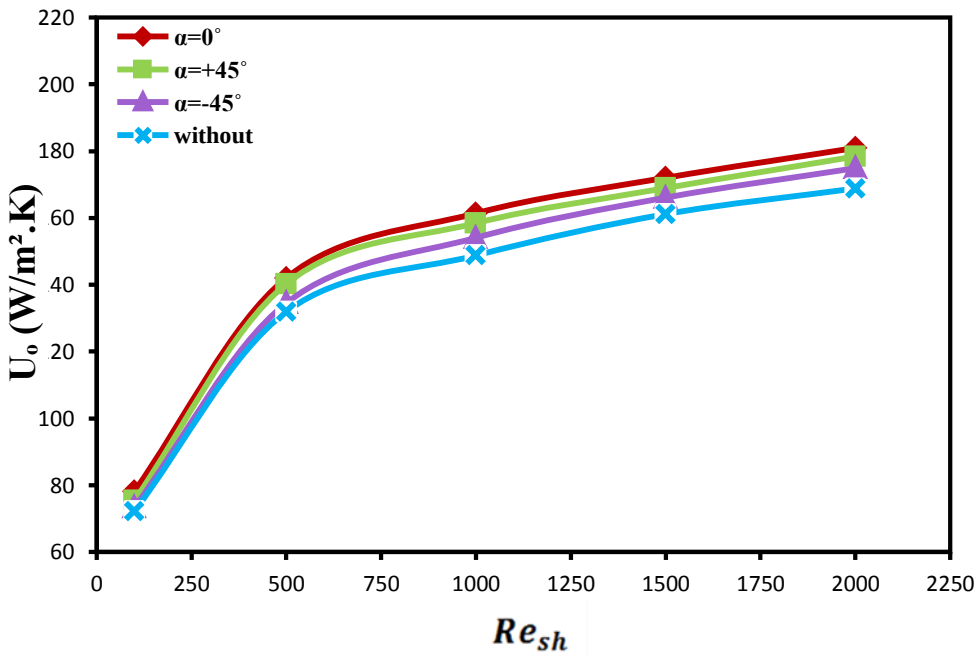

Fig. 5.15 Variation of overall heat transfer with shell side Reynolds number for different inclination angle of baffles(α) at Re_t=600, dh=16.9mm, T_{ci}=300K and T_{hi}=360K.

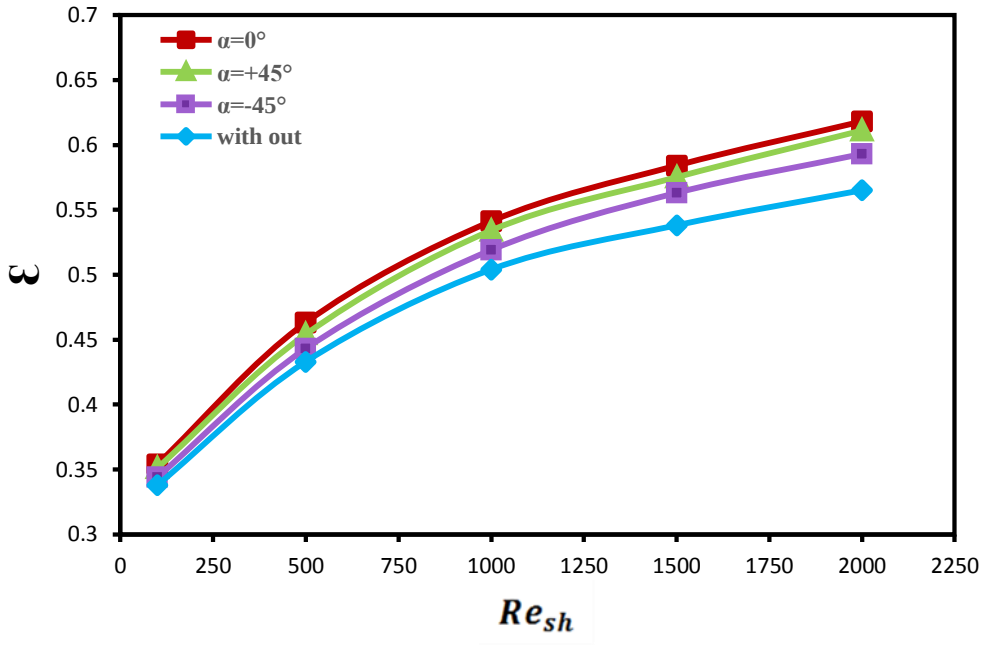

Fig. 5.16 Variation of heat exchanger effectiveness with shell Reynolds number for different inclination angle of baffles(α) at Re_t=600, dh=16.9mm, T_{ci}=300K and T_{hi}=360K.

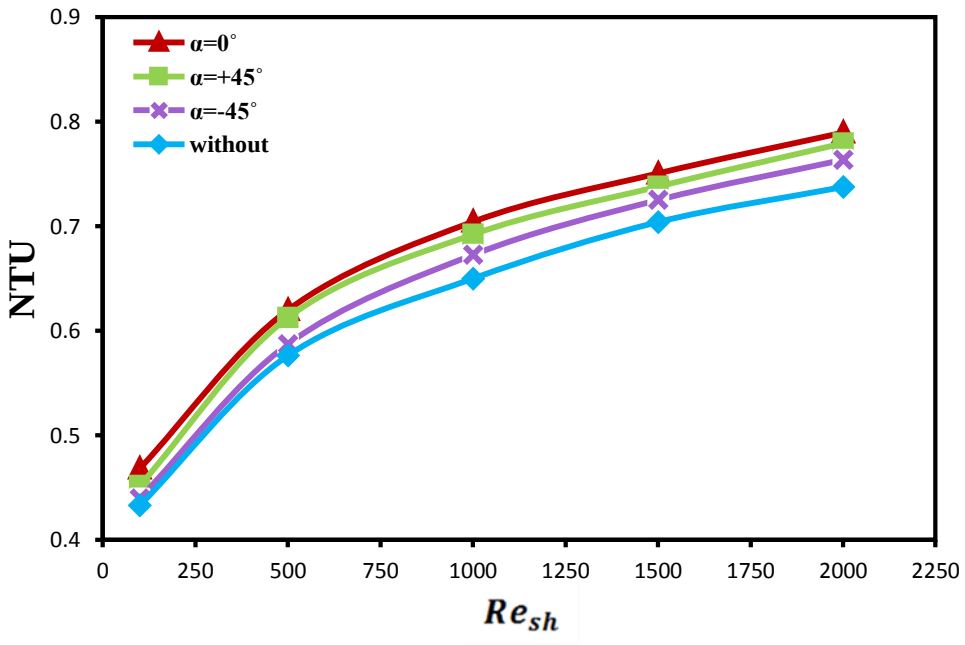

Fig. 5.17 Variation of number of heat transfer unit (NTU) with shell side Reynolds number for different inclination angle of baffles(α) at Re_t=600, dh=16.9mm, T_{ci}=300K and T_{hi}=360K.

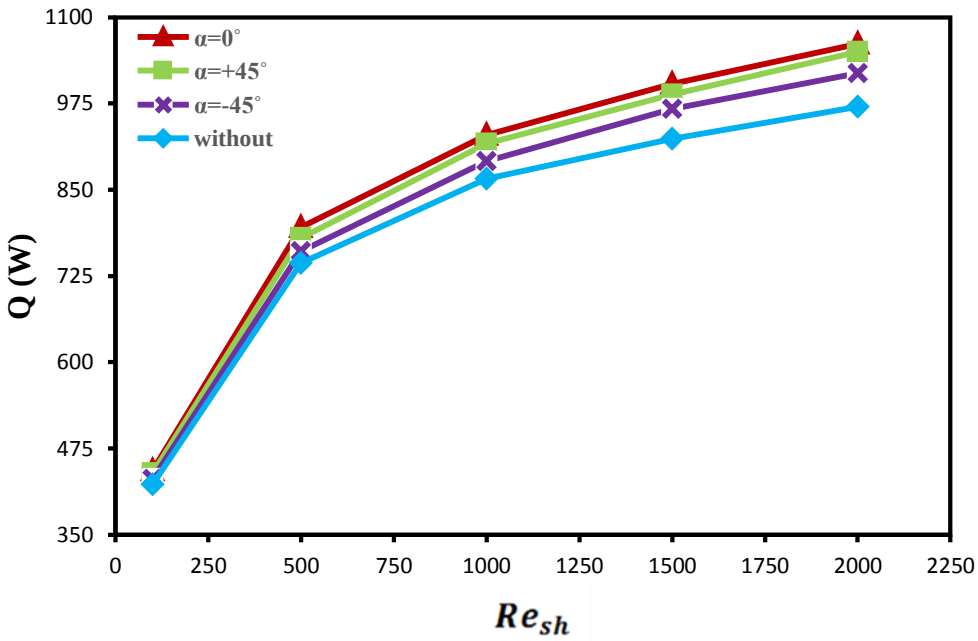

Fig. 5.18 Variation of total heat transfer rate with shell side Reynolds number for different baffles inclination angle(α) at Re_t=600, dh=16.9mm, T_{ci}=300K and T_{hi}=360K.

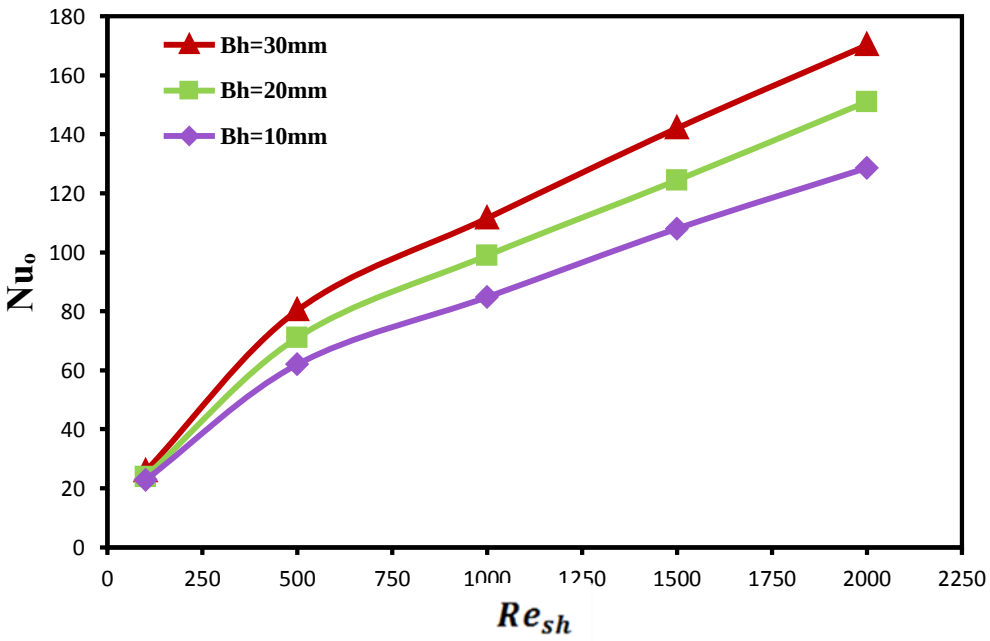

Fig. 5.19 Variation of average Nusselt number with shell side Reynolds number for different baffles height (Bh) at Re_t=600, dh=16.9mm, T_{ci}=300K and T_{hi}=360K.

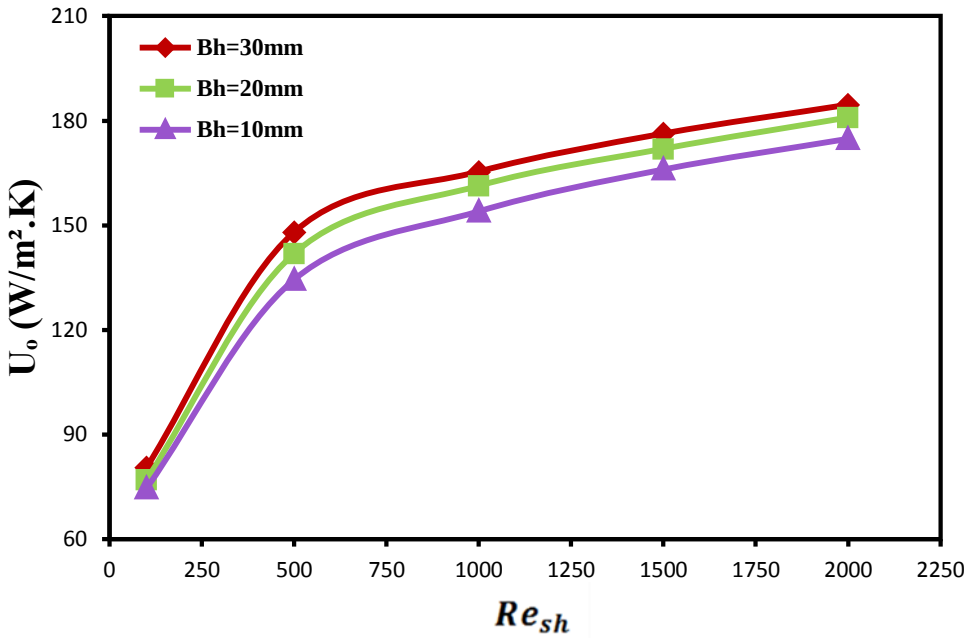

Fig. 5.20 Variation of overall heat transfer with shell side Reynolds number for different baffles height (Bh) at Re_t=600, dh=16.9mm, T_{ci}=300K and T_{hi}=360K.

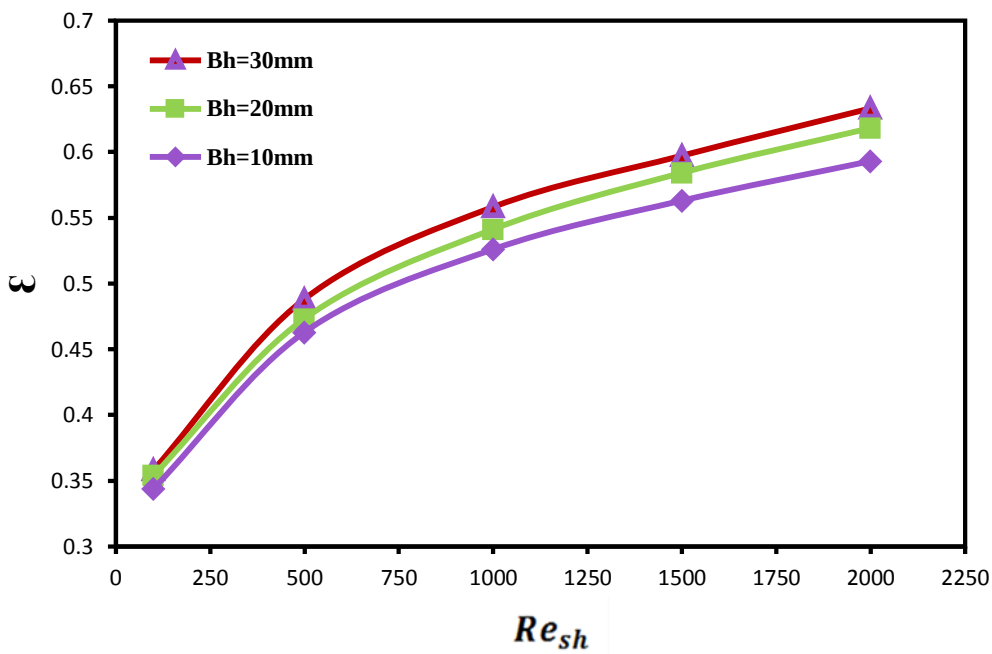

Fig. 5.21 Variation of heat exchanger effectiveness with shell side Reynolds number for different baffles height (Bh) at Re_t=600, dh=16.9mm, T_{ci}=300K and T_{hi}=360K.

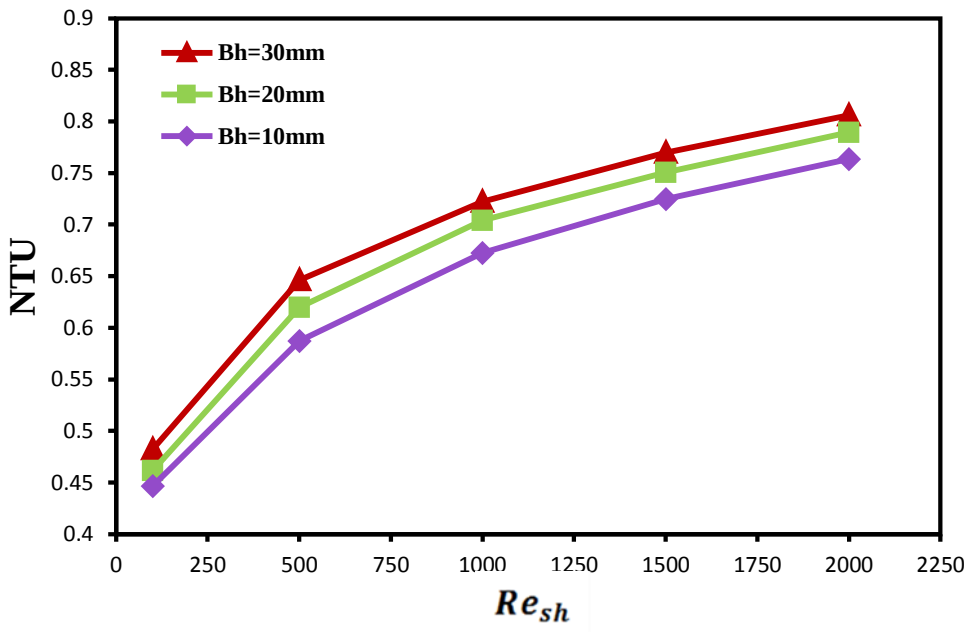

Fig. 5.22 Variation of number of heat transfer unit with shell Reynolds number for different baffles height (Bh) at Re_t=600, dh=16.9mm, T_{ci}=300K and T_{hi}=360K.

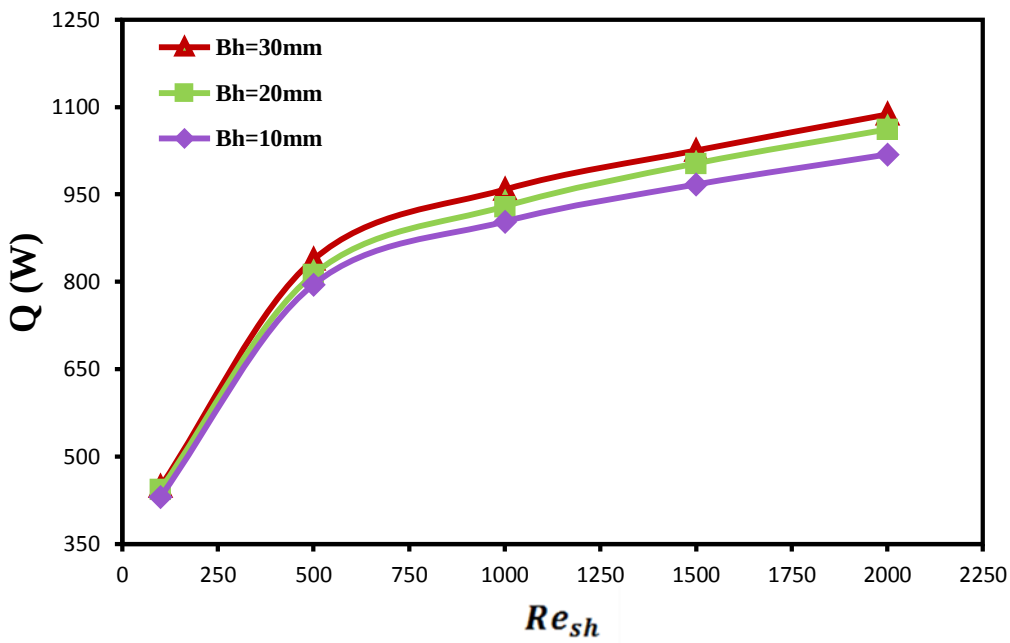

Fig. 5.23 Variation of total heat transfer rate with shell side Reynolds number for different baffles height (Bh) at Re_t=600, dh=16.9mm, T_{ci}=300K and T_{hi}=360K.

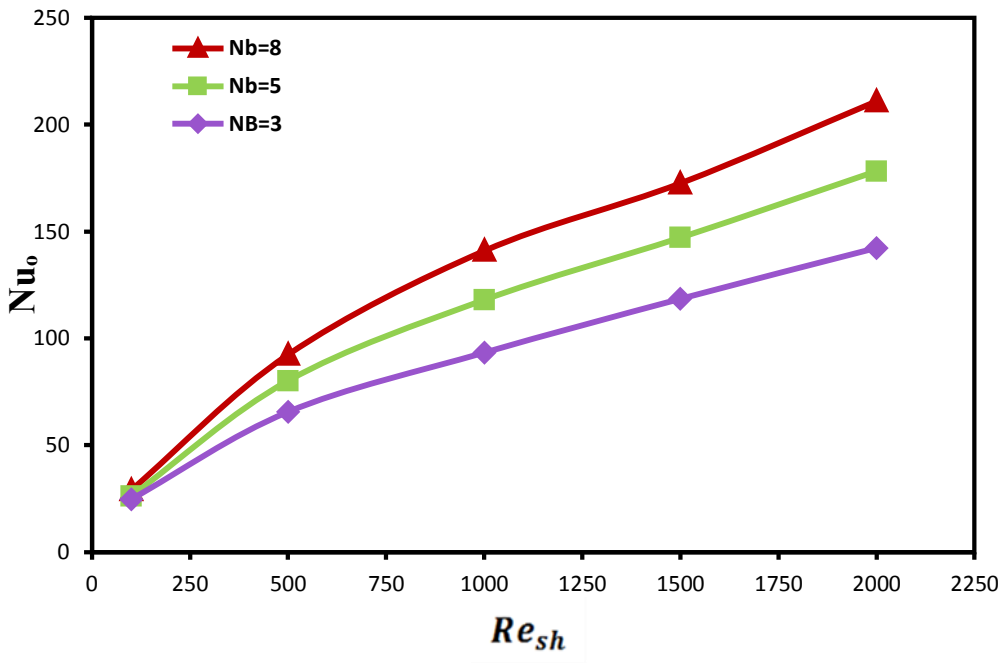

Fig. 5.24 Variation of average Nusselt number with shell side Reynolds number for different number of baffles (Nb) at Re_t=600, dh=16.9mm, T_{ci}=300K and T_{hi}=360K.

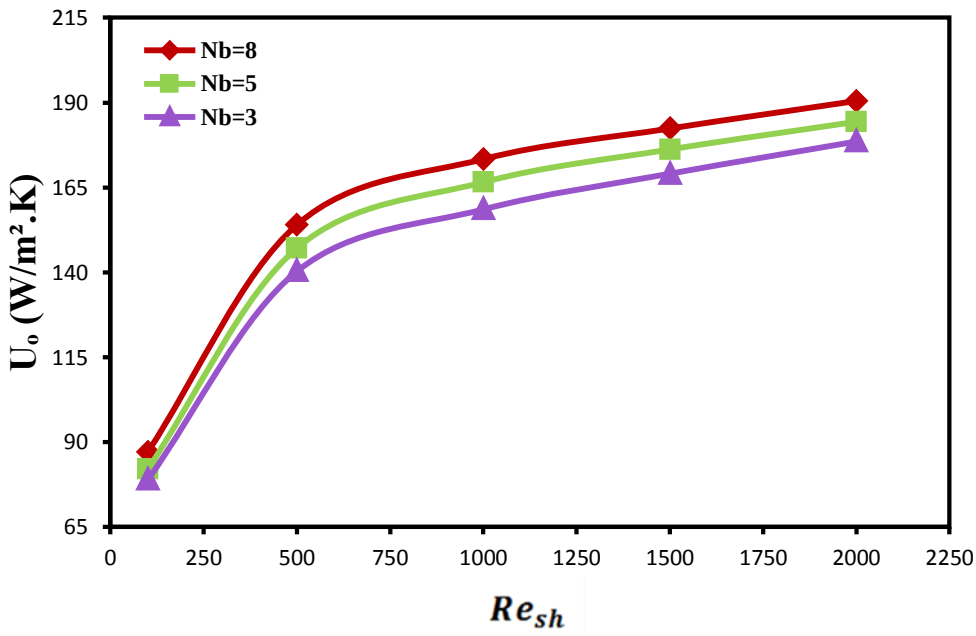

Fig. 5.25 Variation of overall heat transfer with shell side Reynolds number for different number of baffles(Nb) at Re_t=600, dh=16.9mm, T_{ci}=300K and T_{hi}=360K.

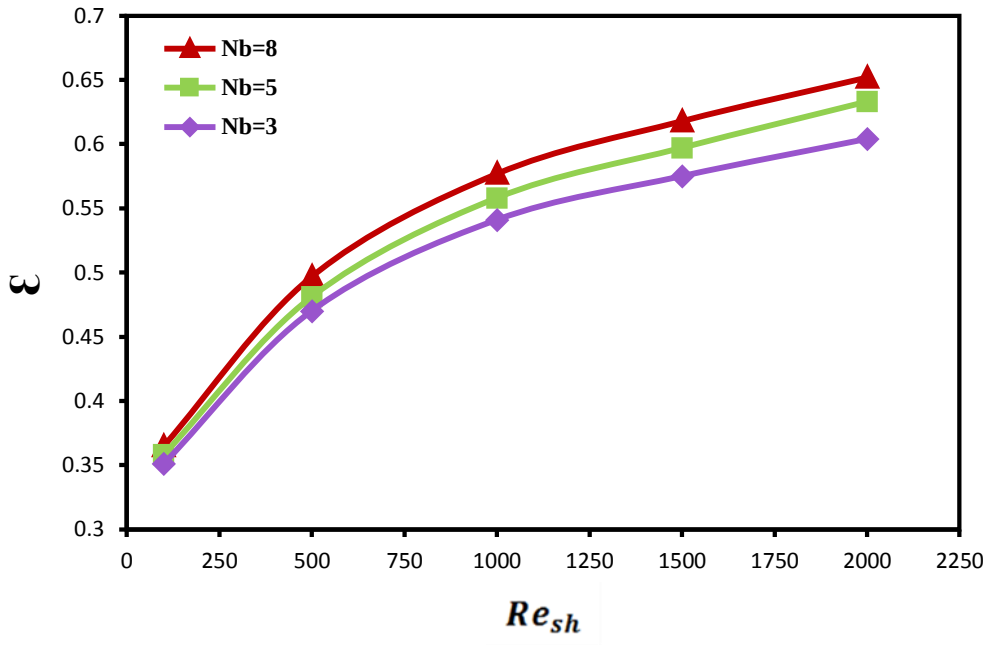

Fig. 5.26 Variation of heat exchanger effectiveness with tube Reynolds number for different volume concentrations at Re_t=600, dh=16.9mm, T_{ci}=300K and T_{hi}=360K.

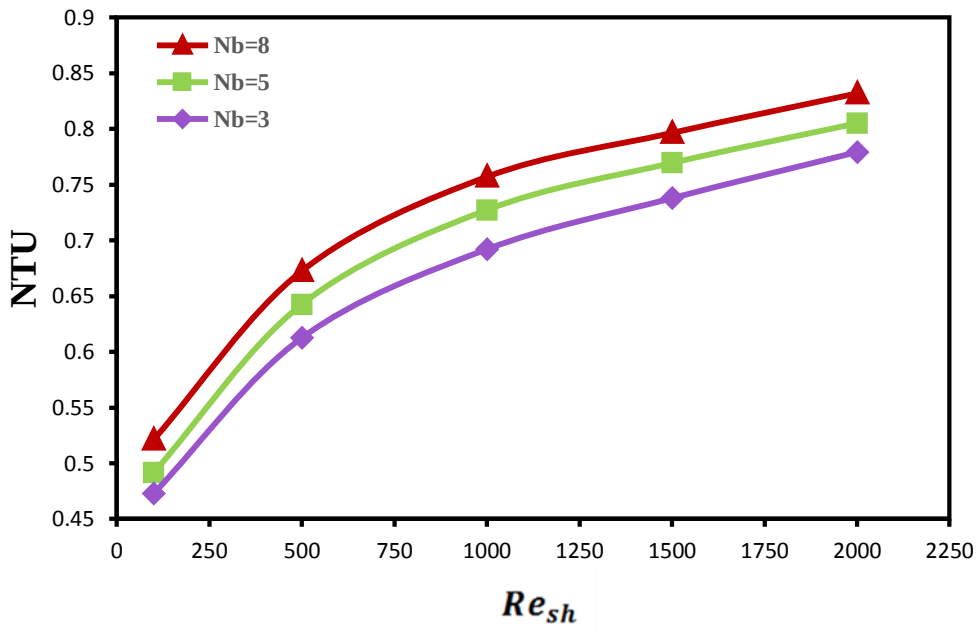

Fig. 5.27 Variation of number of heat transfer unit with tube Reynolds number for different volume concentrations at Re_t=600, dh=16.9mm, T_{ci}=300K and T_{hi}=360K.

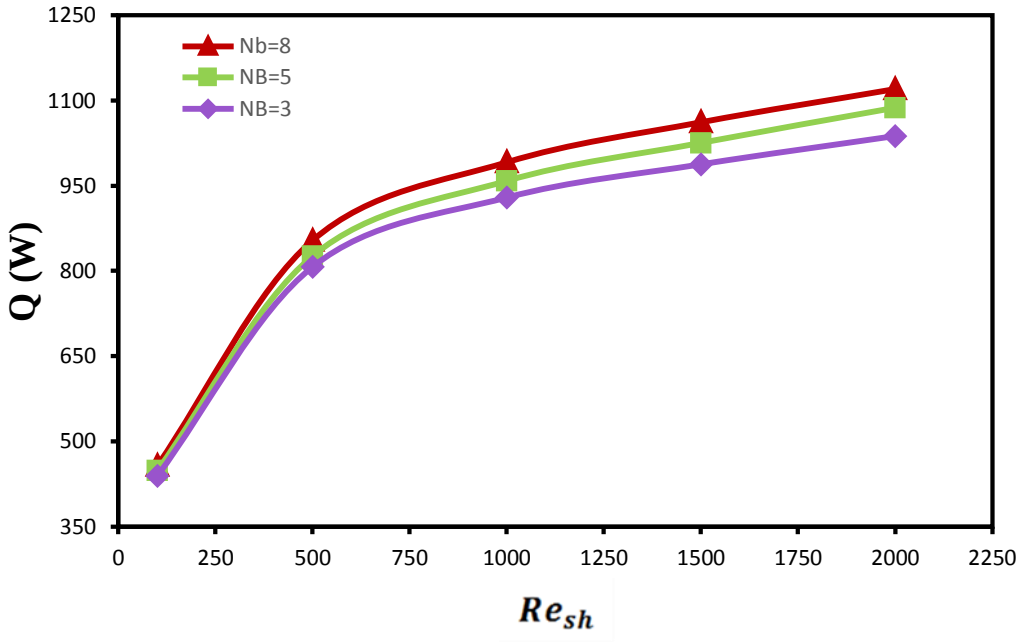

Fig. 5.28 Variation of total heat transfer rate with shell side Reynolds number for different number of baffles(Nb) at Re_t=600, dh=16.9mm, T_{ci}=300K and T_{hi}=360K.

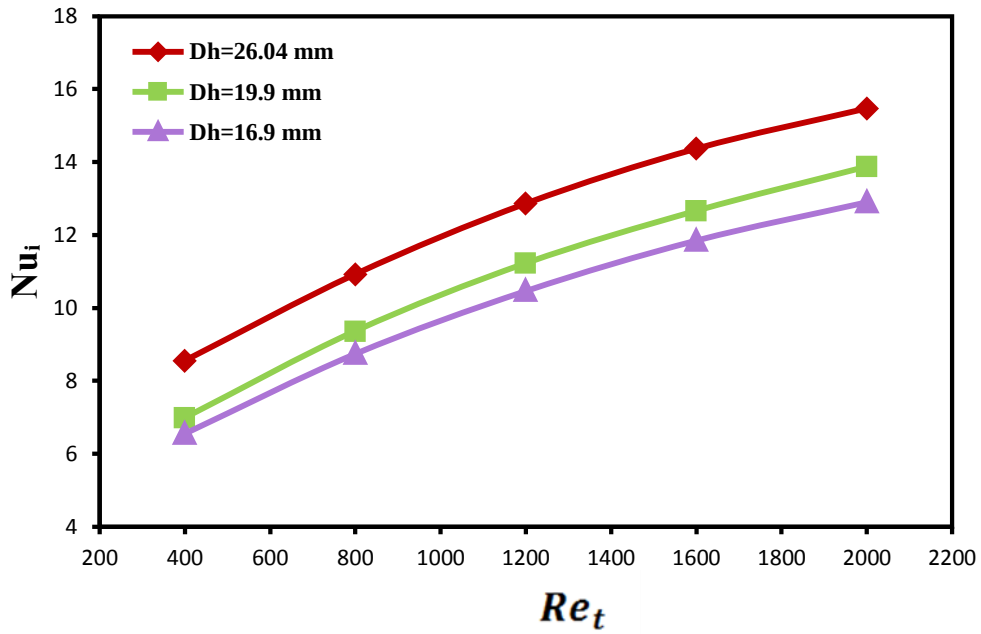

Fig. 5.29 Variation of average nusselt number with tube Reynolds number for different diameter of tube at Re_{sh}=1000, T_{ci}=300K and T_{hi}=360K.

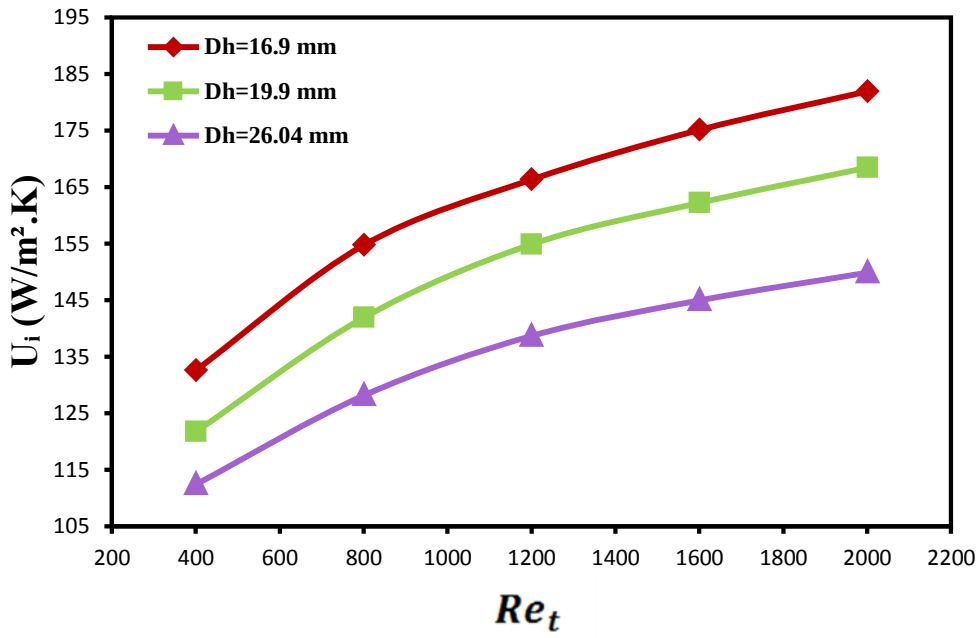

Fig. 5.30 Variation of overall heat transfer with tube Reynolds number for different diameter of tube at Re_{sh}=1000, T_{ci}=300K and T_{hi}=360K.

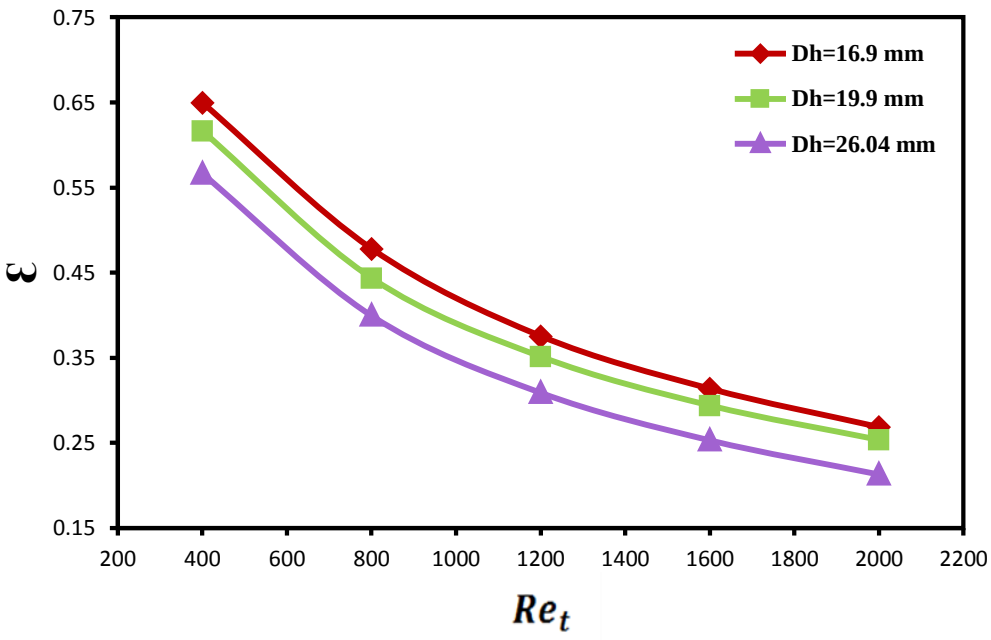

Fig. 5.31 Variation of heat exchanger effectiveness with tube Reynolds number for different diameter of tube at Re_{sh}=1000, T_{ci}=300K and T_{hi}=360K.

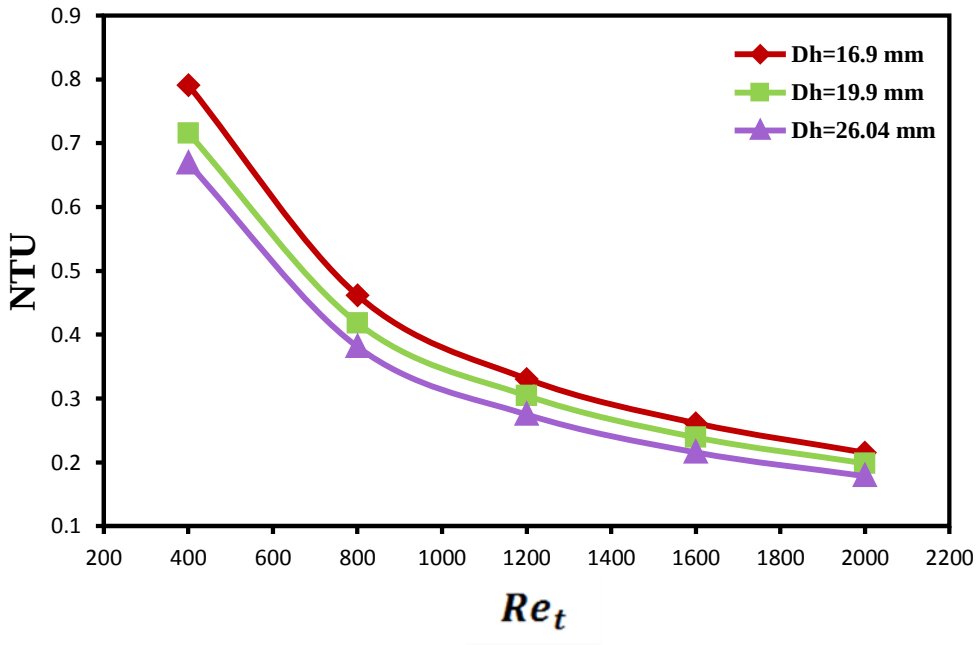

Fig. 5.32 Variation of number of heat transfer unit with tube Reynolds number for different diameter of tube at Re_{sh}=1000, T_{ci}=300K and T_{hi}=360K.

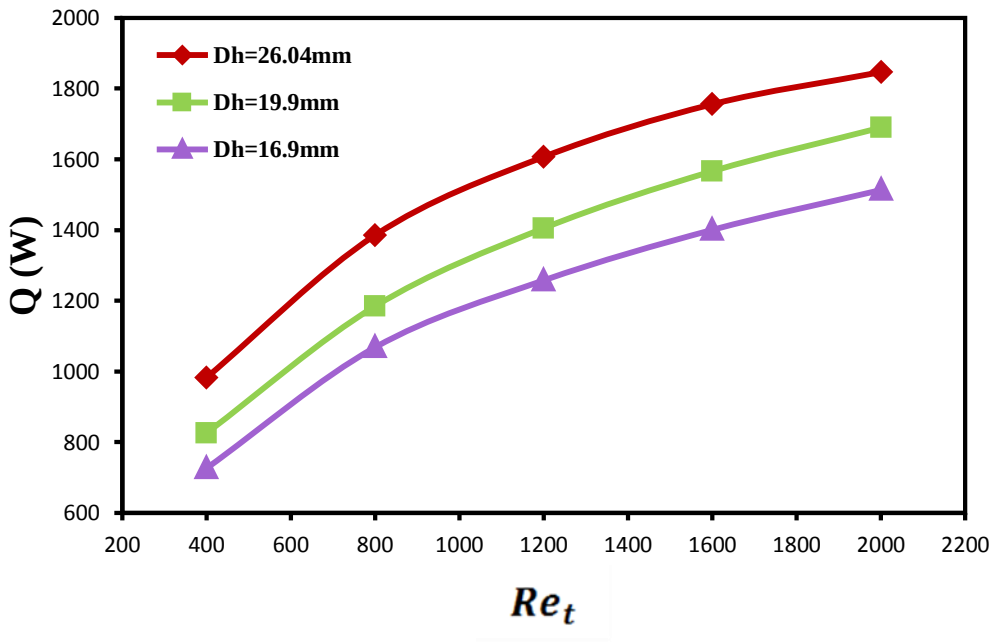

Fig. 5.33 Variation of total heat transfer rate with tube Reynolds number for different diameter of tube at Re_{sh}=1000, T_{ci}=300K and T_{hi}=360K.

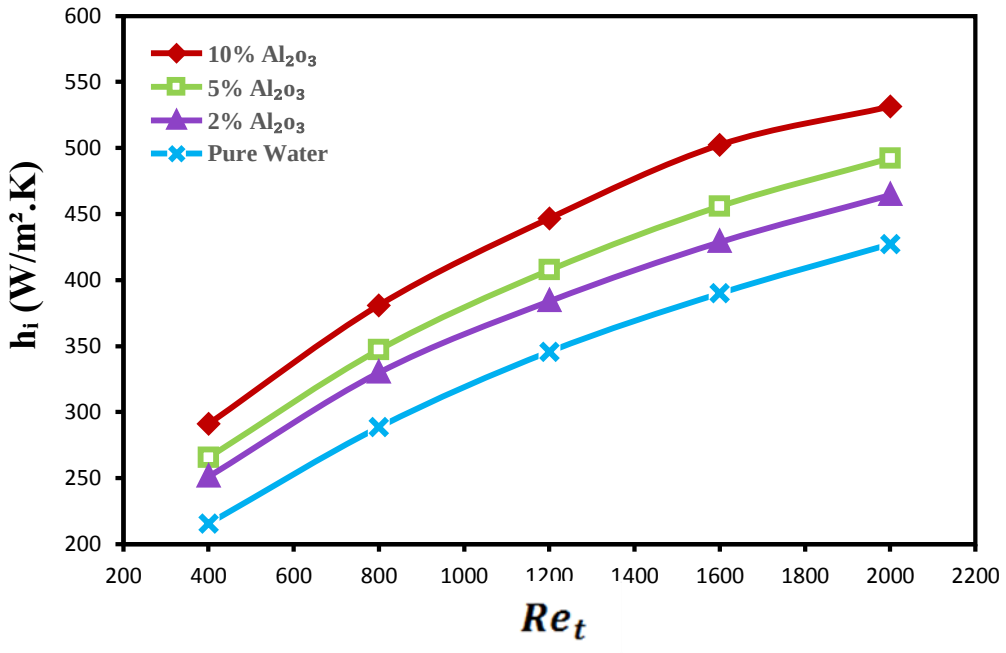

Fig. 5.34 Variation of average heat transfer coefficient with tube Reynolds number for different volume concentrations at α(0˚), Re_{sh}=1000, Nb=5, Bh=25mm, T_{ci}=300K and T_{hi}=360K.

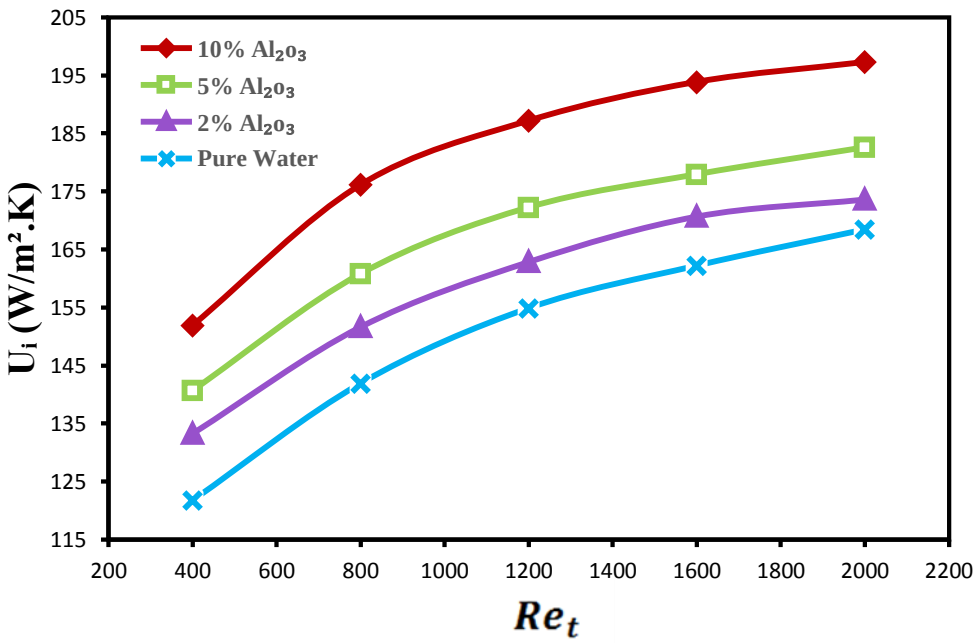

Fig. 5.35 Variation of overall heat transfer with tube Reynolds number for different volume concentrations at α(0˚), Re_{sh}=1000, Nb=5, Bh=25mm, T_{ci}=300K and T_{hi}=360K.

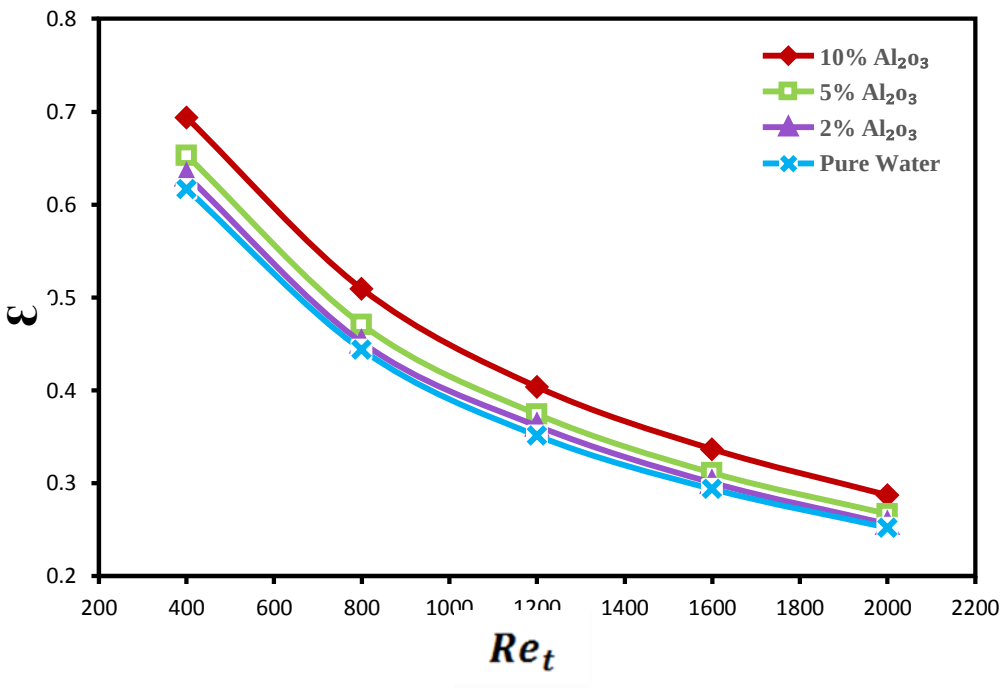

Fig. 5.36 Variation of heat exchanger effectiveness with tube Reynolds number for different volume concentrations at α(0˚), Re_{sh}=1000, Nb=5 and Bh=25mm, T_{ci}=300K and T_{hi}=360K.

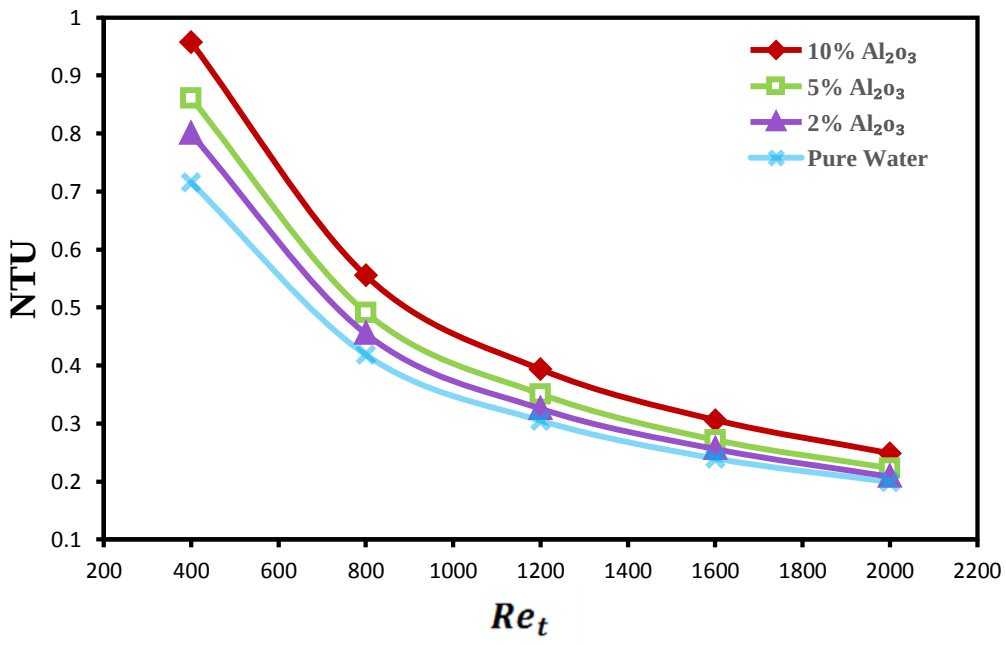

Fig. 5.37 Variation of number of heat transfer unit with tube Reynolds number for different volume concentrations at α(0˚), Re_{sh}=1000, Nb=5, Bh=25mm, T_{ci}=300K and T_{hi}=360K.

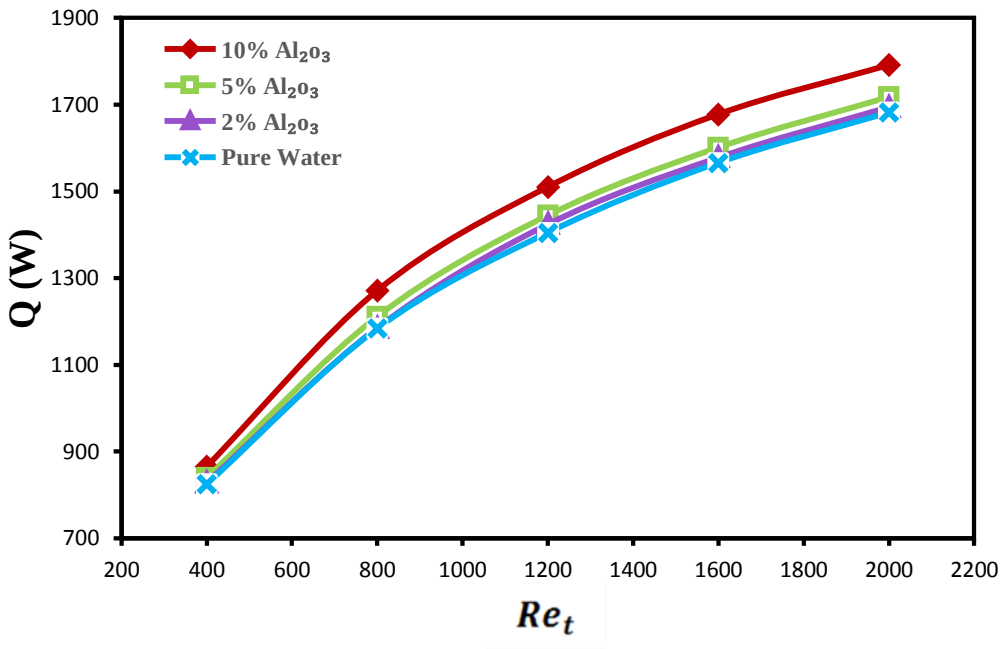

Fig. 5.38 Variation of total heat transfer rate with tube Reynolds number for different volume concentrations at α(0˚), Re_{sh}=1000, Nb=5, Bh=25mm, T_{ci}=300K and T_{hi}=360K.

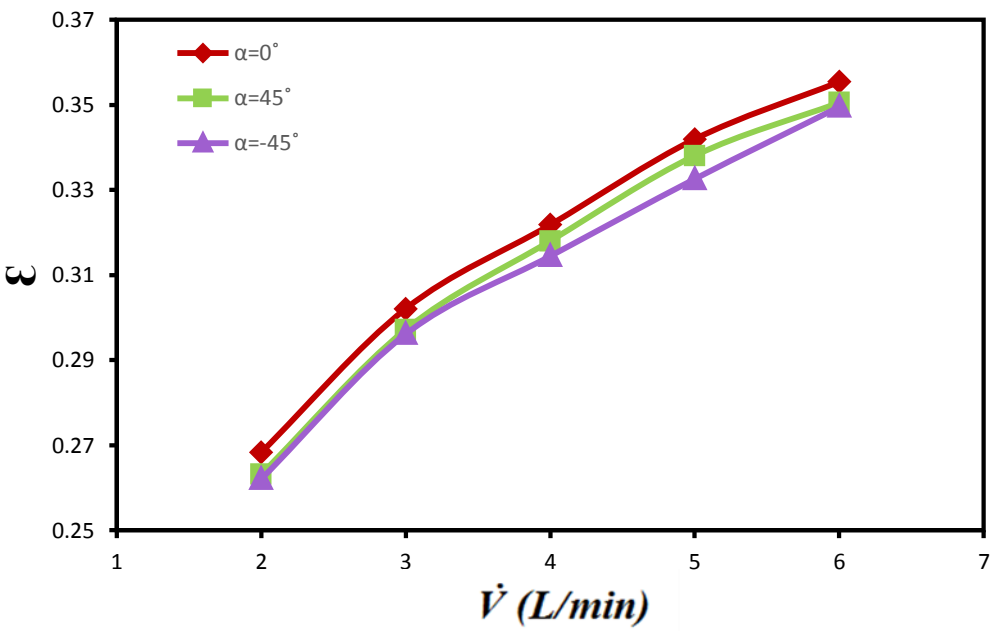

Fig. 5.39 Variation of heat exchanger effectiveness with volumetric flow rate shell side for different inclination angle of baffle at Nb=5 and Bh=20mm.

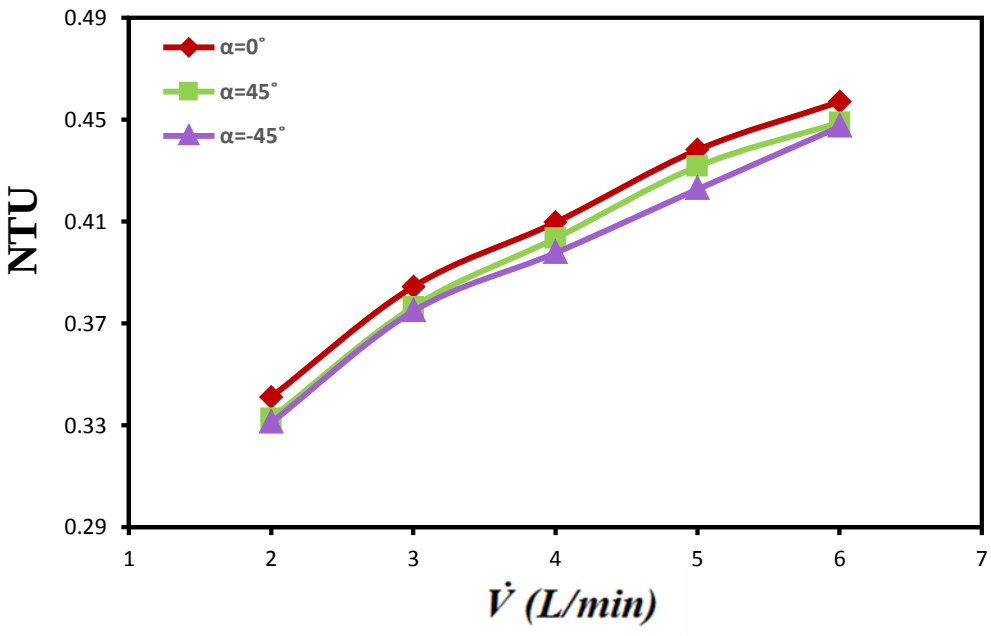

Fig. 5.40 Variation of number of heat transfer unit with volumetric flow rate shell side for different inclination angle of baffle at Nb=5 and Bh=20mm.

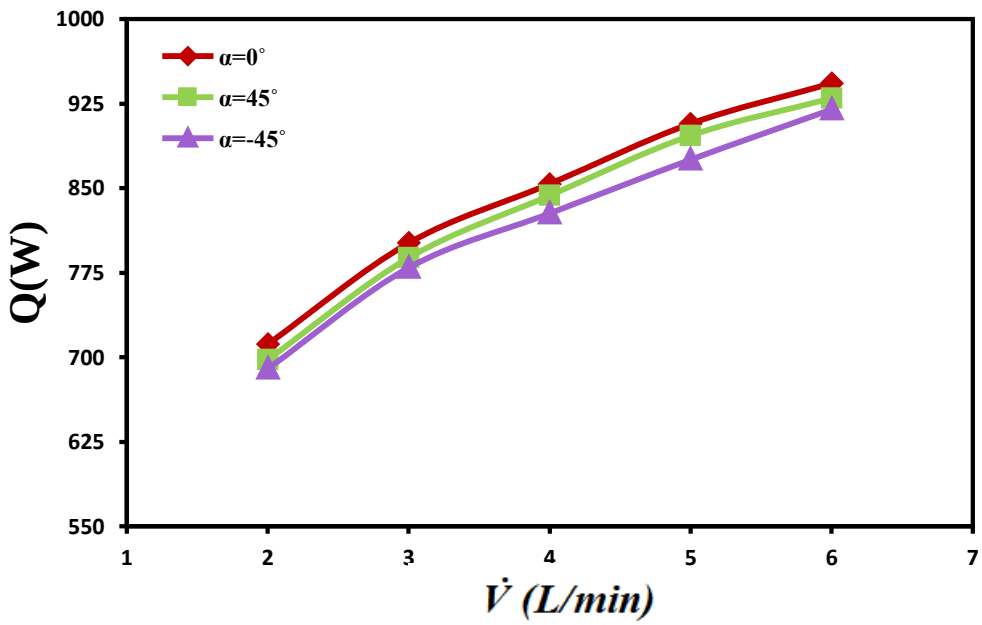

Fig. 5.41 Variation of number of heat transfer unit with volumetric flow rate of the shell side for different inclination angle of baffle at Nb=5 and Bh=20mm.

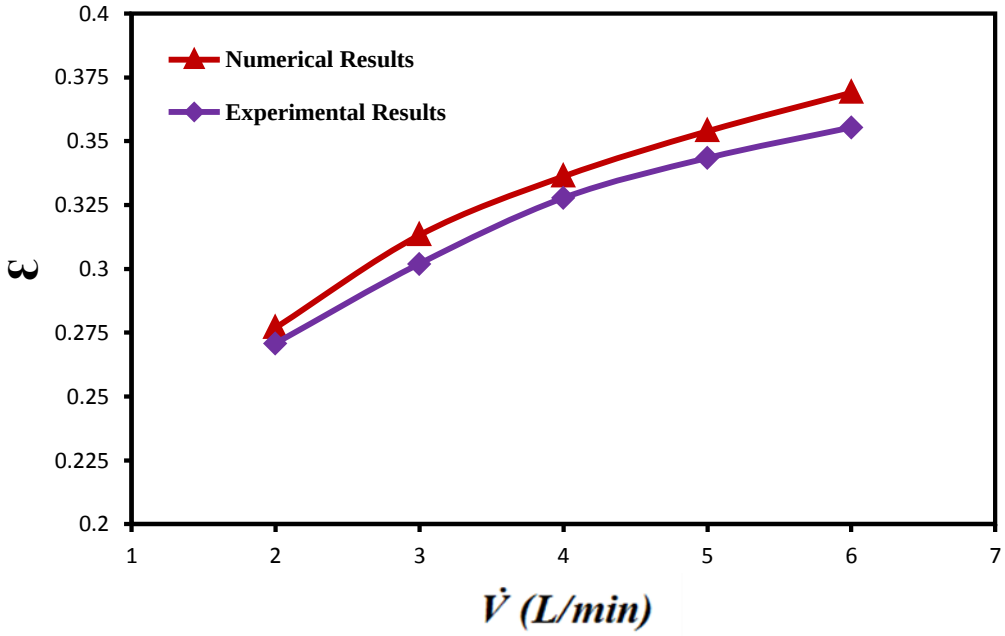

Fig. 5.42 Comparison of predicted and experimental of heat exchanger effectiveness with volumetric flow rate of shell side at α (0˚), Nb=5 and Bh=20mm.

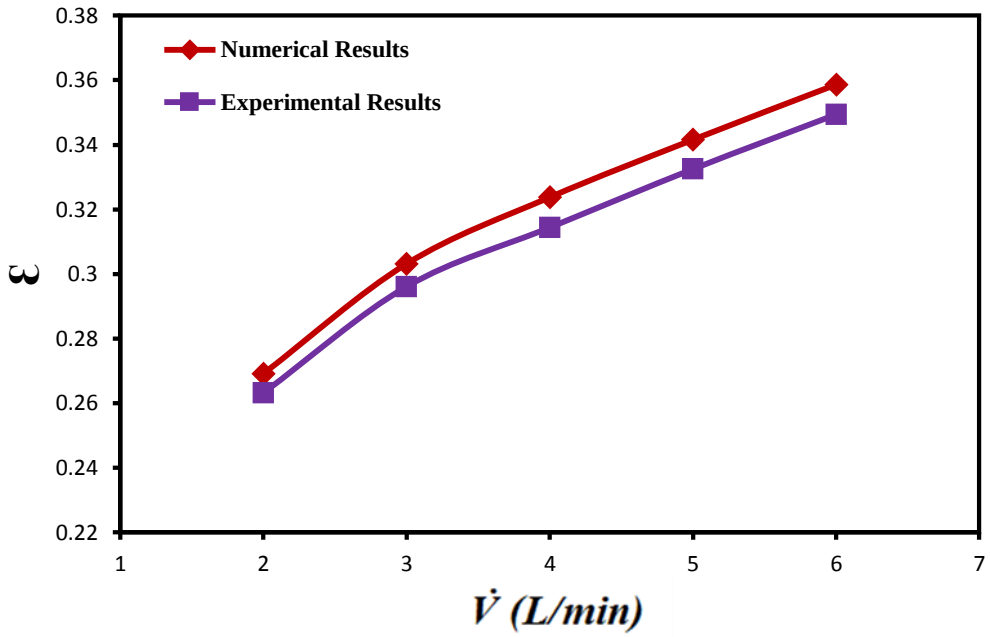

Fig. 5.43 Comparison of predicted and experimental of heat exchanger effectiveness with volumetric flow rate of shell side at α (+45˚), Nb=5 and Bh=20mm.

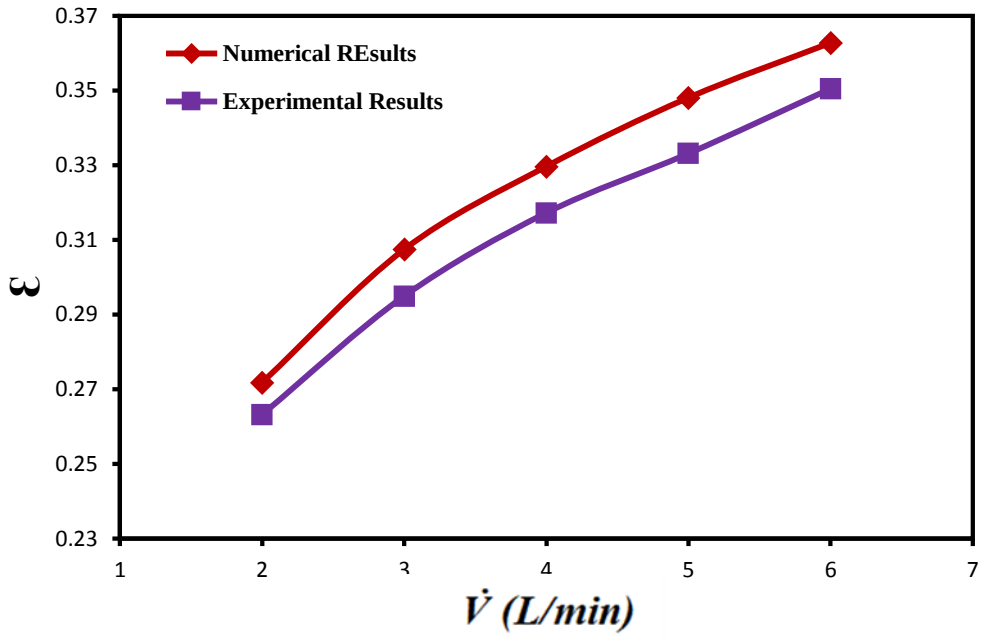

Fig. 5.44 Comparison of predicted and experimental of heat exchanger effectiveness with volumetric flow rate of shell side at α (-45˚), Nb=5 and Bh=20mm.

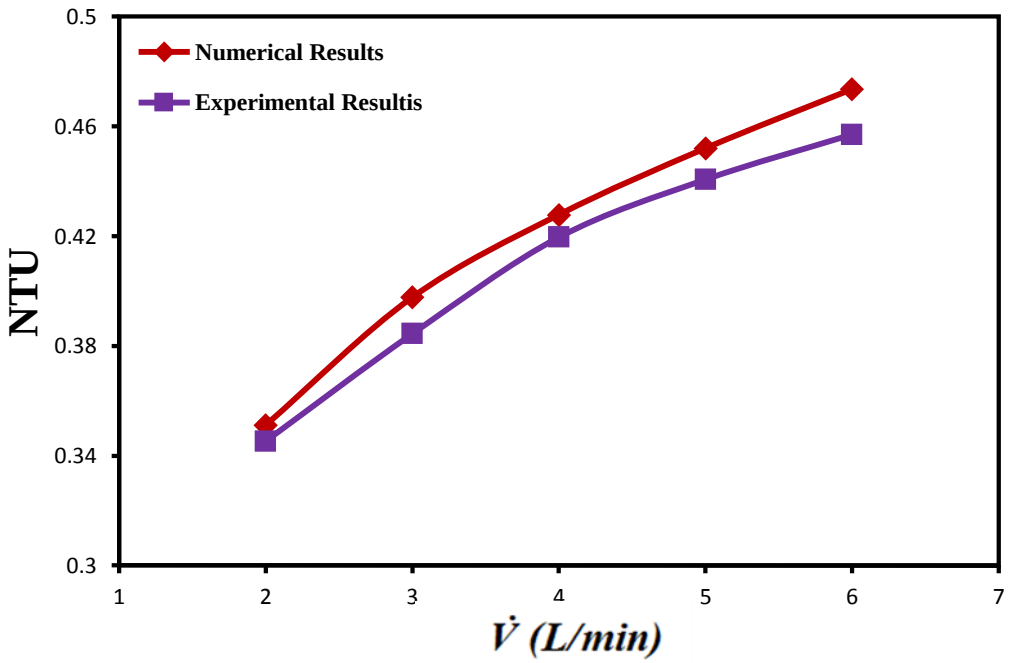

Fig. 5.45 Comparison of predicted and experimental for number of transfer unit with volumetric flow rate of shell side at α (0˚), Nb=5 and Bh=20mm.

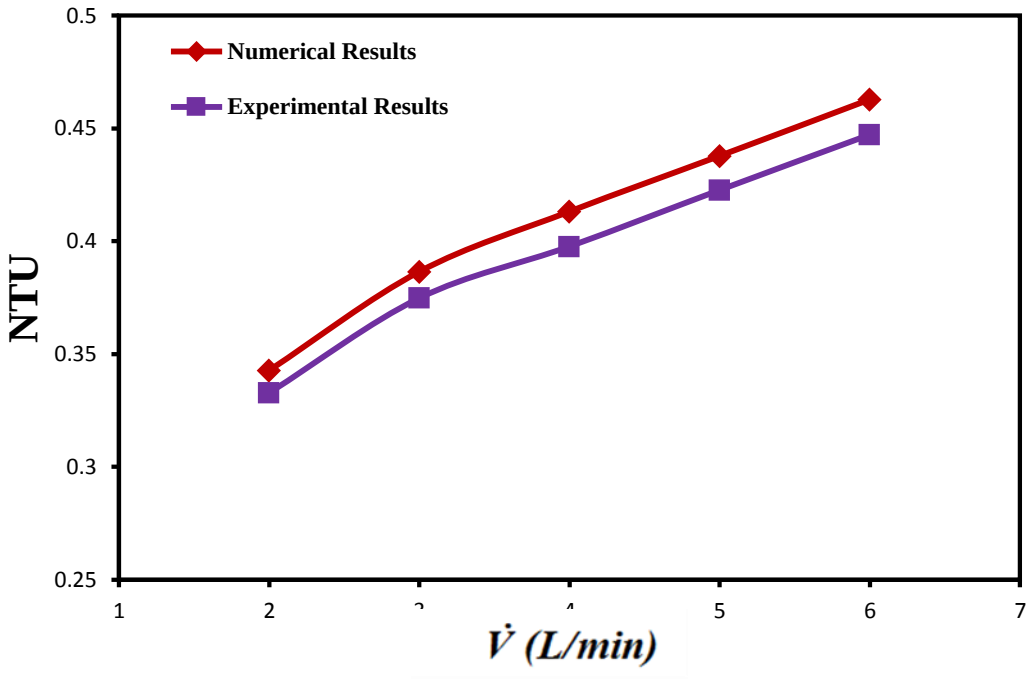

Fig. 5.46 Comparison of predicted and experimental for number of transfer unit with volumetric flow rate of shell side at α (+45˚), Nb=5 and Bh=20mm.

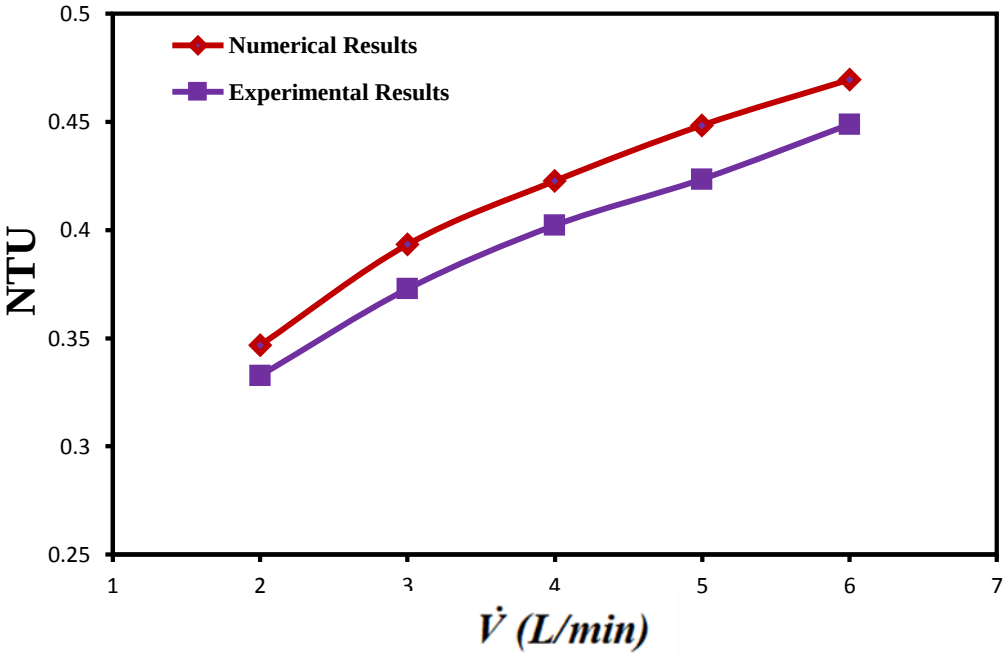

Fig. 5.47 Comparison of predicted and experimental for number of transfer unit with volumetric flow rate of shell side at α (-45˚), Nb=5 and Bh=20mm.

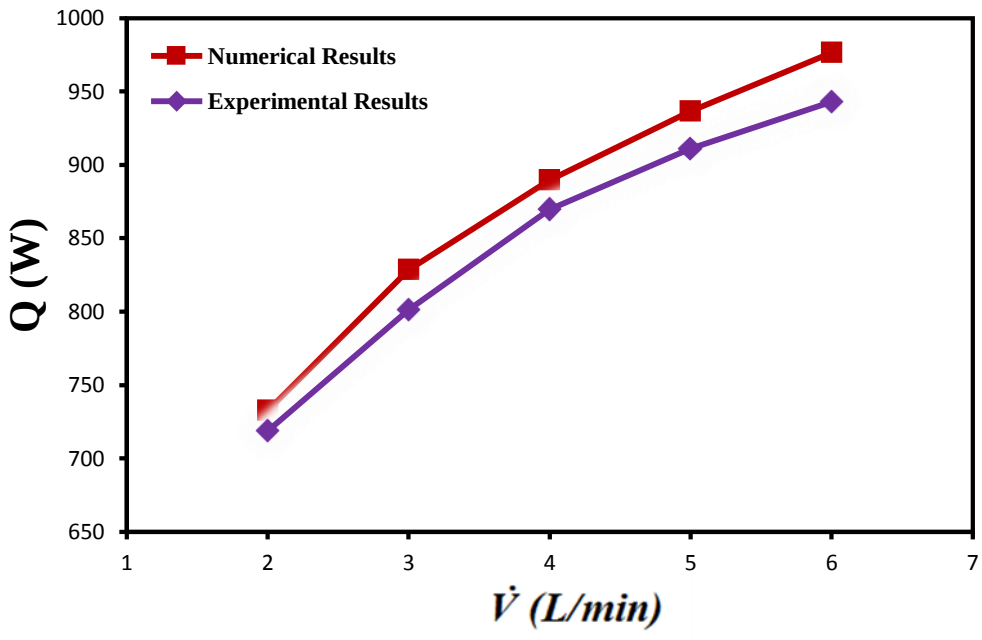

Fig. 5.48 Comparison of predicted and experimental for heat transfer rate with volumetric flow rate of shell side at α (0˚), Nb=5 and Bh=20mm.

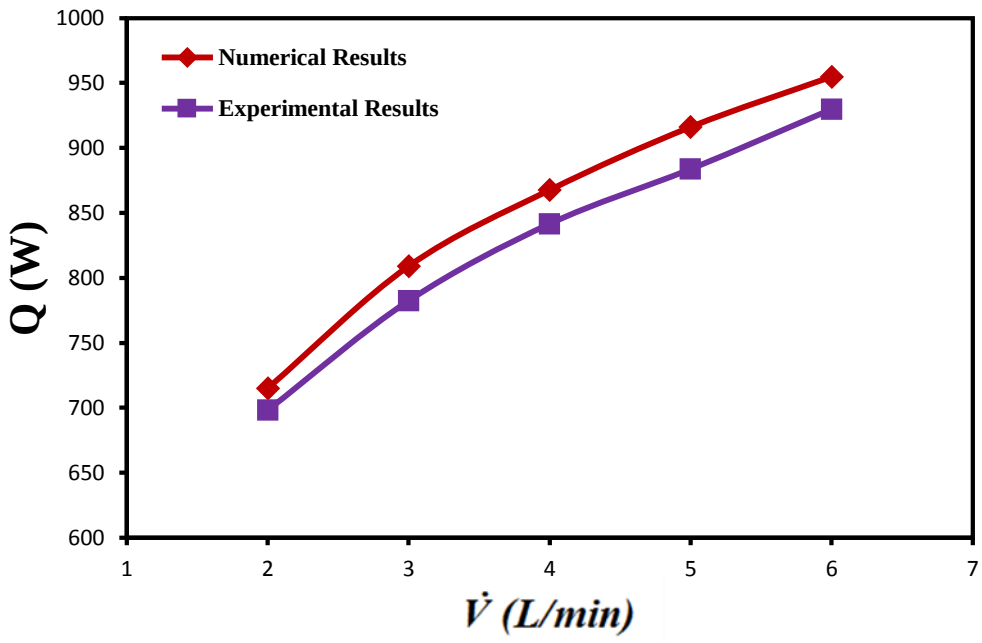

Fig. 5.49 Comparison of predicted and experimental for heat transfer rate with volumetric flow rate of shell side at α (+45˚), Nb=5 and Bh=20mm.

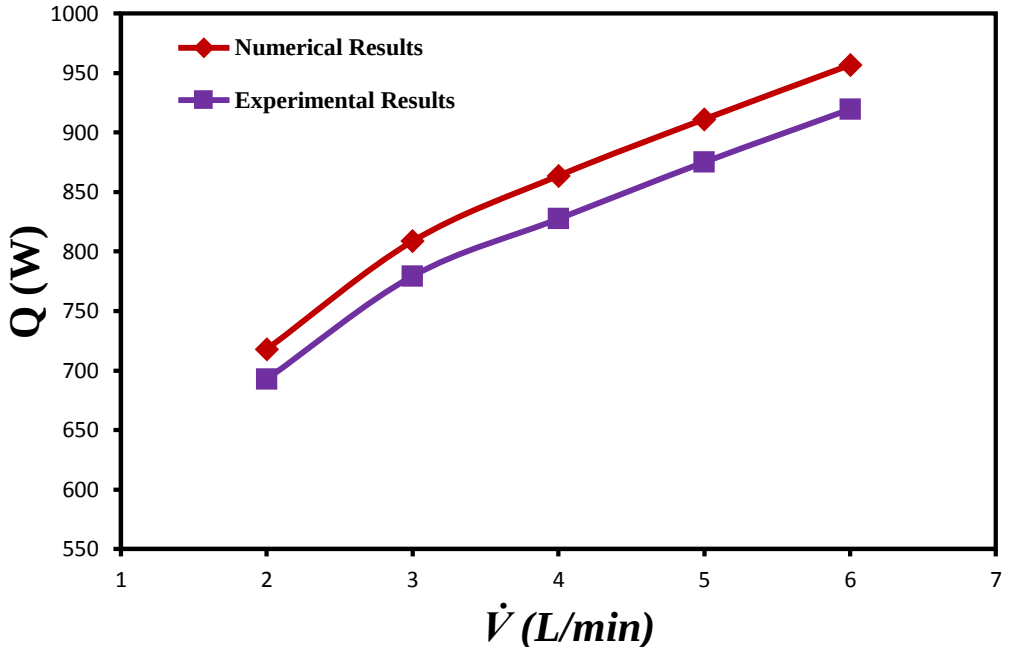

Fig. 5.50 Comparison of predicted and experimental for heat transfer rate with volumetric flow rate of shell side at α (-45˚), Nb=5 and Bh=20mm.

CHAPTER SIX

CONCLUSIONS AND RECOMMONDATOINS

Chapter Six

Conclusions and Recommendations

6.1 General

The main purpose of this project is to investigate the hydraulic and thermal characteristics of laminar flow in three-dimensional steady-state conditions for shell and U-tube heat exchanger. This chapter present the conclusions gained from this study and give recommendations for future work for developing.

Commercial computational fluid dynamics code FLUENT is employed to examine the flow structure as well as the hydraulic and thermal characteristics of numerical model. The governing equations are solved using finite volume method with certain assumptions and appropriate boundary conditions to provide a clear understanding of modeling aims and conditions for the current study. The effect of inclination angle of baffles(α), Reynolds number (*Re*), space between baffles (Nb), the height of baffles(Bh), hydraulic diameter (D_h) and addition volume concentration of nanofluid(Φ). are studied on the thermal and hydrodynamic flow fields. Also, experimental work is done to characteristic fluid flow and heat transfer behaviors of U-tube heat exchanger.

6.2 Conclusions

The main conclusions drawn from this project can be summarized as follows:

1. The current work presents the first study includes the comparison between

the experimental and theoretical results for the U-tube heat exchanger with the coupling boundary condition with a high accuracy results.

2. Increasing the Re_{sh} increases the heat transfer rate. The highest percentages of the heat transfer rate are found 11.38% at $Re_{sh} = 2000$, α=0º, Nb=8 and Bh=30mm.
3. The thermal performance of the heat exchanger enhances with each of Increasing the baffle number(Nb), increasing the height of baffle (Bh) and increasing tube hydraulic diameter.
4. low flow rate there is a little effect of baffles on heat exchanger performance compare with high flow rate.
5. For the experimental test, Re_{sh} has a greater influence in increasing effectiveness, while Re_t has less influence on effectiveness. The effectiveness increased with increasing of Re_{sh}.
6. The experimental test of the inclination angle baffle show that, the highest value of heat transfer rate is found at α=0º. These experimental results were compared with numerical results and good agreement is obtained.
7. The higher values of the heat transfer coefficient with effectiveness are found 9.38% in the case of α=0º. But, there is small variation in effectiveness between them when Re_{sh}< 500.
8. The increase of heat transfer coefficient with increased volume concentrations is due to increase the thermal conductivity of nanofluid, Also the increasing in effectiveness 13.8% in case of 10% volume concentrations Al_2O_3-water is larger than in base water.
9. After the optimization procedure, baffles and nanofluid are selected to be effective parameters to enhanced heat transfer and effectiveness.

6.3 Recommendations

According to this study the recommendations for the future work could be presented as follows:

1. Using turbulent flow case (i.e. $2500 \leq Re \leq 10000$) for shell and U-tube heat exchanger with varying baffle inclination angle to investigate its influences of thermal and flow fields.
2. Using more than U-tube inside the shell.
3. Using different type of nanofluid.
4. The hydraulic and thermal performance of U-tube heat exchangers could be investigated experimentally by using Nanofluid as a cooling fluid.

REFERENCES

References

[1] Martin J.N., “Studies of shell side performance of shell-and-tube heat exchanger” PhD thesis, Mech. Eng. Dpt., University of Aston in Birmingham, 1984.

[2] Holman J. P., "Heat transfer", SI Metric edition, McGraw - Hill Book Company, 1989.

[3] Satyabrata Kanungo, “Numerical Analysis to Optimize the Heat Transfer Rate of Tube-in-Tube Helical Coil Heat Exchanger” MSC. thesis, Mech. Eng. Dpt. National Institute of Technology Rourkela,2014.

[4] http://www.wcr-regasketing.com, “Heat exchanger applications.” http:// www.wcr-regasketing.com/heat-exchanger-applications.htm, 2010.

[5] Bhatt.D and M. J. Priyanka, "Shell and tube heat exchanger performance analysis," the International Journal of Science and Research Volume, vol. 3, pp. 1872-1881, 2012.

[6] Paul William M., “Flow and Pressure Drop on the Shellside of Cylindrical Heat Exchanger” PhD thesis, Mech. Eng. Dpt., University of Aston in Birmingham, 1988.

[7] Chandra.B sekhar, D.Krishnaiah, F.Anand Raju,” Thermal Analysis of Multi Tube Pass Shell and Tube Heat Exchanger” International Journal of Innovative Research in Science, Engineering and Technology,2007.

[8] Talib Mushtaq, "Assisting and opposing mixed convective heat transfer study in an inclined circular pipe using nanofluids" M. Sc. Thesis, Mech. Eng. Dpt., University Tenaga Nasional.

[9] Xuan.Yand Q. Li, "Heat transfer enhancement of nanofluids," International Journal of heat and fluid flow, vol. 21, pp. 58-64, 2000.

[10] Nawar Salih “Numerical Comparative Study of Flow and Heat Transfer Between Base Fluid & Nanofluids in Curved Duct” M. Sc. Thesis, Mechanical engineering Department, College of Engineering, Basra University, 2012.

[11] Patankar, S.V., "Numerical heat transfer and fluid flow", Hemisphere Publishing Corporation, 1980.

[12] Martin Fisher, “An Experimental and Numerical Investigation into Compact Heat Exchangers” PhD thesis, Mech. Eng. Dpt., University of Warwick May 2000.

[13] Ferziger, J.H., and Perić, M., "Computational Methods for Fluid Dynamics", Springer-Verlag, Berlin, 2nd edition, (1997).

[14] Timothy Barth and Mario Ohlberger, “Finite volume methods: foundation and analysis", Institute of Applied Mathematics, Freiburg University, 2004.

[15] Ali Kadhim Mohammed, “FLOW BOILING INSIDE VERTICAL TUBES” Msc thesis, Department of Mechanical, Thermal Engineering Technology, March, 2014.

[16] Sukhrinder Pal S.N, “Shell-side Transfer in Shell-and-Tube Heat Exchangers” PhD thesis, Che. Eng. Dpt., University of Aston in Birmingham, 1981.

[17] Vukić. M. V, G. Vučković, P. Živković, Ž. Stevanović, and M. Tomić, "3D numerical simulations of the thermal processes in the shell and tube heat exchanger," Facta Universitatis, Series: Mechanical Engineering, vol. 11, pp. 169-180, 2014.

[18] Cucumo.M, V. Ferraro, D. Kaliakatsos, M. Mele, A. Galloro, R. Schimio, et al., "Thermohydraulic Analysis of a Shell-and-Tube “Helical Baffles” Heat Exchanger," International Journal of Heat and Technology, vol. 34, pp. S255-S262, 2016.

[19] Lei. Y.-G, Y.-L. He, R. Li, and Y.-F. Gao, "Effects of baffle inclination angle on flow and heat transfer of a heat exchanger with helical baffles," Chemical Engineering and Processing: Process Intensification, vol. 47, pp. 2336-2345, 2008.

[20] Ozden.E and I. Tari, "Shell side CFD analysis of a small shell-and-tube heat exchanger," Energy Conversion and Management, vol. 51, pp. 1004-1014, 2010.

[21] Raj. K. T. R and S. Ganne, "Shell side numerical analysis of a shell and tube heat exchanger considering the effects of baffle inclination angle on fluid flow using CFD," Thermal Science, vol. 16, pp. 1165-1174, 2012.

[22] Rehman. U. U, "Heat transfer optimization of shell-and-tube heat exchanger through CFD studies," 2012.

[23] Santosh K. Hulloli, "Thermal analysis of tubular heat exchangers using ANSYS," International Journal of Engineering Research, Volume, pp. 21-25, 2014**.**

[24] Rahim.A and S. S. Jameel, "SHELL SIDE CFD ANALYSIS OF A SMALL SHELL-AND-TUBE HEAT EXCHANGER CONSIDERING THE

EFFECTS OF BAFFLE INCLINATION ON FLUID FLOW," in National Conference on Trends and Advances in Mechanical Engineering, 2012.

[25] Vyas A. and Sharma, "An Experimental Analysis Study to Improve Performance of Tubular Heat Exchangers," Int. Journal of Engineering Research and Applications (www. ijera. com): ISSN, pp. 2248-9622, 2013.

[26] Shinde. S. S. and Hadgekar. M. P. V, "Numerical comparison on Shell side performance of Helixchanger with center tube with different helix angles," International Journal of Scientific and Research Publications, vol. 3, 2013.

[27] Ajithkumar and Ganesha, "CFD Analysis to Study the Effects of Inclined Baffles on Fluid Flow in a Shell and Tube Heat Exchanger," International Journal of Research in Advent Technology, vol. 2, 2014.

[28] Arjun and Gopu, "Design of shell and tube heat exchanger using computational fluid dynamics tools," Research journal of engineering sciences, vol. 3, pp. 8-16, 2014.

[29] Liu, Liu.Z, and W. Liu, "3D numerical study on shell side heat transfer and flow characteristics of rod-baffle heat exchangers with spirally corrugated tubes," International Journal of Thermal Sciences, vol. 89, pp. 34-42, 2015.

[30] Amirtharaj. P.S. P, Allaudinbasha.S, Janagan.M, Karthikeyan.K, Muthukumar.S, “Design and analysis of Shell and Tube Heat Exchanger with Inclined Baffles” International Journal of Scientific Development and Research” Vol.1. 2016

[31] Shahmohammadi1.P, Beiki1” A numerical investigation of γ-Al2O3-water nanofluids heat transfer and pressure drop in a shell and tube heat exchanger “Trans. Phenom. Nano Micro Scales, 4(1): 29-35, Winter - Spring 2016. Iran.

[32] Farajollahi.B, Etemad. S. G, and Hojjat, "Heat transfer of nanofluids in a shell and tube heat exchanger," International Journal of Heat and Mass Transfer, vol. 53, pp. 12-17, 2010.

[33] Guerrieri.D, Viana.F, Fragoso. S. C, and Avelino. M. R, "Shell-and-tube heat exchangers using nanofluids," in Proceedings of the 4th Brazilian Congress of Thermal Sciences and Engineering. Rio de Janeiro, RJ, Brazil: ABCM, 2012.

[34] Mukesh Kumar.P, Kumar.J, Suresh.S, and Praveen Babu.K, "Experimental study on parallel and counter flow configuration of a shell and helically coiled tube heat exchanger using Al2O3/water nanofluid," J. Mater. Environ. Sci, vol. 3, pp. 766-775, 2012.

[35] Albadr J, Tayal.S, and Alasadi.M, "Heat transfer through heat exchanger using Al2O3 nanofluid at different concentrations," Case Studies in Thermal Engineering, vol. 1, pp. 38-44, 2013.

[36] Ramesh R, Dr. R. Vivekananthan, “Application of Al2O3 Nanofluid for Enhance Heat Transfer Rate in Shell and Tube Heat Exchanger” Journal of Mechanical and Civil Engineering, Vol.11, PP 29-33,2014.

[37] kumar Surana.A, Koppula J. S, Harshit.S, Kumar.U, and RAJAGOPAL, "Numerical investigation of shell and tube heat exchanger using Al2O3 nanofluid," International Journal of Thermodynamics, vol. 20, pp. 59-68, 2017.

[38] Frank M. White, "Viscous Fluid Flow", Second Edition, McGraw -Hill, Inc., 1991.

[39] Walshaw A. C., Jobson D. A., "Mechanics of fluids" Second edition SI Units, Longman Group Limited, London, 1972.

[40] Latif M. Jiji, "Heat convection", Springer - Verlag Berlin Heidelberg, 2006.

[41] Merle C. Potter, John F. Foss, "Fluid Mechanics", Great Lakes Press, INC. Okemos, MI 48864, 1982.

[42] Talib Mushtaq " Numerical simulation of counter flow microchannel heat exchanger with different channel geometries and working fluids" PhD. Thesis, Mech. Eng. Dpt., Basrah University (2009).

[43] Bejan. A, Kraus A.D, Heat Transfer Handbook, John Wiley, New Jersey, 2003.

[44] Incropera, F.P., and DeWitt, D.P., "Fundamentals of heat and mass transfer", John Wiley & Sons, Inc., New York, 4th edition, (1996).

[45] AL-tayyeb A. K, “Heat Transfer and Nanofluid Flow Characteristics in Microchannel Heat Sink with Different Shapes” MSC. Thesis, Mech. Eng. Dpt., University Putra Malaysia,2013.

[46] John D. Anderson, "Computational fluid dynamics, the basics with Applications", International Edition, McGraw - Hill, INC. 1995.

[47] Patankar, S.V., "Numerical heat transfer and fluid flow", Hemisphere Publishing Corporation, 1980.

[48] Ghaith Najm Obaid, “Hydrodynamics and Thermal Characteristics Study of Turbulent Flow in a Model of Gas Turbine Blade” MSC. Thesis, Mech. Eng. Dpt., Basrah University (2013).

[49] Versteeg H. K., Malasekera W., "An introduction to computational fluid dynamics (The finite Volume method)", Addison Wesley Longman Limited, 1995.

[50] FLUENT 6.3 User's Guide, Fluent Inc. 2006.

[51] Satyabrata K., “Numerical Analysis to Optimize the Heat Transfer Rate of Tube-IN-Tube Helical Coil Heat Exchanger” Msc. Thesis, Mech. Eng. Dpt., National Institute of Technology Rourkela in Odisha,2014.

APPENDIX

Appendix A
Calibration of Thermocouples

Fig. (A-1). Shows The calibration of thermocouple consists of recording each of the measured temperature by the sensor and the indication of a standardized thermometer. The calibration process occurred in a constant bath temperature for each temperature recording. The result of the calibration is shown in Fig. (A-1).

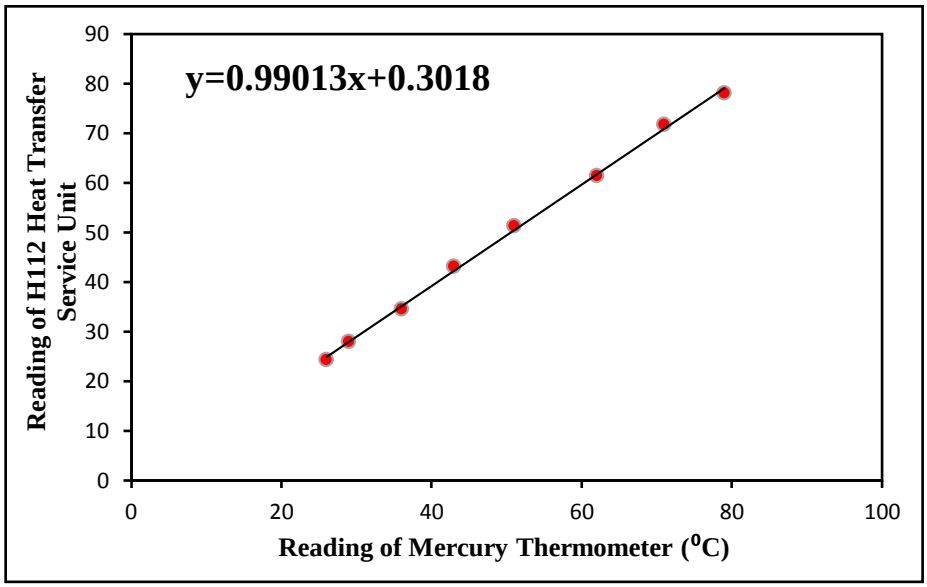

Fig. (A-1) Calibration of the Thermocouples.

Appendix B

Calibration of Rotameter

The calibration process consists of recording the volume flow rate which measured by the standard method and the indication of Rotameter. Whereas, in the standard method a cylinder with known volume and timer (stop watch) to measure the time need to fill the cylinder are used. Then by dividing the volume of cylinder by the observation time obtain the volume flow rate, the calibration process occurred at constant ambient temperature. The results of the calibration curve as in Fig. (B-1).

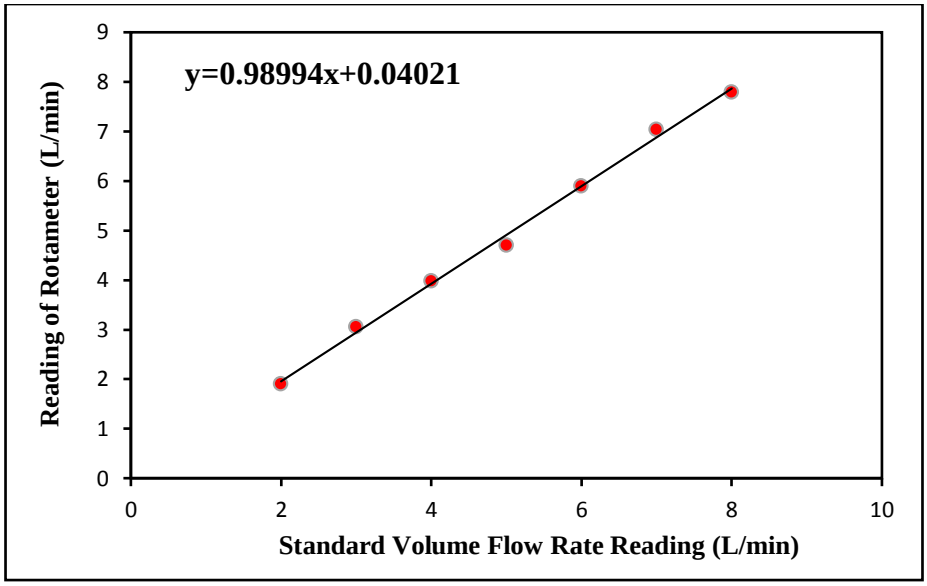

Fig. (B-1) Calibration of Rotameter.

Appendix (C):

Submitted Paper from the Thesis

THREE DIMENSIONAL STUDY OF HEAT TRANSFER AND FLOW CHARACTERISTICS IN SHELL-AND U-TUBE HEAT EXCHANGER WITH BAFFLES AND NANOFLUID.

Prof Dr Sadoun F.Albahadili*

Technical Engg college Basrah

Southern Technical University

BASRAH-IRAQ

Assist prof Dr Ahmed K.Alshraa

Engineering college Misan

Misan University

MISAN-IRAQ

Engg Murtadha S.Albahadili

Technical Engg college Basrah

Southern Technical University

MISAN-IRAQ

ABSTRACT

In this paper the three dimensional model of cylindrical coordinates, at laminar fluid flow and heat transfer in shell-and-tube heat exchanger (STHE) is examined. The thermo-hydraulic performance of heat exchangers is predicted with finite volume method by CFD simulations using ANSYS 15.0 code. Shell-and-tube heat exchanger is consisting of one pass of warm water, laminar flow on the shell side and two passes single tube of a laminar cold water with Al_2O_3 nanofluid. To enhance heat transfer the annular baffles are inserted on inner surface of the shell side, and on the facing distances from the outer surface of the length of tube. Annular baffles are inserted with staggered position on the shell and tube to achieve good fluid circulation. On the tube baffles are designed with different angle inclination, number, height Reynolds number ranging from 100 to 2000 with and without nanofluid. At the shell side only height and number are varied. Baffles angle inclination, number and diameter show clear influence on the flow velocity streamline. The results show high effect of baffles and nanofluid on the heat exchanger performance.

Keywords: Shell-and-tube; Numerical simulation; baffle inclination angle; nanofluid.

INTRODUCTION

The heat exchange between flowing fluids is one of the important processes in engineering applications. It can be classified depending upon their application, process fluids, and mode of heat transfer and flow. One important type of heat exchangers called tubular or shell and tube which are widely used. Shell-and-tube heat exchangers (STHE) are extensively used in petroleum refining, chemical engineering, and power generation, among others. Baffles, placed on the shell side space, are providing the cross flow direction of shell side fluid. **Shah mohammedi.P and Beikihe.H** [1] studied the effect of γ-Al2O3 nanoparticles on heat transfer rate, baffle spacing and pressure drop in the shell side of small shell and tube heat exchangers was investigated numerically under turbulent regime. They used γ-Al2O3-water nanofluids and pure water in the shell side and the tube side of heat exchangers, respectively. **Akshay Kumar Surana et al [2]** carried out the effect of number of tubes, unequal baffle spacing and tube diameter on heat transfer and pressure drop characteristics of a typical shell and tube type heat exchanger. Upon geometrical optimization, they studied the influence of Al2O3

Best Presentation Award

Name & Surname SAADOON ALBAHADİLİ

Paper Title THREE DIMENSIONAL STUDY OF HEAT TRANSFER AND FLOW CHARACTERISTICS IN SHELL-AND U-TUBE HEAT EXCHANGER WITH BAFFLES AND NANOFLUID

INTERNATIONAL CONFERENCE ON ENERGY AND THERMAL ENGINEERING

ICTE'17

APRIL 25-28, 2017

Assoc. Prof. Ahmet Selim DALKILIÇ
ICTE'17 Conference Chairman

Appendix (D):

Submitted Paper from the Thesis

Journal of University of Duhok, Vol. 20,No.1 (Pure and Eng. Sciences), Pp 404-415, 2017
eISSN: 2521-4861 & pISSN: 1812-7568
https://doi.org/10.26682/sjuod.2017.20.1.37

NUMERICAL INVESTIGATION OF HEAT TRANSFER AND FLOW CHARACTERISTICS IN SHELL-AND U-TUBE HEAT EXCHANGER WITH BAFFLES

PROF SADOUN FAHAD*, ASSIST PROF AHMED KADHIM ALSHARA** and ENG. MURTATHA SAEED***
*&**Technical Engg college Basrah- Southern Technical University-Iraq
*** Engineering college Misan- University of Misan-Iraq

ABSTRACT

In this paper the numerical model of cylindrical coordinates, three dimensional of a laminar heat transfer and fluid flow inside shell and tube heat exchanger is examined. The thermo-hydraulic performance of heat exchangers is predicted with finite volume method by CFD simulations using ANSYS 15.0 code. Shell-and-tube heat exchanger is consisted of one pass of warm water laminar flow at the shell side and two passes single tube of laminar cold water. The annular baffles are inserted on shell side, and on the facing distances of the length of tube from the outer surface. Baffles are inserted with staggered position on the shell and tube to achieve good fluid circulation. Also baffles on the tube side are varied with angle inclination, number and diameter while only number and length on the shell side. The tube baffles angle inclination as (45°, 0° and -45 °) and without baffles and the range of Reynolds number from 100 to 2000. The results show high effect of baffles angles on the heat exchanger performance at high Reynolds number. Maximum heat transfer from hot fluid occurs at baffle with angle 0° and high 30mm. Also baffles number increases Nusselt number at high fluid flow rate while a little effect of baffle height and number on the fluid pressure drop is absorbed as obtained by Mica et.al [1].

KEYWORDS: Shell-and-tube; Numerical simulation; baffle inclination angle.

1. INTRODUCTION

The heat exchange between fluids in engineering applications is one of the important processes. It is classified depending upon their process fluids, application, and mode of flow and heat transfer. One type of heat exchangers called tubular or shell and tube which are widely used. Shell-and-tube heat exchangers are used extensively in chemical engineering, petroleum refining, and power generation, among others. **Vukic. et al [2]** investigated local heat transfer and pressure drop on the shell side of shell-and-tube heat exchangers with segmental baffles for different baffle spacing. They found for same Reynolds number, the pressure drop and average heat transfer increase by increasing baffle spacing due to a reduced leakage through the baffle-shell clearance. **Vukic. et al [3,4]** carried out experimental and numerical heat and flow in shell and tube heat exchanger to show effect of number of segmental baffles, baffle cut size, baffle distance, the first and the last baffle position to inlet and outlet nozzle, size of the constructive on effectiveness of the shell and tube heat exchanger. They used heat exchanger with one pass shell and two pass 24 tubes (U-tube) in shell. Three packages of segmental baffle cuts of 22, 27 and 32% are located in the shell. There are 5 segmental baffles in every package. The results showed the heat exchange depending on the geometry of shell side. **Abdur Rahim et al. [5]** studied the effects of baffle inclination angle on flow and heat transfer of a heat exchanger with segmental baffles, three inclination angles of baffle 0°, 10° and 20°. These results concluded for the tubular heat exchanger that 20° baffle inclination angle hold a best performance comparing to 10° and 0° inclinations. **Amirtharaj et al. [6]** studied heat and flow in shell and tube heat exchanger with various design styles of baffle. They used CFD analysis for two models of shell and tube heat exchanger, the first with segmental baffles and second with inclined baffles. The Kern method was used to do the mathematical calculation. Results showed high effect of the performance of heat transfer for heat exchanger (shell and tube) with inclined baffles. **Thundil et al. [7]** carried out the effects of different baffle inclination angles on the heat transfer and fluid flow characteristics of a heat exchanger (shell and tube) for three inclination angles of baffle namely 0°, 10°, and 20°. They compared the performance of two tubular heat exchangers, the first with segmental baffles inclined on the direction of fluid flow and the

UNIVERSITY OF DUHOK
COLLEGE OF ENGINEERING

DUHOK 2017
ICRIE
CONFERENCE
RECENT INNOVATIONS IN ENGINEERING

Certificate of Attendance

Murtatha Saeed

has attended the 2nd International Conference of the College of Engineering, University of Duhok: Recent Innovations in Engineering

26th – 27th April 2017

Prof. Dr. Jowhar Rasheed Mohammed
Chairman of the conference

University of Duhok
Dean office
College of Engineering

Appendix (E):

Submitted Paper from the Thesis

Numerical and experimental study of heat transfer in shell-and U-tube heat exchanger with baffles

Abstract

In this paper the numerical and experimental investigations of the shell-and-tube heat transfer are presented. The thermal performance of heat exchangers is predicted with finite volume method by CFD simulations using ANSYS 15.0.1 software. The experimental part includes analyzing the thermal performance for laminar flow of U-tube heat exchanger unit. The effect of mass flow rate of hot and inclination angle of baffles were studied. The experimental rig for Shell-and-tube heat exchanger is consisting of one pass of warm water flow on the shell side and two passes single tube of cold water. The annular baffles were inserted on shell side, and on the facing distances from the outer surface of the length of tube. Baffles were inserted with staggered position on the shell and tube to achieve good fluid circulation [4]. The tube heat exchanger with different design style of angle inclination baffle (45º, 0º, -45º) and without baffles with Reynolds number ranging from 100 to 2000 was compared with numerical result. The results show high effect of baffles angles on the heat exchanger performance at high Reynolds number. Maximum heat transfer from hot fluid occurs at baffle with angle 0° and high 30mm.The experimental results show that the increase in the inlet hot mass flow rate led to increase in the heat transfer rate. Also, mass flow rate for shell side played a major role in effectiveness. Furthermore, it can be concluded that 0° baffle inclination angle gives a best performance compared to +45° and -45° inclination angles. All the experimental results were compared with theoretical results which analysis for model as shown in Fig. (1) and good agreement was obtained.

Appendix (F):

Submitted Paper from the Thesis

Experimental study of heat transfers in shell-and U-tube heat exchanger with baffles

Abstract

In this paper the experimental investigations of heat transfer for the cylindrical three dimensional of laminar flow in shell-and-tube heat exchanger are presented. Shell-and-tube heat exchanger is consisting of one pass of warm water flow on the shell side and two passes single tube of cold water. The annular baffles were inserted on shell side, and on the facing distances from the outer surface of the length of tube. Baffles were inserted with staggered position on the shell and tube to achieve good fluid circulation [1]. The effect of hot fluid Reynolds number on the thermal performance was studied. Also baffles on the tube side are varied with angle inclination. The tube heat exchanger with different design style of angle inclination baffle (45º, 0º, -45º) with mass flow rate ranging (2-6) L/min. The results show high effect of baffles angles on the heat exchanger performance at high Reynolds number. Maximum heat transfer from hot fluid occurs at baffle with angle 0º.

الخلاصة

أجريت دراسة تجريبيه وعدديه لجريان المائع وانتقال الحرارة ذي جريان انسيابي ثلاثي الابعاد وبإحداثيات أسطوانية في مبادل حراري نوع القشرة والانبوب باستخدام الحواجز والمائع النانوي (Al_2O_3). تم حساب أداء المبادل الحراري والهيدروليكي باستخدام طريقة الحجوم المحددة من خلال نمذجه ديناميك الموائع الحسابي والبرنامج الجاهز ANSYS 15.0.1. يتكون المبادل الحراري من القشرة بممر واحد للماء الساخن وممرين للأنبوب على شكل حرف (U) للماء البارد. الحواجز الحلقية تم تثبيتها على السطح الداخلي للقشرة وبأبعاد متساوية وكذلك على السطح الخارجي للأنبوب. ثبتت الحواجز بشكل متعاقب للقشرة والانبوب لضمان أفضل تدوير للمائع الساخن. تم دراسة المبادل الحراري مع الحواجز بزوايا مختلفة (+45º , 0º -45º) وبدون حواجز بحدود عدد رينولد متغير (100-2000).

الهدف الرئيسي لهذه الدراسة هو تحديد تأثير كل من زاوية ميل الحاجز، عدد الحواجز، ارتفاع الحاجز، القطر الهيدروليكي للأنبوب ونسبة تركيز المائع النانوي بالنسبة للماء على أداء المبادل الحراري. تم دراسة تأثير المتغيرات على الحرارة من خلال معدل عدد نسلت والفعالية بينما على الجريان يشمل هبوط الضغط ومعدل معامل الاحتكاك.

تبين النتائج النظرية تأثير عالي لزويا الحواجز على أداء المبادل الحراري عند زيادة عدد رينولد. أكبر معدل لانتقال الحرارة بين المائعين يحدث عند الحاجز ذي الزاوية (0º) وارتفاع 30 وبنسبة زيادة في معدل انتقال الحرارة 15.402%. كما ان أكبر معدل تحسين لمعامل انتقال الحرارة الإجمالي بنسبة 6.73% باستخدام المائع النانوي (Al_2O_3) ذي تركيز 10% بسبب زيادة الموصلية الحرارية للمائع. كما وان زيادة عدد الحواجز تؤدي الى تحسين عالي للفعالية ليصل الى حوالي 7.94% في حالة عند عدد الحواجز 8 وعدد رينولد 2000 مقارنه مع الحالة عدد الحواجز 3.

الجزء التجريبي يشمل تحليل الأداء الحراري للجريان المنساب للمائعين داخل المبادل الحراري. تم دراسة تأثير عدد رينولد للمائع الساخن وزوايا الحواجز. تبين النتائج التجريبية

زيادة معدل انتقال الحرارة بزيادة معدل جريان الحجمي للمائع. كما وانه معدل الجريان الحجمي خلال القشرة يلعب دورا بارزا في تحسين الفعالية. كذلك نستنتج ان زاوية ميل الحاجز (0°) تعطي أفضل أداء مقارنتا بزاوية ميل الحاجز ($+45^o$) و(-45°). جميع النتائج التجريبية تم مقارنتها بالنتائج النظرية للموديل وكان هنالك تطابق بالنتائج.

دراسة نظريه وتجريبيه لتأثير الشكل الهندسي للعوائق والمائع النانوي على أداء المبادل الحراري ذي القشرة والانبوب على شكل حرف U

رسالة مقدمة الى

مجلس الكلية التقنية الهندسية/البصره - الجامعة التقنية الجنوبية كجزء من متطلبات نيل درجة الماجستير في علوم هندسة تقنيات الحراريات

من قبل

مرتضى سعيد محمد

ايلول 2017